Real-Time Optimal Control of a Plug-in Hybrid Electric Vehicle Using Trip Information

by

Mahyar Vajedi

A thesis
presented to the University of Waterloo
in fulfillment of the
thesis requirement for the degree of
Doctor of Philosophy
in
Systems Design Engineering

Waterloo, Ontario, Canada, 2016

I hereby declare that I am the sole author of this thesis. This is a true copy of the thesis, including any required final revisions, as accepted by my examiners.

I understand that my thesis may be made electronically available to the public.

Abstract

The plug-in hybrid electric vehicle (PHEV) is a promising option for future sustainable transportation. It offers better fuel economy and lower emissions than conventional vehicles. This thesis has developed a novel energy-optimal powertrain controller for PHEVs. The controller will be broadly applicable to all PHEV models; however, it will be fine-tuned to the Toyota Prius Plug-in Hybrid for testing and validation. The controller will take advantage of advancements in vehicle intelligent and communications technologies, such as Global Positioning System (GPS), Intelligent Transportation System (ITS), Geographic Information System (GIS), radar, and other on-board sensors, to provide look-ahead trip data. These data are critical to increasing fuel economy as well as driving safety.

This PhD research has developed three energy-optimal systems for PHEVs: Trip Planning module, Route-based Energy Management System (Route-based EMS), and Ecological Cruise (Eco-Cruise) Controller. The main objective of these energy-optimal systems is to minimize the total energy cost, including both electricity derived from the grid and fuel. The upper-level system is Trip Planning, using an algorithm designed to take advantage of previewed trip information to optimize State of Charge (SOC) profiles. The Route-based EMS optimally distributes propulsion power between the batteries and engine. Finally, the Eco-Cruise controller adjusts the speed considering upcoming trip data.

Real-time implementation has remained a major challenge in the design of complex control systems. To address this hurdle, simple and efficient models and fast optimization algorithms are developed for each energy-optimal strategy. A Real-time Cluster-based Optimization is developed to solve the Trip Planning problem in real-time. The Route-based EMS is developed based on Equivalent Consumption Minimization Strategy (ECMS) to optimally distribute propulsion power between two energy sources. And, a Nonlinear Model Predictive Control (NMPC) is utilized to obtain optimum traction or regenerative torques in Eco-Cruise controller.

Model-in-the-Loop (MIL) and Hardware-in-the-Loop (HIL) testing are critical steps in control validation and in ensuring real-time implementation capability. The MIL results show that the novel energy-optimal powertrain controller can improve the total energy cost by up to %20 compare to benchmark rule-based controller. The HIL test results demonstrate that the computational time for energy-optimal strategies are less than the target sampling-time, and they can be implemented in real-time.

Acknowledgements

I would like to express my deepest gratitude to my supervisor Professor Nasser L. Azad, for his motivation and valuable guidance during my PhD study. This research would not have been possible without his precious support.

I would also like to thank Professor John McPhee for his insightful comments and encouragement at different stages of my PhD research.

My special thanks to my PhD examination committee, Professors Baris Fidan and William Melek, for their valuable time, attention, and efforts toward the improvement of this thesis.

I am grateful for my colleagues in the SHEVS Lab and Motion Research Group, A. Taghavipour, R.S. Razavian, N. Mehrabi, R. Masoudi, M. Chehrehsaz, H. Adibi, B. Ghannadi, A. Mozaffari, M. Shourijeh, A. Seaman, A. Hall, J. Banerjee, A. Ing, S. Kim, B. Sakhdari, S. Tajeddin, P. Golchoubian, Y. Masoudi, S. Hassanpour, C. Shum, E. Samadani, S. Ekhtiari, M. Batra, A. Maitland, A. Keblawi, and Y. Liang, for their efforts and collaboration that made working in the lab a wonderful experience.

I thank Dr. Ken Butts and Toyota Technical Center for their suggestions which greatly assisted the research.

I acknowledge the NSERC, OCE, and Toyota for financial support of this research.

Last but not the least, I would like to thank my family for their unfailing support. My special gratitude and love goes to my parents, for giving me the opportunity to pursue my education.

Dedication

To my loved ones.

Table of Contents

List of Tables

List of Figures

Abbreviation

ACC	Adaptive Cruise Control
ADAS	Advanced Driving Assistant Systems
AER	All Electric Range
A-ECMS	Adaptive Equivalent Consumption Minimization Strategy
CAFE	American Corporate Average Fuel Economy
CDCS	Charge Depleting - Charge Sustaining
DP	Dynamic Programming
ECMS	Equivalent Consumption Minimization Strategy
Eco-Cruise	Ecological Cruise Controller
ECU	Electronic Control Unit
EMS	Energy Management System
EV	Electric Vehicles
FTP	Federal Test Procedure
GIS	Geographic Information Systems
GPS	Global Positioning Systems
HEV	Hybrid Electric Vehicle
HIL	Hardware-in-the-Loop
HMI	Human Machine Interface
HWFET	Highway Fuel Economy Driving Schedule
ICE	Internal Combustion Engine
ITS	Intelligent Transportation System
LMPC	Linear Model Predictive Control
MIL	Model-in-the-Loop
MPC	Model Predictive Control
MSSM	Modified Simple Shooting Method
NMPC	Nonlinear Model Predictive Control
PHEV	Plug-in Hybrid Electric Vehicle
PMP	Pontryagin's Minimum Principle
PSO	Particle Swarm Optimization
RCO	Real-time Cluster-based Optimization
RCP	Rapid Control Prototyping
RTI	Real Time Interface
SOC	State of Charge
SDP	Stochastic Dynamic Programming
TPBV	Two Points Bouldery Value Problems
RMSE	Root Mean Square Error

SSM	Simple Shooting Method
SFTP	Supplemental Federal Test Procedure
UDDS	Urban Dynamometer Driving Schedule
VPA	Vehicle Powertrain Architecture
VPC	Vehicle Powertrain Controller

Nomenclature

P_d	Power demand
T_d	Wheel torque demand
F_d	Resistance force
v	Vehicle speed
ρ	Air density
C_d	Drag coefficient
f	Rolling resistance coefficient
m	Vehicle mass
θ	Road grade
A	Frontal area of the vehicle
g	Gravity acceleration
r	Wheel radius
PR	Power Ratio
η_t	Power-split transmission efficiency
η_m	Motor-generator efficiency
P_b	Battery electrical power
$\tilde{P}_b$	Mechanical power delivered by the battery
P_e	Engine power
V_{oc}	Battery open circuit voltage
R_b	Battery resistance
I	Load current
P_{acc}	Acceleration power
P_{dec}	Deceleration power
$v^\star$	Threshold speed for the engine starting
m_f	Fuel consumption
Q_{max}	Maximum battery capacity
η_{ch}	Charger efficiency
k_f	Unit price of gas
k_e	Unit price of grid electrical energy
η_b	Battery efficiency
H_{LHV}	Low heat value of the fuel
S	Equivalency factor
ω_m	Motor angular velocity
T_m	Motor torque
ω_e	Engine angular velocity
T_e	Engine torque

ω_g	Generator angular velocity
T_g	Generator torque
v_h	Speed of the host vehicle
x_h	Position of the host vehicle
v_p	Speed of the preceding vehicle
x_p	Position of the preceding vehicle
a_p	Acceleration of the preceding vehicle
u	Control command (input)

Chapter 1

Introduction

1.1 Background

Energy and environmental issues are among the most serious concerns facing today's society, with the automotive industry figuring prominently in the global dialogue. At its current trajectory, the transportation sector is expected to become the largest greenhouse gas producer over the next 50 years [1], and will continue to rank among the world's leading energy consumers. This situation has spurred significant investment in the research and development of fuel efficient, sustainable transportation systems that will minimize, and eventually replace, non-renewable, fossil-based energy sources with clean, renewable ones.

Electric vehicles (EV) consume electric energy from the grid, which can be provided from renewable resources. In addition, EVs demonstrate outstanding energy efficiency, at roughly 70%, in comparison with conventional Internal Combustion Engine (ICE) vehicles,

which have peaked at just 30% efficiency [2]. Therefore, EVs are increasingly considered viable long-term solutions to the sustainable transportation challenge. However, broad take-up of current EV technologies has been hampered by their limited operating range (about 150 km) and high initial costs.

PHEVs are promising options for near-term improvements to transportation sustainability. Utilizing two sources of energy, batteries (to power an electric motor) and gasoline (to power an ICE), allows them to achieve much higher energy efficiencies than conventional ICE vehicles, without sacrificing performance. Furthermore, with an ability to store electric energy directly from the grid, PHEVs offer the combined advantages of both electric and Hybrid Electric Vehicles (HEVs). That is, they can operate in full electric mode in urban areas (zero emissions, zero fuel consumption) and provide the extended range and efficiency typical of HEVs during highway driving (low emissions, low fuel consumption).

The potential to maximize energy efficiency and minimize environmental impacts through vehicle electrification has captured the attention of most automotive manufacturers. In response to energy and environmental concerns, governments across the world have established strict vehicle standards, such as the American Corporate Average Fuel Economy (CAFE), which require automotive companies to dramatically reduce fleet emissions and improve efficiencies on a very tight timeline. Most, if not all, major automotive manufacturers have made major investments in HEV, PHEV, and/or EV development, not only to meet future market demands, but also to maintain their annual average fuel economy within the range allowable by government standards.

1.2 Motivation and challenges

Due to rising fuel cost and emission concerns, PHEVs are increasingly considered a viable alternative to conventional vehicle technologies. Although these vehicles demonstrate significantly improved vehicle performance, high initial and maintenance costs have proved an impractical trade-off for most consumers. According to the report by National Academy of Sciences [1], EVs and PHEVs, which were once expected to dominate the automotive industry by 2020, will likely capture only 5% of the market in the next decade.

To increase demand for PHEVs, long-term operation cost issues must be resolved. In other words, vehicle systems should be enhanced to improve fuel efficiency, which in turn, will provide long-term cost advantages over conventional vehicles. One approach is to improve total energy cost through advanced powertrain control systems, in particular the optimal trip planning module, Energy Management System (EMS), and ecological cruise controller. Trip planning modules optimize electrical energy profiles based on long-range trip information for any driving scenario. EMS strategies compute the power distribution between two sources of energy (fuel and battery). Ecological cruise controllers adjust vehicle speeds to minimize total energy cost.

Although PHEVs offer improved efficiencies similar to conventional HEVs, they also present new challenges in energy-optimal powertrain control problem. It is difficult to find control solutions that can optimally distribute power demand between the two sources of energy. This difficulty largely stems from the fact that PHEVs differ from HEVs in two key ways: they can fully charge the battery by connecting to the grid and they can operate in charge depletion mode, reducing the battery SOC to the minimum permissible value.

Furthermore, the ability to restore the electrical energy during regenerative braking makes ecological cruise control for PHEVs more complicated than that for a conventional vehicle. Therefore, approaches to the development of energy-optimal controllers for PHEVs must consider these differences in the dynamics of the system, initial conditions and constraints.

A global optimum solution for the PHEV powertrain control problem can only be addressed with advance knowledge of driving conditions. Access to these data enables optimal distribution of electrical energy throughout any trip. We can take advantage of recent advancements in GPS, GIS, Intelligent Vehicle Technologies, such as Vehicle-to-Vehicle (V2V) and Vehicle-to-Infrastructure (V2I) Communication Systems, and radar sensor to predict future driving conditions and create more effective energy-optimal controllers.

In particular, control systems that optimize EMS and enable ecological cruise control are very complex, making real-time implementation a significant challenge. Several global optimization methods that aim to provide an optimum powertrain control strategy already exist; however, computationally they are extremely costly, particularly for long trips, and cannot be implemented in real time. This PhD research will address these challenges by developing a novel energy-optimal controller for power-split PHEVs, with real-time implementation capability.

1.3 Objectives and methods

The goal of this PhD research was to design a real-time energy-optimal controller to minimize total energy cost, including both fuel and electrical energy taken from the grid. To

enhance the performance of the controller, prediction of future driving conditions were incorporated. The energy-optimal controller has been designed for real-time implementation. To address the potential for practical implementation, the controller has been fine-tuned to a commercial PHEV architecture, the Toyota Prius Plug-in Hybrid, for testing and validation purposes. The devised energy-optimal controller consists of three main systems:

- Trip Planning module
- Route-based EMS
- Eco-Cruise controller

The real-time implementation capability of the energy-optimal controller is achieved through efficient control-oriented models and fast optimization techniques. Control-oriented models are sufficiently simple and fast for real-time implementation, and are accurate enough to characterize the system. These models have been validated using a high-fidelity model, which is more complex and considers more system details. The high-fidelity model of baseline PHEV has been developed in Prof. Nasser L. Azad and Prof. John McPhee's research group by A. Taghavipour [3] and M. Chehresaz [4] (Please see Section 3.2).

In each aforementioned energy-optimal system, a proper and fast optimization algorithm is developed based on the problem characteristics such as desired computational speed, number of variables and optimization parameters, and dynamics of the system. The Trip Planning module deals with huge number of variables and optimization parameters, especially during long trips. Therefore, a Real-time Cluster-based Optimization (RCO) algorithm is developed for this module that reduces the number of optimization

parameters using clustering technique. Then, Dynamic Programming (DP) is applied to solve the simplified optimization problem. Route-based EMS is based on ECMS strategy, which is fast technique for solving EMS problems. This thesis improves EMS performance by incorporating trip information. Finally, the NMPC technique is utilized for solving the Eco-Cruise control problem. NMPC can solve multi-objective control problems and can handle constraints on states and inputs. Therefore, it's a promising technique for the Eco-Cruise controller which optimizes both the total energy cost and driving safety while considering constraints on vehicle speed and powertrain variables.

This PhD research evaluates the new energy-optimal controller using following strategies:

- Energy-optimal controller performance compared against:
  - Autonomie software rule-based controllers; and
  - Global optimum control methods: Dynamic Programming and Pontryagin's Minimum Principle (PMP).
- MIL simulations to evaluate the new controllers; and
- HIL tests to evaluate the real-time implementation capability of the energy-optimal controller.

1.4 Document organization

This thesis is organized as follows: Chapter 2 reviews state-of-the art HEV and PHEV control strategies, including both EMS and speed controllers. This discussion also addresses current methods used to incorporate trip information within control strategies that aim to improve vehicle performance. Chapters 3, 4, and 5 cover the steps in the design of the proposed Trip Planning, Route-based EMS, and Eco-Cruise controller. Finally, Chapter 6 discusses the conclusions and future work, and outlines anticipated contributions of the proposed research.

Chapter 2

Literature review

This chapter reviews recent advances in HEV and PHEV research, spanning Trip Planning algorithms, EMS strategies, and cruise control techniques. It also investigates approaches to improve control system efficiency. The chapter concludes with a summary of the relevant literature and an overview of the significant contributions of the designed energy-optimal control system.

2.1 Trip planning

This section investigates algorithms used to improve powertrain control systems based on knowledge of upcoming driving conditions. Two general approaches are currently used to predict future traffic conditions: model-based and data-driven methods [5]. In model-based methods, future traffic speed is calculated based on traffic flow theory. Data-driven methods, on the other hand, predict upcoming traffic speeds based on current and past

traffic data, without incorporating a traffic model. Neural networks are among the most popular data-driven prediction methods. For example, Park [6, 7] utilized an artificial neural network to model traffic conditions based on trip information obtained from GPS and ITS, then used this information to improve EMS performance and, subsequently, fuel efficiency.

Some researchers used model-based driving condition predictions in the speed controller systems to improve fuel efficiency. Recent examples include studies by Keulen et al. [8–10]. They obtained optimum future speed trajectory for an HEV, based on trip information. Then, they fed this data to a cruise controller to ensure that the vehicle followed the optimum speed trajectory. In another work [11], Keulen et al. presented an optimized EMS controller for hybrid electric trucks based on trip information. They calculated optimal future speed trajectories using trip information. By implementing an online EMS controller, they obtained the optimum deceleration rate during the regenerative braking, to achieve the maximum energy recovery. They showed that the fuel consumption can be reduced considerably by using the proposed control approach.

Gong et al. [12, 13] proposed a two-scale DP method to produce optimized energy management schemes for PHEVs. In this method, they first calculated the power demand governed by trip information, and then optimized the SOC profile using the linear model of the battery. They investigated the use of Gas-kinetic based models and neural networks to incorporate trip modelling into EMS, finding that Gas-kinetic models are complicated by several parameters, while neural networks offer better trip modelling accuracy and are more feasible for real-time implementation. They used traffic data to train the neural network and utilized future traffic conditions in the EMS of a parallel PHEV. In another PHEV

EMS study, Gong et al. [14, 15] used a statistical approach to obtain traffic information, specifically applying a Markov chain model to generate a velocity trajectory. The predicted velocity trajectory was then utilized to tune the controller and augment the EMS strategy to improve vehicle performance.

Bin et al. [16] utilized an adjustable segment scheme that regulates the length of trip segments based on trip information, to minimize the computational effort required for effective EMS. They compared the simulation results against earlier-mentioned DP results, which numerically calculated power demand and SOC, and found that the two-scale DP method is more computationally efficient.

Katsargyri et al. [17,18] optimized the battery SOC profile of power-split PHEVs based on trip information. They employed the rule-based controller offered by the PSAT software to track the optimum SOC and proposed a receding horizon approach in the segmentation procedure. They replaced the original route, which had a large number of segments, with a virtual route. In the virtual route, they considered the few initial segments of the original route plus the last segment, which was considered equivalent to all the remaining segments. Using DP, they obtained the optimum SOC of each segment and used the first segment's SOC as a reference point in the EMS strategy. They showed that this method had a lower computational cost than the optimal solution of the original route.

2.2 HEV/PHEV energy management strategies

In order to obtain optimal fuel economy, an EMS strategy that optimizes energy flow between the two power sources is a key requirement. EMS schemes can be divided into two main categories: reactive and route-based strategies. Reactive EMS strategies use current driving information in their controller scheme; therefore, they can find only the near-optimal solution for the problem. Rule-based controllers, Charge Depleting Charge Sustaining strategy (CDCS), Stochastic Dynamic Programming (SDP), and the ECMS strategy belong to this group.

Rule-based approaches typically utilize maps constructed from engineering expertise, or more formal methods such as optimization [19]. These are rigid strategies that yield high performance for known drive cycle patterns, but they are not optimized. In the CDCS strategy, the vehicle is propelled primarily using energy from the battery in charge depleting (CD) mode, until a predefined level of SOC is reached. Then, the EMS controller switches to charge sustaining (CS) mode to keep the SOC at the predefined level.

The SDP method is an appealing EMS approach because it provides an ability to optimize system performance with respect to a probabilistic distribution of different drive cycles [20]. Bashash [21] and Moura [22, 23] utilized the SDP method to establish an appropriate EMS strategy for power-split PHEVs. Bashash predicted the PHEV's power demand based on stochastic data. Moura used SDP to derive an optimal EMS strategy for a PHEV platform. The strategy aims to minimize both fuel cost and battery maintenance cost. His simulation results showed that, at first, more electric power is consumed to quickly deplete the battery SOC when the battery resistance growth is high. Then, a

blended strategy is the more efficient strategy when the SOC is low.

Look-ahead trip and driving conditions that cover the entire drive cycle should also be incorporated in a truly optimized EMS scheme. Considerable research has been undertaken to reduce fuel consumption and vehicle emissions with the help of preview trip information [24–28]. Gonder [29, 30] investigated the efficacy of using route-based control algorithms to improve the fuel economy of HEVs. He showed that look-ahead control improves fuel consumption approximately 2% to 4%. This may seem a negligible improvement; however, it represents an opportunity for significant fuel savings. Based on estimated annual HEV fuel consumption in 2006, a 2% to 4% improvement in efficiency could potentially reduce annual fuel consumption by 6.5 million gallons in the US alone.

Taking advantage of trip information increases the complexity of the energy management problem, and makes the real-time implementation of these control strategies very challenging in practice. Several optimal control approaches for HEV and PHEV energy management schemes were studied in the literature [31], including: DP, PMP, Model Predictive Control (MPC), and Adaptive-ECMS (A-ECMS). To clarify previous EMS research directly related to this thesis, the following discussion focuses on the aforementioned optimal control techniques.

2.2.1 Dynamic programming

DP is a global optimization method that can optimally solve a vehicle's power distribution based on trip information. This method is computationally expensive, and often impractical for real-time implementation, particularly for complex problems. Lin [32, 33] has found

near-optimal rules in the EMS controller of parallel HEVs based on DP global minimum results. Using this method, he obtained an optimal power distribution between the engine and electric motor, and showed rather large improvements in fuel efficiency.

Gonder et al. [34] studied several PHEV EMS strategies during CD mode, including all-electric-range and blended strategy. They compared these strategies in terms of travel distance and prior knowledge of the trip. The results showed that the all-electric-range operation mode has all the benefits of a full electric vehicle, but would require more expensive electric components (a larger battery and electric motor). On the other hand, the blended strategy showed the best fuel efficiency for long-distance travel. O'Keefe and Markel [35] demonstrated that in optimal battery charge distribution strategies, SOC reaches the minimum level exactly when the trip terminates.

2.2.2 Pontryagin's minimum principle

The PMP technique finds the global optimal solution for control problems based on minimizing the Hamiltonian. This technique can minimize the performance index in the presence of states and inputs constraints. Razavian et al. [36, 37] developed a real-time EMS strategy for a series HEV using the PMP technique. This controller works independently of speed trajectory, requiring only the cruise time and the amount of energy used during regenerative braking to tune its parameters. With this approach, the optimal control problem was reduced from the integral cost minimization to the instantaneous Hamiltonian minimization, enabling real-time implementation of the EMS strategy. To evaluate the performance of the controller, it was applied to a high-fidelity HEV model developed in

MapleSim. The simulation results demonstrated a significant improvement in fuel economy.

Ebbesen et al. [38] considered battery life in the optimum EMS strategy of a parallel HEV using the PMP technique. Ebbesen has claimed that they developed the first state of health model for Li-ion batteries. Because electrochemical models are extremely complex, they cannot be implemented in real-time EMS strategies. Therefore, Ebbesen used a throughput-based capacity fade model in his study. In this model, it is assumed that the battery's energy capacity is equivalent to the remaining number of cycles before its end-of-life, under constant conditions.

2.2.3 Model predictive control

Model predictive control is a promising method for exploiting the potentials of modern concepts and fulfilling automotive requirements, because of its ability to handle constrained multi-input multi-output optimal control problems [39]. Application of MPC to hybrid vehicles has been investigated before. Wang [40] proposed a real-time control system for different hybrid architectures using the MPC concept. Kim [41] utilized MPC to calculate an optimal torque split in the parallel HEV. Borhan [42, 43] applied MPC to a power-split HEV, ignoring the dynamics of the powertrain against other faster dynamics for the model inside the controller. He implemented several different controllers, such as a nonlinear MPC, linearized MPC, and the rule-based controller strategy offered by the PSAT software, to evaluate performance. The results illustrate that, in comparison with the other controllers studied, nonlinear MPC provides the largest improvement to fuel economy.

Taghavipour et al. [44] applied MPC to a power-split PHEV and used DP as a benchmark for evaluating the EMS performance. In another work [45], the authors developed an EMS strategy based on MPC approach and applied it to a high-fidelity model of a power split PHEV in the MapleSim software in order to minimize fuel consumption.

2.2.4 Equivalent consumption minimization strategy

ECMS has been widely employed for building EMS schemes. This approach is helpful in developing an optimal control system that minimizes total energy consumption whether electric energy (consumed by the battery) or fuel (consumed by the engine) [46–55]. Since electric energy consumed by the battery and fuel consumed by the engine are not directly comparable, the ECMS technique is used to develop an optimal control system that minimizes total fuel consumption. Tulpule et al. [56] applied the ECMS technique to series and parallel PHEVs, taking into consideration two different strategies: CD and Blended. The results demonstrated greater efficiencies for both architectures, depending on trip conditions. Musardo et al. [57] proposed an A-ECMS method based on driving conditions, which calculates the equivalency factor in ECMS technique for parallel HEVs.

Among the different PHEV architectures available, the power-split configuration has particular advantages. It decouples the engine crankshaft from the road, and allows electric machines to move the engine operation point to where fuel efficiency is at its maximum. Yiming He [58] adopted the A-ECMS for power-split PHEVs. Wollaeger [59] showed that a near-optimal EMS strategy can be achieved by depleting the battery SOC with respect to the driving distance. This optimal strategy assumes that we have prior knowledge of the

travelling distance, while speed trajectory remains unknown. Stockar et al. [60,61] proposed a novel supervisory EMS strategy for series-parallel PHEVs. They applied the ECMS to calculate the overall vehicle CO_2 emissions, taking into account emissions indirectly produced during electric power generation. They applied PMP to find the optimum power distribution between the engine and motor-generators.

2.3 Cruise controller

Reports released by the World Health Organization indicate that the annual worldwide costs resulting from road traffic injuries are approximately $518 billion [62]. The evidence indicates that human perception error is the most significant factor, contributing to 90% of road traffic accidents. This fact has brought the automotive control engineers to develop Advanced Driving Assistant Systems (ADAS). The main goal of ADAS systems is to decrease the constraints on human judgment during the driving cycle, which will in turn result road transportation safety improvement [63–65]. Adaptive Cruise Control (ACC) is one of the most important ADAS technologies, and has attracted increasing interest from automotive engineers. ACC works based on the information received from on-board sensors, for instance radar, to adjust vehicle speed to maintain a proper distance with the proceeding vehicle on the road [66, 67].

2.3.1 Adaptive cruise controller

ACC systems aim to increase traffic flow and reduce accidents, and thus represent a big step towards improving overall traffic and transportation system efficiency. ACC takes advantage of sensor technologies to measure headway distance, and a controller uses the obtained data to adjust both velocity and distance to the next vehicle according to current driving and environmental conditions. Employing much more effective ACCs can significantly enhance the driving safety and performance of vehicles [68,69]. ACC systems can be divided into two main groups: rule-based approaches and model-based approaches. Sliding mode [70], optimal control [71], and model predictive control [72] are all examples of model-based approaches.

Ferrara and Vecchio [73] proposed a collision avoidance ACC system to reduce the incidence of collisions involving passengers and other vulnerable road users. They used a supervisory control technique that switches the control mode between normal condition and collision avoidance, based on trip data. In normal condition, the sliding mode control system has been utilized to follow the desired distance from the leading vehicle. If the supervisory control detects a possible collision, the control mode is switched to collision avoidance, which activates the emergency braking or performs a collision avoidance manoeuvre.

Moon et al. [74] integrated ACC with collision avoidance. They proposed a control scheme that operates the vehicle in three modes based on specific driving situations, including comfort-mode, large- deceleration mode, and severe-braking mode. The driving situation is recognized by two indexes: the time-to-collision index and non-dimensional

warning index. The latter is calculated based on vehicle spacing. They used manual driving data in the no-crash condition to tune the controller parameters. Full vehicle testing demonstrated that the ACC system could drive the vehicle similar to the human driving and avoid the collision.

2.3.2 Ecological cruise controller

Some researchers have begun to investigate ecological cruise controller for conventional vehicles. Huang [75] used constrained nonlinear programming to predict the optimal throttle, gear shifting and velocity trajectory of heavy trucks. Hellstom [76] incorporated MPC in real-time, set the optimum speed trajectory as a set point of the cruise control system, and then implemented his solution on a heavy diesel truck. The results showed that look-ahead cruise control provides better fuel efficiency than conventional cruise control systems, especially on hilly roads. The look-ahead control system improves fuel economy by efficiently reducing the vehicle's speed as it proceeds towards a downhill slope and increasing it before an uphill climb. Zhaun et al. [77] claim they were the first to formulate a solution to the nonlinear problem, but specifically for application to trains. They proposed an output regulation approach that incorporates measurement feedback and has the locomotive follow a prescribed speed profile.

MPC theory has received a great deal of attention for automotive control applications, as its formulation is best suited for online optimizations, as well as dealing with constraints in large multivariate systems [78–81]. The scope of MPC technique application has also been extended to ITS, in which the principal focus is on using upcoming information from

the intended route to adjust the control variable of vehicles. A significant number of studies in the literature demonstrate the applicability of MPC controllers for ITS applications. Li et al. [82] used MPC in their ACC system design. They proposed a multi-objective controller, which simultaneously considers fuel economy and speed tracking. Kamal et al. [83] took advantage of the MPC theory to design a novel ecological driving system for running a vehicle on roads with up-down slopes. The simulation results demonstrated that the use of MPC controllers can significantly decrease the fuel consumption.

Wang et al. [84] analysed driver assistance systems and concluded that using a control strategy with the ability to predict the future dynamics of proceeding vehicles' speed can result in efficient ACC. In this way, they demonstrated that MPC theory has a high potential to be used for ACC systems. Groot et al. [85] used the MPC theory to design an integrated predictive traffic and emission control. They observed that the MPC technique can be fused with a mixed-logic dynamical model description to efficiently control system performance. Lin et al. [86] applied the MPC technique to reduce the traffic delays and traffic emissions on urban roads. Their simulation demonstrated that the predictive nature of MPC significantly contributes to the efficiency of results. Kamal et al. [87, 88] used MPC in designing a predictive control scheme capable of using the upcoming information on traffic flow to adjust vehicle distance under a bounded driving torque condition. An exhaustive comparative study for different traffic conditions demonstrated the efficacy of the MPC-based ACC.

2.4 Summary

This chapter introduced optimal powertrain control strategies including trip planning, energy management strategy, and cruise controller. Also, it described what have been done for designing optimal powertrain control strategies in the literature. Its found that using advance knowledge of the entire driving cycles can improve powertrain controllers. Processing trip date increases the complexity of control systems, and presents significant challenges for real-time implementation.

Most research to date has been conducted with the goal of developing efficient control systems for traditional gasoline powered or conventional hybrid vehicles. Some recent studies have reported progress towards energy management of power-split PHEVs, which have more complicated dynamics and provide more flexibility to reduce total energy cost. There exist only rare reports in the literature addressing the applicability of ACCs for HEVs and PHEVs. A complicated architecture of a PHEV propulsion system can restore energy during regenerative braking. Therefore, the ecological cruise control problem in PHEV is more complicated than that for a conventional vehicle. This thesis develops a novel energy-optimal controller for PHEV that addresses these challenges.

Chapter 3

Real-time trip planning module development and evaluation

This chapter presents the Trip Planning module as a part of the devised energy-optimal controller. This module takes advantage of long-range trip data to optimize SOC profiles. Parts of this chapter are extracted from the author's published papers [89–91].

3.1 An overview of the real-time energy-optimal control scheme

Vehicular powertrain control strategies benefit immensely from real-time data provided by GPS, ITS, and other infrastructure sensors. These technologies provide critical short- and long-range traffic data, as well as important trip information such as the trip distance,

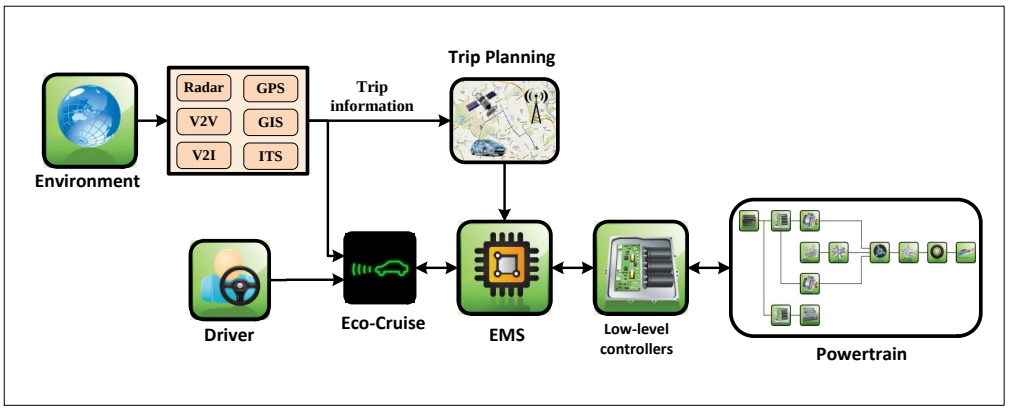

Figure 3.1: Schematic of the energy-optimal controller.

road grade, the positions of stopping points, bridge ramps, etc. Together, these inputs enable accurate prediction of future driving conditions, more efficient control of vehicle components and, subsequently, better system performance.

Figure 3.1 presents our proposed architecture for the energy-optimal controller of PHEVs, which takes advantage of the above-mentioned real-time inputs. It consists of three main subsystems: the Trip Planning module, Route-based EMS, and Eco-Cruise controller.

The Trip Planning contains an optimization algorithm designed to find the optimum SOC profiles based on trip information. The algorithm minimizes the total energy cost of the trip, including both fuel and electrical grid energy expenditures, while taking into consideration the constraints on the PHEV's powertrain components. Eco-Cruise controller calculates the optimum propulsion and braking torques, considering fuel economy and driving safety. Finally, the Route-based EMS uses the optimum SOC profiles to determine the power distribution between the engine and motor-generators, in real-time. Total energy cost, driving safety, and comfort must be taken into account to build a properly energy-

Table 3.1: Energy-optimal control system objectives

System	Safety	Energy cost	Comfort
Trip Planning module		✓	
Route-based EMS		✓	
Eco-Cruise controller	✓	✓	×

✓ : direct criteria, × : indirect criteria

optimal control system. Table 3.1 shows the criteria employed in each sub-controller.

There is broad variance in the rates at which trip conditions change. For example, travel paths and traffic data tend to change infrequently and relatively slowly, whereas vehicle speed, power demand, and the working points for both the engine and motor-generator change often and very quickly. This has concomitant impacts on the desired update rates for the Trip Planning and Route-based EMS. Even though these sub-systems are implemented in real-time, the Trip Planning can receive updates at a much slower rate than is required by the Route-based EMS. This chapter describes and presents simulation results outlining the development of the Trip Planning, while the Route-based EMS and Eco-Cruise controller are presented in the Chapters 4 and 5, respectively.

The Trip Planning optimizes SOC profiles by considering constraints on powertrain components. Fig. 3.2 shows a schematic of the controller. First, the route is divided into segments using a trip model. Then, the fuel consumption and ΔSOC of each segment are calculated based on the power distribution between the engine and the battery. Finally, the optimum SOC profiles are obtained using the fast RCO algorithm. Progress towards designing the Trip Planning is described below.

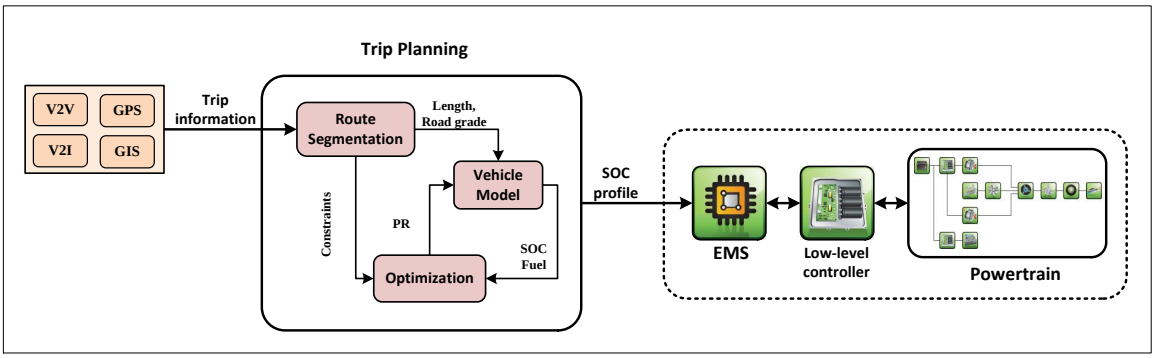

Figure 3.2: Schematic of the Trip Planning

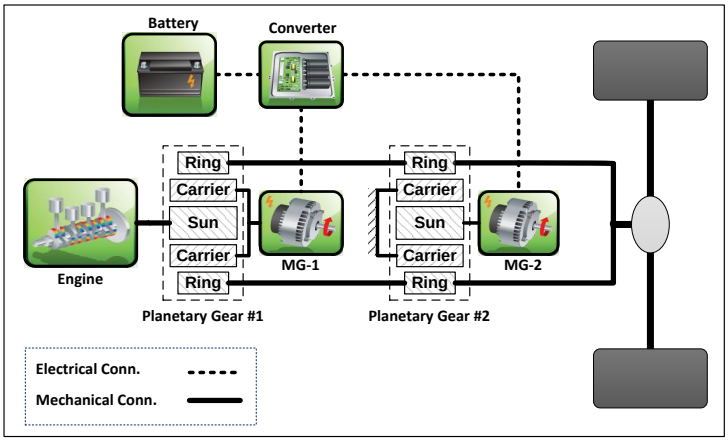

Figure 3.3: Schematic of the power-split PHEV

3.2 High-fidelity model

The baseline PHEV powertrain includes an engine and two electric machines, MG-1 and MG-2, both of which can operate as a generator and as a motor. These components are coupled to the wheels through a power-split transmission system consisting of two planetary gear sets, as shown in Fig. 3.3.

The ring gears of both planetary gears are coupled to the wheels. The sun gear and

planet carrier of the first planetary gear are coupled with MG-1 and the engine, whereas the sun gear and planet carrier of the second planetary gear are coupled to MG-2 and the chassis. In this configuration, the power-split transmission decouples the engine crankshaft from the road and allows the electric machines to adjust the engine's operation so that it functions at its maximum fuel efficiency point.

In a power-split system, the engine use can be minimized in low-efficiency operating conditions. For example, the engine is turned off when driving at low speeds and when the vehicle accelerates from a standstill. In these cases, electricity generated from the battery is the only power source used to operate the vehicle. While driving at normal speeds, the power-split system distributes the engine power in two ways. One power stream is used to drive the wheels, while the other is applied to MG-1, which operates as a generator. The electric power produced by the generator is converted to mechanical power in MG-2 and then transmitted to the final drive.

Control system design, tuning, testing, and validation activities typically incorporate several different types of model, which can be broadly divided into: high-fidelity, control-oriented, and online-optimization models. High-fidelity models are complex and describe the plant in detail, but are computationally expensive to run. Control-oriented or online-optimization models are sufficiently simple and fast for real-time implementation, and are accurate enough to characterize the system.

The high-fidelity model of the baseline PHEV powertrain is developed in the Autonomie software to evaluate the performance of the designed controller. Autonomie is a next generation of PSAT software, developed by Argon National Lab. The high-fidelity model

is employed for the evaluation of a controller's performance through MIL and HIL testing. It can also be utilized for both the parameter identification and model validation of control-oriented models.

A top level Simulink model of the PHEV is shown in Fig. 3.4, including the driver, vehicle powertrain architecture (VPA), and vehicle powertrain controller (VPC). The VPA, VPC, driver and environment blocks are interconnected via buses that contain information about the vehicle. The main info bus leaves the VPA and collects all the signals from the vehicle's powertrain systems (VPA). Then this main VPA info bus enters the VPC, driver and environment blocks. The environment blocks also send a bus, with all of the signals, into the VPC. The main VPA info bus and environment bus come together, along with input from the driver, before they enter the VPC, where they are used by the control strategy to adjust system behaviour. Afterwards, signals from all of the VPC subsystems enter the VPA [92].

3.2.1 Powertrain model

Figure 3.5 shows the powertrain configuration built in Autonomie. The main components of the powertrain are an internal combustion engine (Eng), two electric motors (more specifically, a traction motor (MG-2) and a generator (MG-1)), and a battery pack (B). Table 3.2 shows the characteristics of Toyota Prius Plug-in Hybrid.

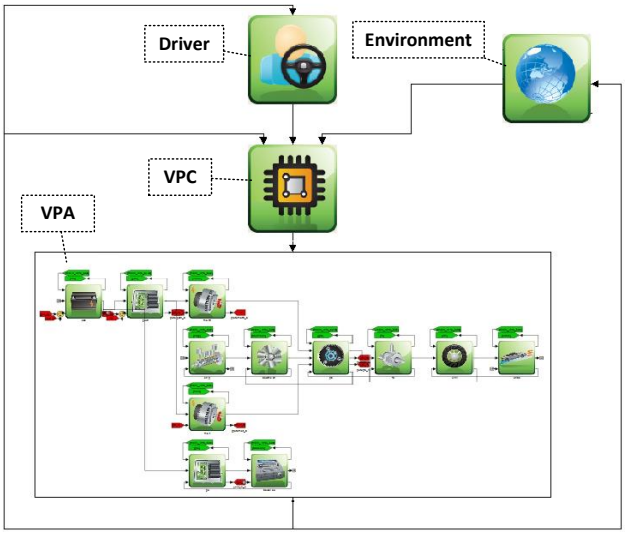

Figure 3.4: Interconnection of blocks in the Autonomie model of the PHEV

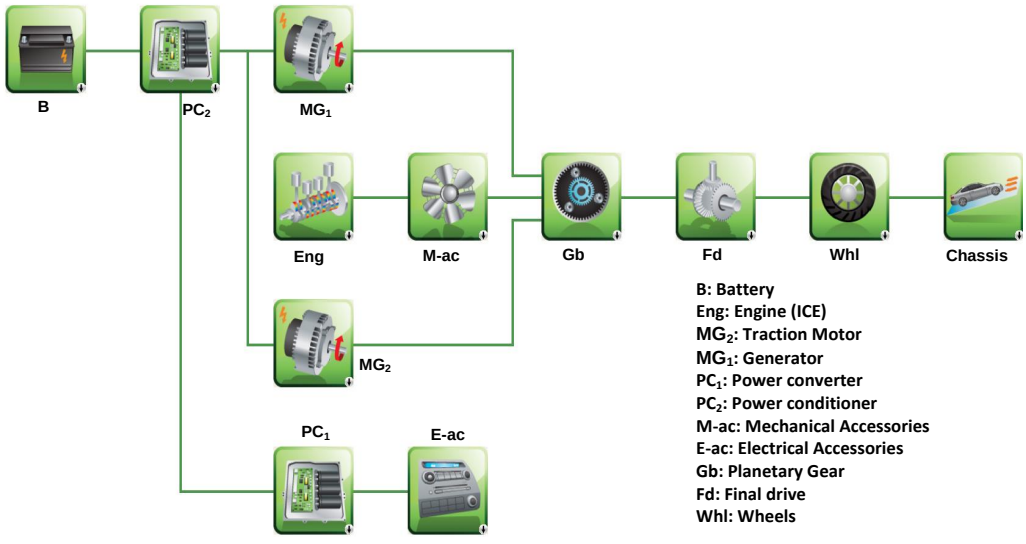

Figure 3.5: Power-split PHEV powertrain configuration

Table 3.2: The characteristics of Toyota Prius Plug-in Hybrid.

Parameter	Symbol	Unit	Value
Drag coefficient	C_D	-	0.26
Frontal area	A	m^2	2.25
Vehicle mass	m	kg	1525
Rolling resistance	f	-	0.008
Engine power	P_e	kW	73
Motor power	P_m	kW	50
Generator power	P_g	kW	30
Number of battery cells	N_b	-	56
Battery cell nominal voltage	V	V	3.7
Battery nominal capacity	Q	Ah	21
Wheel radius	r	m	0.3

Engine

The internal combustion engine was modeled using look-up tables based on the engine torque and speed. The ICE of Prius 2012 is a 1.8L spark ignition engine with a maximum power of 73 kW. Fig. 3.6 depicts the ICE efficiency maps for the Prius.

Electric motor-generators

The Prius is equipped with two permanent magnet electric motors. The efficiency of these electric motor-generators are represented by two look-up tables, as shown in Fig. 3.7.

Battery

The Lithium-ion battery pack is characterized using dual polarization circuit model. Battery variables such as open circuit voltage (V_{oc}), Internal resistance (R_b), and polarization

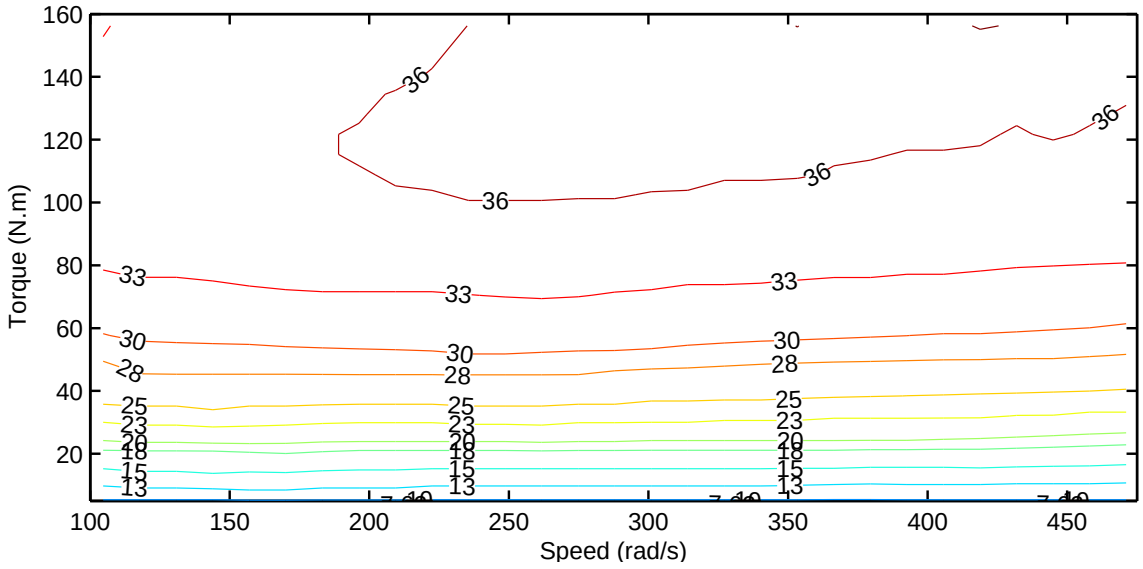

Figure 3.6: Engine efficiency map.

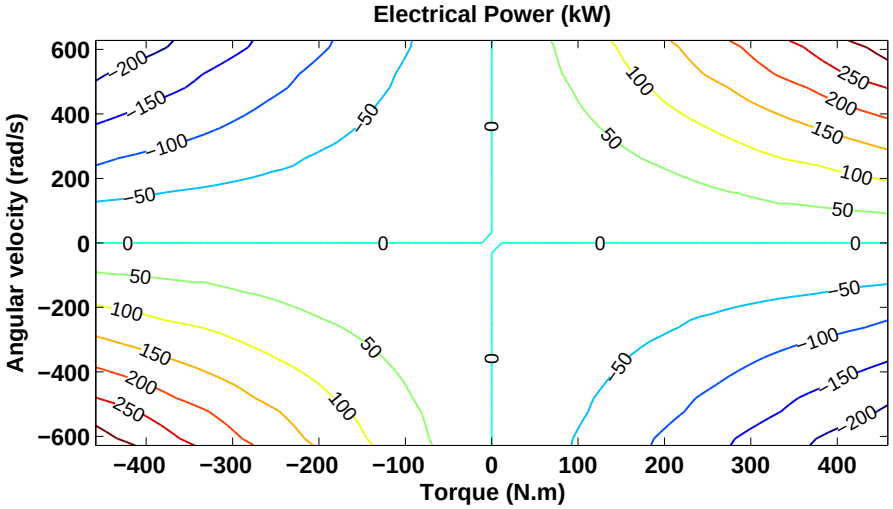

Figure 3.7: Motor-generator electrical power map.

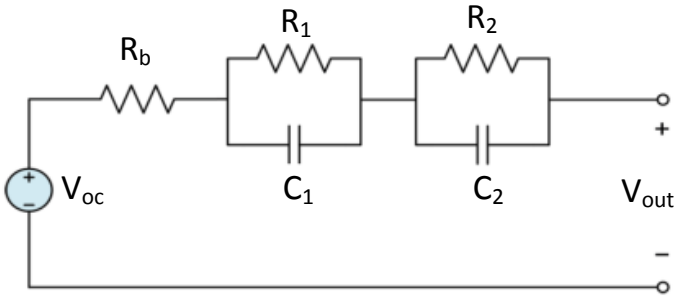

Figure 3.8: Schematic of dual polarization battery model.

variables ($R_1,\ R_2,\ C_1,\ C_2$) are obtained using look-up tables. The initial SOC and the minimum SOC are set to 0.9 and 0.2, respectively.

3.2.2 Driver model

The driver model block controls the speed of the vehicle. It contains of both feedforward and feedback controller. The feedforward controller is fast but not accurate. On the other hand, the feedback controller is more accurate but it needs feedback from the system that makes it relatively slow. The feedforward controller calculates desired torque based on the longitudinal dynamics (Eq. 3.1), and the feedback controller adjusts the desired torque using a PID controller.

$$T_{loss} = R \times (mg\sin\theta + \frac{1}{2}\rho A C_D v^2 + C_r mg\cos\theta + ma) \tag{3.1}$$

where R is the wheel radius, θ is the road grade, a is the vehicle acceleration, C_r and C_D are the rolling resistance and drag coefficients, respectively.

3.2.3 Powertrain controller

The Autonomie rule-based EMS strategy is similar to the CDCS strategy. The only difference is that the rule-based EMS operates the engine in CS mode when the power demand is high. Based on this strategy, the engine would be turned on when the requested power is above a threshold or the battery SOC is lower than a threshold, or the electric motor cannot provide the requested wheel torque. First, the engine power command P_{eng} is calculated to determine the engine ON/OFF status.

$$P_{eng} = P_d + P_{e,b} \tag{3.2}$$

where P_d is the requested power, $P_{e,b}$ is the additional power to maintain the SOC of the battery during the CS operation. P_d is calculated from the vehicle longitudinal dynamics. $P_{e,b}$ is obtained from the Eq. .

$$P_{e,b} = k_p(SOC_{ref} - SOC) + \frac{k_i}{s}(SOC_{ref} - SOC) + P_0 \tag{3.3}$$

where, k_p and k_i are the proportional and integral gains, respectively. P_0 is obtained from the look-up table.

The controller determine the engine On/Off status using the engine power and SOC; i.e., if P_{eng} is more than threshold for a certain SOC, the engine is turned on and vice versa.

In the Low-level controllers (shown in Fig. 3.9), the torques of each powertrain component are computed based on torque demand and the optimum engine power. The angular

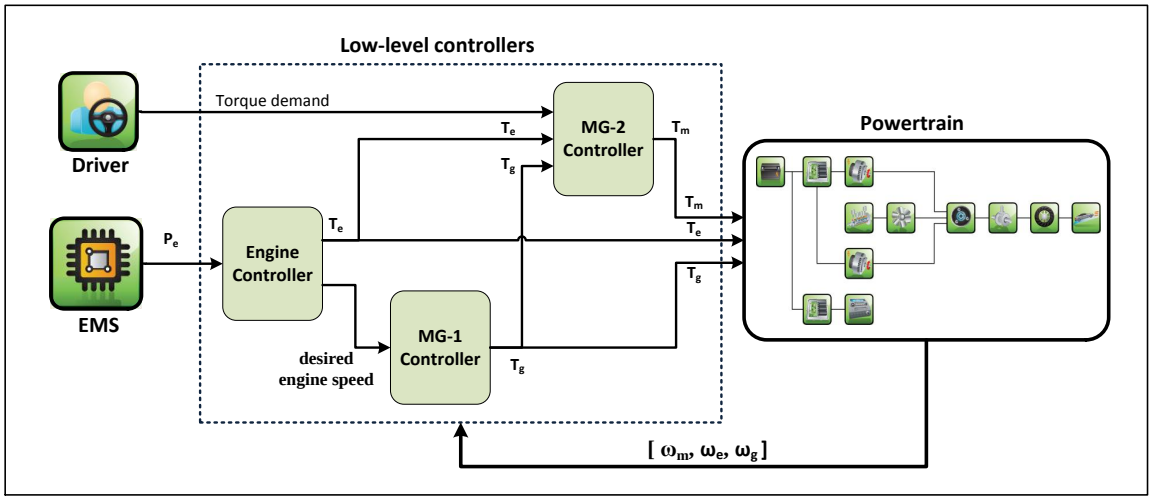

Figure 3.9: Schematic of the low-level controllers.

velocity and torque of the engine are obtained from look-up tables based on optimum working point of the engine. Then, Generator torque (T_g) is controlled to track the optimum angular velocity of the engine. A PID controller adjust the electric motor torque in a way that wheel torque follow the desired torque which is calculated from driver model.

3.3 Online-optimization model

The high-fidelity model is very detailed and thus too complex and computationally expensive for real-time applications. Therefore, the online-optimization model is developed for the Trip Planning module. The inputs of the online-optimization model are trip data and Power Ratio (PR) between two energy sources. This model predicts future speed trajectory and calculate total energy cost using a simple but sufficiently accurate powertrain model.

3.3.1 Powertrain model

In the online-optimization model, the powertrain components are represented based on their power instead of torque & angular velocity or voltage & current. Therefore, this model is simpler than the high-fidelity model. First, the vehicle's power demand is determined from Eq. 3.4.

$$\begin{aligned} P_d &= (m\dot{v} + F_d)\,.v \\ F_d &= \tfrac{1}{2}\rho A C_d v^2 + mgf\cos\theta + mg\sin\theta \end{aligned} \tag{3.4}$$

where P_d is the power demand, F_d is the resistance force, v is the vehicle speed, ρ is the air density, C_d is the drag coefficient, f is the rolling resistance coefficient, m is the vehicle mass, θ is the road grade, A is the frontal area of the vehicle, and g is the gravity acceleration.

Based on Eq. 3.4, the vehicle longitudinal dynamics is derived:

$$\begin{aligned} m\dot{v} &= \frac{P_d}{v} - C_1 v^2 - C_2 \\ C_1 &= \frac{1}{2}\rho A C_d \\ C_2 &= mgf\cos\theta + mg\sin\theta \end{aligned} \tag{3.5}$$

The power distribution between the battery and engine is determined based on the power

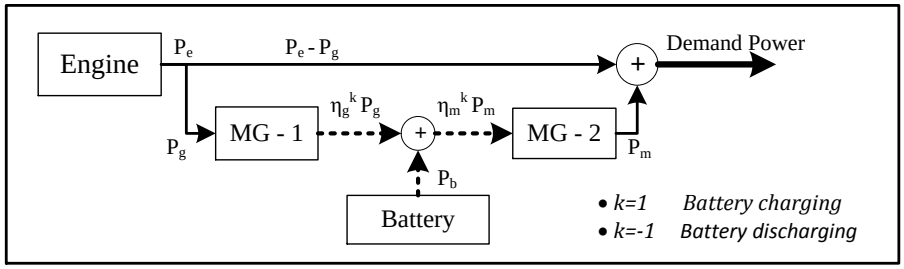

Figure 3.10: Schematic of the power flow in PHEV powertrain

flow of the power-split architecture (please see Fig. 3.10).

$$PR = \frac{\tilde{P}_b}{P_d} \tag{3.6}$$

$$\tilde{P}_b = \eta_m^k P_b = PR.P_d \tag{3.7}$$

$$\eta_t \; P_e = (1 - PR)P_d \tag{3.8}$$

where η_t is power-split transmission efficiency, η_m is the motor-generator efficiency, P_b is the battery electrical power, and $\tilde{P}_b, P_e$ are the mechanical power, delivered by the battery and engine, respectively. In Eq. 3.7, $k = -1$ during battery charging and $k = 1$ during battery discharging.

In the next steps, a battery model and an engine fuel map are built to enable accurate prediction of fuel consumption and SOC, respectively.

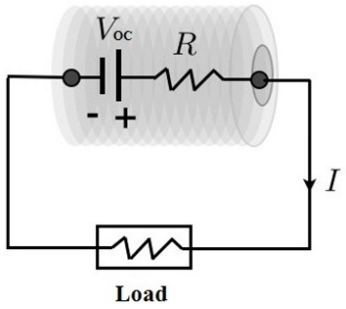

Figure 3.11: Schematic of the battery model.

Battery model

Considering the simple model of the battery pack as shown in Fig. 3.11, the energy balance of the circuit is obtained from Eq. 3.9.

$$-V_{oc}I + R_bI^2 + P_b = 0 \tag{3.9}$$

where V_{oc} is the battery open circuit voltage, R_b is the battery resistance, and I is the load current.

The battery SOC must be defined to evaluate the energy content of the battery. This parameter indicates the percentage of the total available battery capacity. By substituting the load current from Eq. 3.9, SOC is derived [93]:

$$\dot{SOC}(P_b) = \frac{-I}{Q_{max}} = \frac{-V_{oc} + \sqrt{V_{oc}^2 - 4P_bR_b}}{2R_bQ_{max}} \tag{3.10}$$

where Q_{max} is the maximum battery capacity.

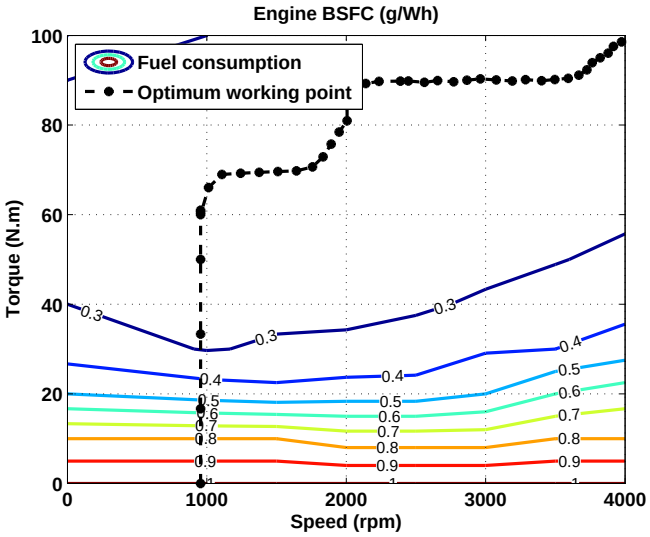

Figure 3.12: Engine fuel map of a baseline PHEV [41]

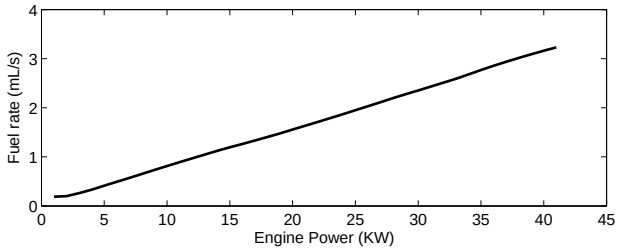

Figure 3.13: Optimum fuel map of the engine.

Engine fuel maps

Figure 3.12 depicts the fuel consumption map of the baseline PHEV engine [44] as a function of the angular velocity (ω_e) and torque of the engine (T_e).

After obtaining the optimum working curve of the engine, the fuel consumption map is derived in terms of the engine power as shown in Fig. 3.13.

3.3.2 Math-based trip model

It is assumed that prior knowledge of route and traffic data is available through on-board and infrastructure-based sensors, such as GPS, ITS, and road maps. This information is crucial to predicting future driving conditions, enabling efficient, real-time control of the vehicle's powertrain, and, subsequently, minimizing total energy consumption.

For a given trip, the route is divided in such a way that key variables, such as the traffic speed profile, maximum permissible speed, and road grade, are constant in each segment. Furthermore, obstacles, such as bridge ramps, traffic lights, or stop signs, are positioned at the margin of the segments. In general, each segment consists of three sections: acceleration, deceleration, and cruise sections. However, based on the conditions of each segment, the acceleration or deceleration section may be excluded.

Figure 3.14 shows an example route divided into 4 segments. In this route, maximum speed limits are shown with a dashed line, and a stop point and bridge ramp are located at the end of the first and second segments, respectively. The third and fourth segments have different traffic speeds. Based on these data, the speed trajectory is obtained, which is shown by the solid line. The third segment does not contain a deceleration section.

Each segment starts with an initial speed, v_a, which, after the acceleration section, reaches the cruise speed v_c. The final speed reduces to v_e at the end of the deceleration section. The speed at the margin of the segments, v_a and v_e, are determined based on trip information. For instance, if there is a stop sign at the beginning or the end of a segment, v_a or v_e will be equal to zero. Speeds used to turn at a junction or pass a bridge ramp can be calculated based on the maximum permissible speed or the recommended safe speed,

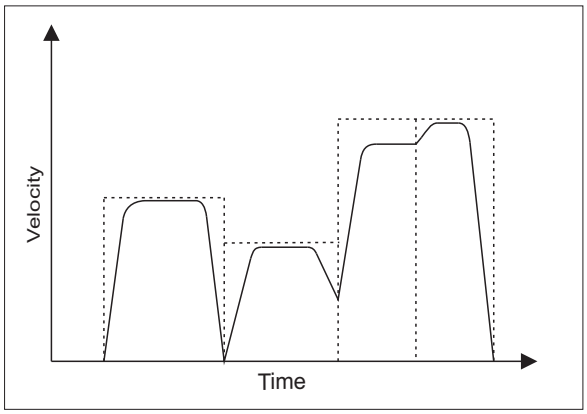

Figure 3.14: Speed trajectories corresponding to different route segments

determined according to the road curvature. The cruise speed is the average traffic speed of the segment or maximum permissible speed.

Based on the proposed speed trajectory, a math-based trip model is developed to calculate total energy consumption. It is assumed that the driver operates the vehicle with constant power during acceleration and deceleration sections (P_{acc}, P_{dec}). Herein, the indices *acc*, *dec*, and *c* denote acceleration, deceleration and cruise modes, respectively.

Acceleration section:

In power-split PHEV architectures, the engine operates inefficiently at low speeds and is therefore turned off. As a result, a threshold speed $v^{\star}$ is defined to determine the starting point for engine operation. Based on $v^{\star}$, the acceleration section can be divided into two parts: *Engine turned Off*, and *Engine turned On*.

i) Engine turned Off ($v < v^{\star}$): In this period, it is assumed that MG-2 propels the vehicle and the battery is the only energy source for the system. The travel time is

obtained by solving longitudinal dynamics from Eq. 3.5:

$$\triangle t_1 = \int_{v_a}^{v^\star} \frac{mv}{P_{acc} - C_1 v^3 - C_2 v} dv \tag{3.11}$$

$$P_{b_1} = \eta_m^{-1}\ P_{acc} \tag{3.12}$$

ii) Engine turned On ($v \geq v^\star$): At high speeds, it is assumed that both the engine and battery contribute energy to the system.

$$\triangle t_2 = \int_{v^\star}^{v_c} \frac{mv}{P_{acc} - C_1 v^3 - C_2 v} dv \tag{3.13}$$

$$P_{b_2} = \eta_m^{-1}\ PR\ P_{acc} \tag{3.14}$$

$$P_{e_2} = \eta_t^{-1}\ (1 - PR)\ P_{acc} \tag{3.15}$$

The fuel consumption m_f, $\triangle SOC$, travel time $\triangle t_{acc}$ and the travel distance $\triangle x_{acc}$ during acceleration section are determined from:

$$m_{f_{acc}} = \dot{m}_f(P_{e_2}).\triangle t_2 \tag{3.16}$$

$$\triangle SOC_{acc} = \dot{SOC}(P_{b_1}).\triangle t_1 + \dot{SOC}(P_{b_2}).\triangle t_2 \tag{3.17}$$

$$\triangle t_{acc} = \triangle t_1 + \triangle t_2 \tag{3.18}$$

$$\triangle x_{acc} = \int_{v_a}^{v_c} \frac{mv^2}{P_{acc} - C_1 v^3 - C_2 v} dv \tag{3.19}$$

Deceleration section:

It is assumed that MG-2 operates as a generator while in regenerative braking mode. The travel time, travel distance, and ΔSOC during the deceleration section can be calculated from:

$$P_{b_dec} = -\eta_m \; PR \; P_{dec} \tag{3.20}$$

$$\triangle SOC_{dec} = \dot{SOC}(P_{b_d}).\triangle t_{dec} \tag{3.21}$$

$$\triangle t_{dec} = \int_{v_c}^{v_e} \frac{mv}{-P_{dec} - C_1 v^3 - C_2 v} dv \tag{3.22}$$

$$\triangle x_{dec} = \int_{v_c}^{v_e} \frac{mv^2}{-P_{dec} - C_1 v^3 - C_2 v} dv \tag{3.23}$$

Cruise section:

In the cruise section, which is the dominant travel mode, the speed is assumed to be constant (v_c). Based on the travel distances of the acceleration and deceleration sections,

the travel time of the cruise section can be calculated by:

$$\triangle t_c = \frac{L_{seg} - (\triangle x_{acc} + \triangle x_{dec})}{v_c} \tag{3.24}$$

$$P_d = C_1 v_c^3 + C_2 v_C \tag{3.25}$$

$$P_{b_c} = \eta_m^{-1}\ PR\ P_d \tag{3.26}$$

$$P_{e_c} = \eta_t{-}1\ (1 - PR)\ P_d \tag{3.27}$$

$$\triangle SOC_c = \dot{SOC}(P_{b_c}).\triangle t_c \tag{3.28}$$

$$m_{f_c} = \dot{m}_f(P_{e_c}).\triangle t_c \tag{3.29}$$

where L_{seg} is the length of the segment.

3.3.3 Parameter estimation

The high-fidelity PHEV model can be utilized to support parameter estimation and validation of the online-optimization model. To estimate unknown parameters, first the parametric model is rewritten in the general form:

$$Z = \theta\ \Phi \tag{3.30}$$

where θ is an unknown parameter, and Z and Φ are measurable variables.

Then, variables Z and Φ are measured by running the high-fidelity model simulation. Finally, the unknown parameter is estimated by minimizing the root mean square error

(RMSE):

$$RMSE = \sqrt{\sum_{i=0}^{N} (Z(i) - \hat{\theta}\ \Phi(i))^2} \tag{3.31}$$

where N is the length of sampling variable vector, and $\hat{\theta}$ is the estimated parameter.

Given its importance to EMS, the battery resistance should be estimated. The ohmic resistance of the battery can be directly measured; however, in order to accurately model the battery, we should consider other phenomena that may affect battery performance, such as activation polarization and concentration polarization. On the other hand, considering the polarization increases the complexity of the system. Therefore, the effective resistance of the battery is estimated based on the results of the high-fidelity model. The parametric model of the battery resistance is derived from Eq. 3.10:

$$(Q_{max}\ S\dot{O}C\ V_{oc} + P_b) = -R_b\ S\dot{O}C^2\ Q_{max}^2 \tag{3.32}$$

The engine efficiency must also be considered. The optimum fuel curve of the engine, Fig. 3.13, is built based on the fuel map. During cruise-controlled driving, the controller adjusts the working point of the engine to its optimum point for maximum fuel efficiency. However, realistically, there are transient times during which the engine does not work efficiently. Engine efficiency (η_e) is defined by evaluating the actual fuel consumption, m_f , based on the optimum fuel curve, $m_f^*(P_b)$.

$$m_f = \eta_e^{-1}\ m_f^*(P_b) \tag{3.33}$$

Table 3.3: Results of parameter estimation for the baseline PHEV.

Parameter	Estimation
Powertrain efficiency	0.89
Engine efficiency	0.88
Battery resistance	0.93
Motor efficiency	0.90
Generator efficiency	0.87

The parametric models of powertrain efficiency (η_t) and motor-generator efficiency (η_m) are written in Eq. 3.34-3.36:

$$(P_d - \tilde{P}_b) = \eta_t \; P_e \tag{3.34}$$

$$\tilde{P}_b = \eta_m^{-1} \; P_b \qquad Charging \tag{3.35}$$

$$\tilde{P}_b = \eta_m \; \tilde{P}_b \qquad Disharging \tag{3.36}$$

Unknown parameters are estimated based on the simulation results for Urban Dynamometer Driving Schedule (UDDS) and Highway Fuel Economy Driving Schedule (HWFET). The parameter estimation results are shown in Table 3.3.

3.3.4 Model evaluation

Simulation results from our high-fidelity PHEV model are used to evaluate our online-optimization model, taking into account both urban (UDDS) and highway (HWFET) drive cycles. First, the trip model is employed to predict future speed trajectories for these two drive cycles based on assumed trip information, stop points and average traffic speed.

Predicted speed trajectories are shown in Fig. 3.15.

Figures 3.16, and 3.17 show a comparison between the simulation results generated from our high-fidelity and online-optimization models using four speed trajectories (UDDS, predicted UDDS, HWFET, and predicted HWFET). In order to maintain similar conditions for both models, the simulations are implemented in two different operating modes: CD and CS. In CD mode, only the MG-2 propels the vehicle, while in CS mode only the engine supplies power to the system and the battery's SOC remains constant. The maximum error between results of the high-fidelity model and online-optimization model are 1.5% and 2% for calculating the SOC and engine fuel consumption, respectively.

3.4 Optimization

Optimization problems that address future driving patterns, where a large number of parameters and constraints must be considered, are particularly challenging to solve in real-time, which is exacerbated over long trips. To reduce the complexity of these problems, this thesis proposes a new real-time approach, an RCO algorithm, to optimize PHEV SOC profiles.

It should be noted that the main objective function of the devised energy-optimal controller is total energy cost. To compare the performance of energy optimal controller against other strategies, we consider a SOC constraint at terminal time. This constraint causes equal electrical energy cost for all strategies. Therefore, the optimization index can change from the total energy cost to the fuel consumption.

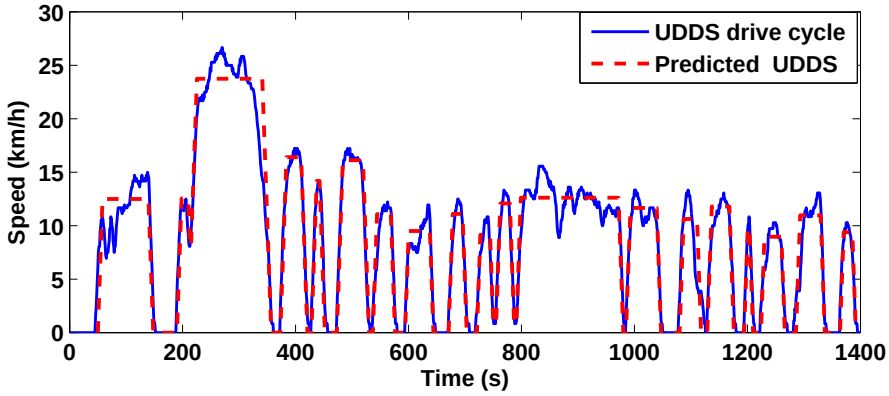

(a) UDDS drive cycle

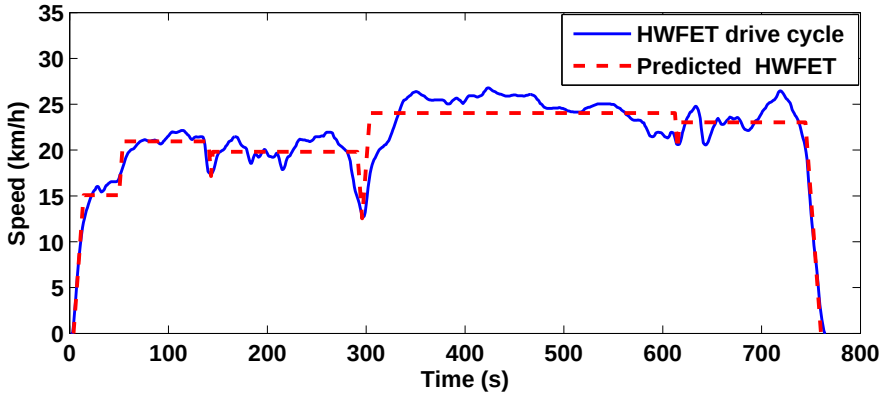

(b) HWFET drive cycle

Figure 3.15: Speed prediction based on future driving condition for UDDS and HWFET drive cycles.

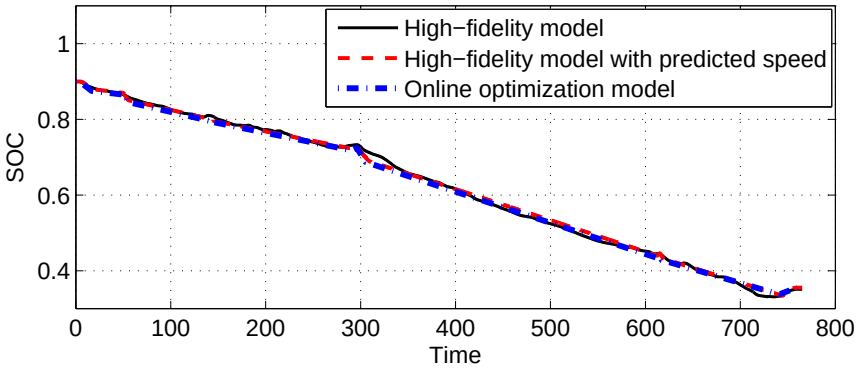

(a) HWFET drive cycle.

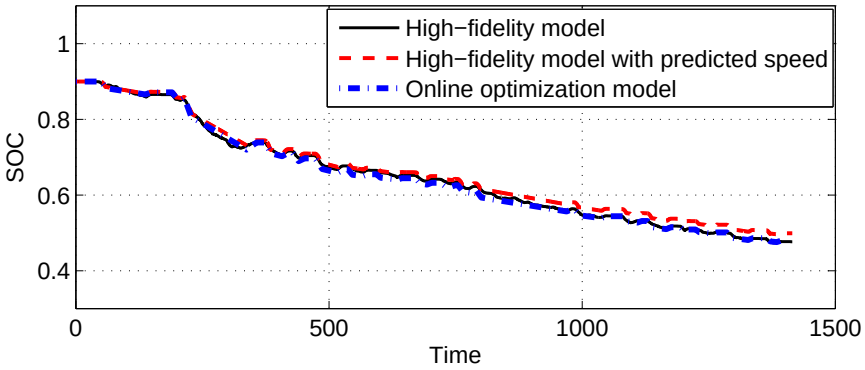

(b) UDDS drive cycle.

Figure 3.16: Comparison between high-fidelity and online-optimization modelling results for PHEVs running in CD mode in highway and urban drive cycles.

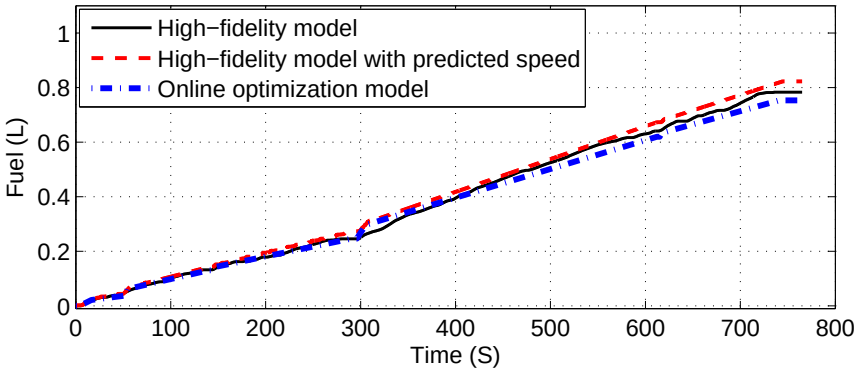

(a) CS mode in HWFET drive cycle.

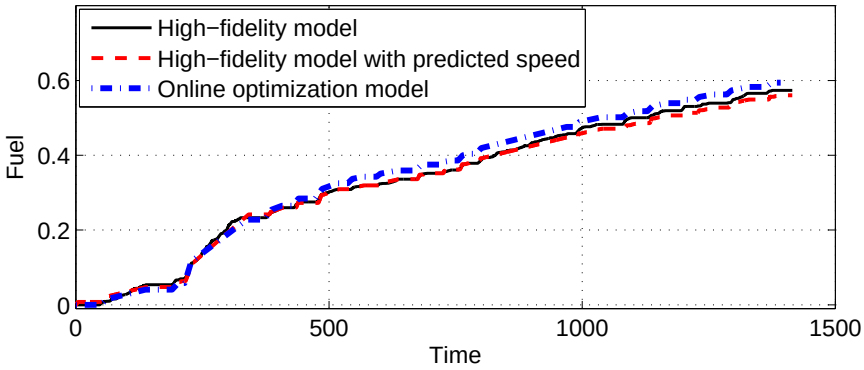

(b) CS mode in UDDS drive cycle.

Figure 3.17: Comparison between high-fidelity and online-optimization modelling results for PHEVs running in CS mode in highway and urban drive cycles.

3.4.1 Dynamic programming

Dynamic programming (DP), a numerical method based on the principle of optimality, was developed by Richard Bellman in the 1950s. Similar to other optimization methods, this global optimization approach aims to minimize the cost function while satisfying performance component constraints. The DP method is widely applicable to complex optimization problems because it applies a decomposition process to break down n-variable problems into n simplified one-variable sub-problems, each of which is solved only once and saved in a table. The solutions for each sub-problem are then combined together to provide an overall solution. This results in a large reduction in computational time and effort [94].

The DP algorithm is applied to find the optimum SOC profile that minimizes total energy cost. In this problem, the SOC is the output of the system, PR is the optimization parameter, and fuel consumption is the objective function. Due to the complexity of the high-fidelity model built in Autonomie, it cannot be applied to DP optimization; therefore, our online-optimization model is employed. The optimal dynamic optimization problem can be formulated in the discrete format as follows:

$$J = \sum_{k=1}^{N} m_f \left(PR(k)\right) .\Delta t_k \tag{3.37}$$

$$SOC(k+1) = SOC(k) + \frac{-V_{oc} + \sqrt{V_{oc}^2 - 4PR(k)P_d(k)\eta^k R_b}}{2R_b Q_{max}} \tag{3.38}$$

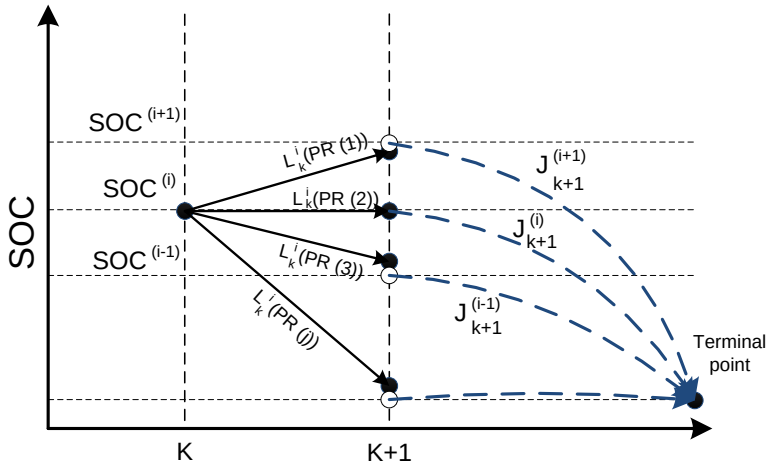

Figure 3.18: Schematic of DP algorithm

In this problem, the following constraint should be satisfied:

$$SOC(t_0) = SOC_0 \tag{3.39}$$

$$SOC(t_f) = SOC_f$$

$$SOC_{min} \leq SOC \leq SOC_{max}$$

$$P_{b_{min}} \leq P_b \leq P_{b_{max}}$$

$$P_{e_{min}} \leq P_e \leq P_{e_{max}}$$

$$0 \leq PR \leq 1$$

In the DP algorithm, the sub-problems of optimization should be solved backward from the terminal condition, as shown in Fig. 3.18. For step k, the sub-problem is to minimize J_k^i with $SOC^{(i)}$ as the initial point of each sub-problem:

$$J_k^i = Min\left[L_k^i(PR(j)) \; + \; J_{k+1}^*\right] \tag{3.40}$$

The cost function is calculated only for the grid points of the SOC. The SOC at next time step (k+1) (filled circle), is determined through discrete state space Eq. 3.38. If this value does not match to the quantized value (empty circle), then the value of J_{k+1}^* is updated using linear interpolation.

3.4.2 Real-time cluster-based optimization

In the PHEV Trip Planning optimization problem, predicted power demand is the input and the power ratio is the optimization parameter. The energy consumption is calculated based on these two variables. It can be assumed that two trip segments with the same power demand also have the same optimum power ratio. This thesis proposes the RCO algorithm that clusters trip segments into groups that share similar power demands, and similar optimum power ratios. Therefore, instead of finding the optimum power ratio of each trip segment, the power ratio is only calculated for each group. In this way, the number of optimization parameters is dramatically reduced.

In general, clustering is the process of grouping objects/data based on their similarities. This process produces a model of data, which is grouped into meaningful sets. Clustering algorithms can be categorized in many different ways. Some of the most important algorithms are hierarchical based, centroid-based and distribution-based algorithms. Based on the application and desired objectives, a robust clustering algorithm can be employed to reduce complexity in optimization problems.

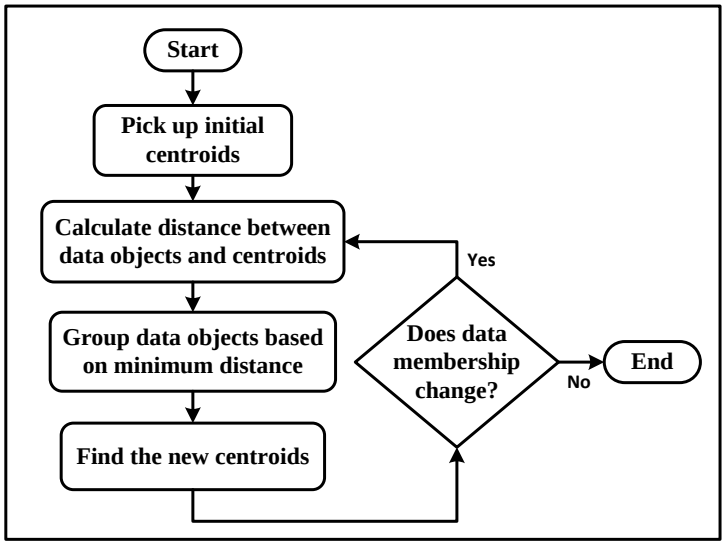

Figure 3.19: Schematic of k-means clustering algorithm

A centroid-based or k-means algorithm is used to cluster the segments in this PhD research. This algorithm works based on some centroid points, which may not be members of any cluster. The data is divided into different groups based on their distances from the centroid points [95].

According to Fig. 3.19, at the first step, k cluster centers (same as the number of clusters) are determined. After defining the k centroids, data points are assigned to clusters based on their distance from the centroids. When all data have been assigned, the k centroids should be recalculated. The algorithm continues by reassigning each point to the nearest centroid. These steps are repeated until recalculation of the centroids yields no change in cluster assignment for the data.

3.5 MIL testing

The Trip Planning is applied to two different test scenarios. In the first, the algorithm is evaluated in different standard driving cycles; while trip data such as the average speed of each segment, segment length, road grade, and maximum speed are known beforehand. In the second test scenario, the benefit of online optimization is investigated by running the simulation when trip data changes.

3.5.1 Following standard driving cycles

This thesis applies the RCO algorithm to the PHEV Trip Planning problem, taking into consideration two drive cycles. The first drive cycle (EPA-UHU cycle) begins and ends with a UDDS cycle, and has a HWFET drive cycle in the middle. The second drive cycle (3xUDDS cycle) combines three UDDS drive cycles. The travel distance of both cycles exceeds the full electric range of the vehicle. Therefore, at the terminal point, the SOC reaches its minimum value and the engine takes over propelling the vehicle.

To implement the RCO algorithm, first the optimal power demands are calculated based on predicted speed. Then, the centroids of groups are obtained and the power demand data cluster into groups. Fig. 3.20 shows the power distribution and clustering results for the EPA-UHU and 3xUDDS drive cycles. The dark bars show the power distribution of the drive cycle during propulsion (positive power demands). Each bar represents the total travel time for the corresponding power demand. The light bars depict each cluster and the center lines show the centroids.

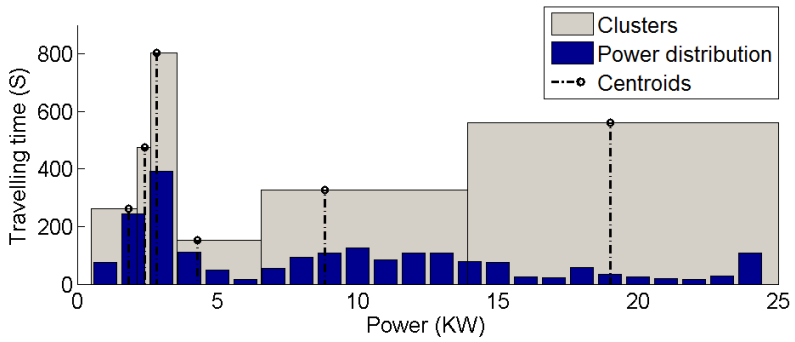

(a) 3xUDDS drive cycle

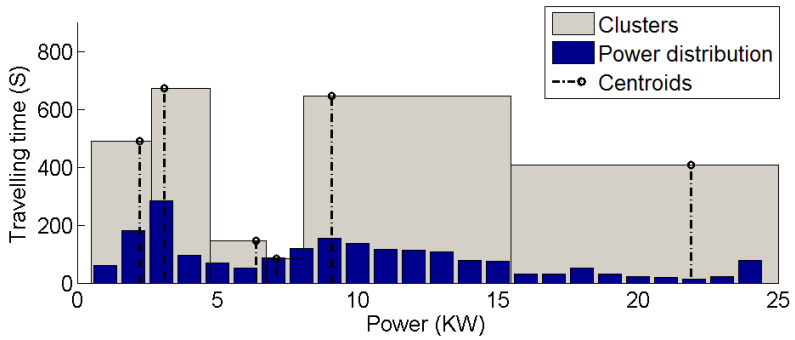

(b) EPA-UHU drive cycle

Figure 3.20: Power distribution and power clustering results for: a)3xUDDS and b)EPA-UHU drive cycles

Table 3.4: Results of RCO algorithm for the EPA-UHU drive cycle.

Group Number	Power (KW)	Power Ratio	Cruise speed range
1	2.2	1	less than 40 km/h
2	3.1	1	40 - 60 km/h
3	6.4	0.3	60 - 70 km/h
4	7.1	1	70 - 80 km/h
5	9.1	0.1	80 - 110 km/h
6	21.9	0.8	During acceleration

The power ratio of each power-group is obtained to minimize total fuel consumption. The optimization results for the EPA-UHU drive cycle is shown in Table 3.4. In the low speed and low power demand groups (groups 1 and 2), the engine did not work efficiently, therefore the vehicle switched to full electric mode. In average cruise speed (groups 3 and 5), the energy management strategy switched to Blended strategy. During acceleration with high power demand, both the engine and electric motor propel the vehicle, while the electric power is dominant ($P_b = 0.8\ P_d$).

Figure 3.21 shows the optimum SOC profile based on RCO and DP approaches for the 3xUDDS and EPA-UHU drive cycles. The RCO results match the global optimum solution generated by the DP algorithm; The maximum error between the optimum SOC profile obtained by RCO and DP approaches are 1.1% and 2.4% for 3xUDDS and EPA-UHU, respectively. However, the RCO algorithm is much less computationally expensive. All simulations are run on a PC with Intel Core 2 Duo CPU (E8500, 3.17GHz) and 4GB RAM. The average computation time of RCO and DP algorithms are 5 s, 35 min for 3xUDDS drive cycle, and 5 s, 28 min for EPA-UHU drive cycle, respectively.

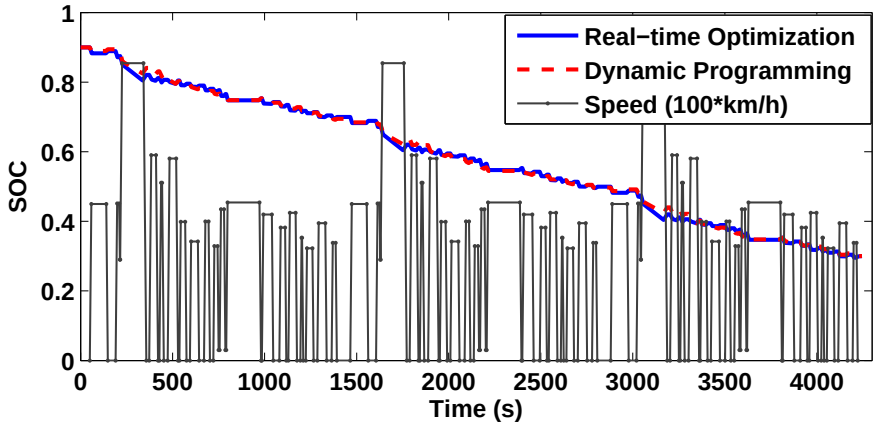

(a) 3xUDDS drive cycle

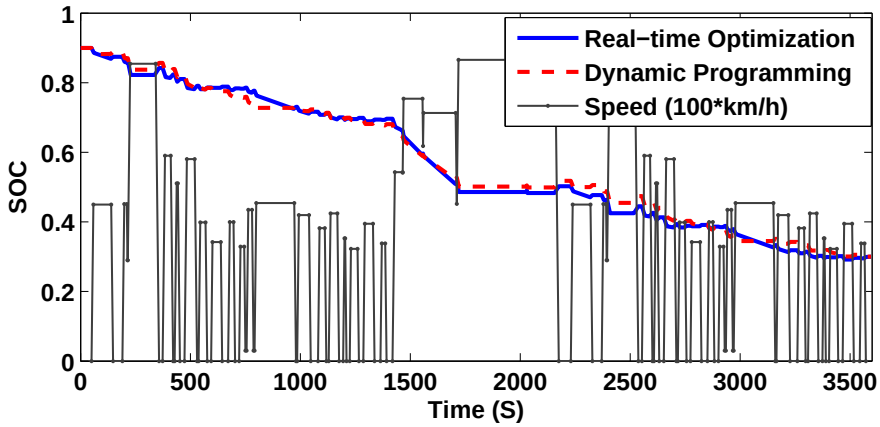

(b) EPA-UHU drive cycle

Figure 3.21: Optimum SOC profiles produced using RCO and DP algorithms for: a)3xUDDS drive cycle and b) EPA-UHU drive cycle

Table 3.5: Characteristics of each case study for online Trip Planning.

Case	Drive cycle	Change in the trip plan
1	3xHWFET	No
2	EPA-HF	No
3	EPA-HF	Yes

3.5.2 Benefit of online optimization

Practically, various sources such as changes in the trip-plan and unpredicted traffic conditions can change trip data. This section investigates the effect of change in trip data on the performance and optimality of the online Trip Planning module through simulations of three different cases. In the first case, the 3xHWFET drive cycle is used; in the second and third cases, the EPA-HF drive cycle. In the last case, trip data change in the following manner: at first, the driver sets a trip-plan in which the predicted speed is that for the 3xHWFET drive cycle. Then, after passing the first highway, the driver changes the trip-plan to that of the FTP-75 drive cycle for the rest of the trip. Fig. 3.22 illustrates the speed trajectories for the three different cases.

Figures 3.23-3.25 show simulation results for the different EMS controller under various conditions. The performance of the controllers can be evaluated from Table 3.6. It is concluded that the Route-based EMS significantly improves fuel economy compared to the rule-based and A-ECMS controllers. However, change in trip data affects the Route-based EMS performance by 1.7% (118 MPG in case-2 and 116 MPG in case-3) .

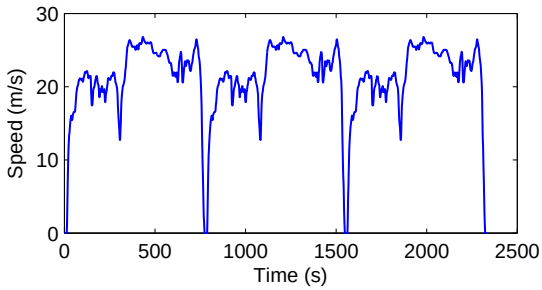

(a) 3xHWFET drive cycle.

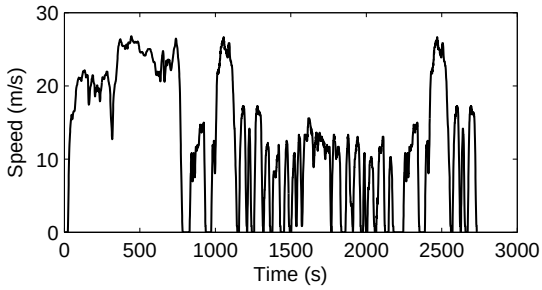

(b) EPA-HU drive cycle.

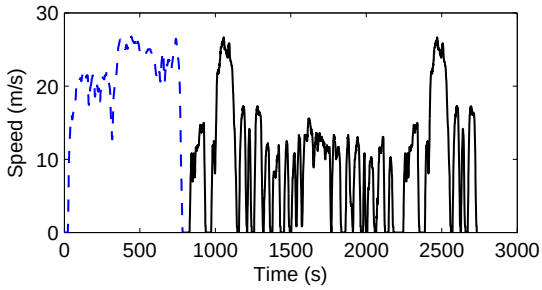

(c) EPA-HU drive cycle with change in trip plane.

Figure 3.22: Speed trajectories applied in different case studies for online Trip Planning.

Table 3.6: Online Trip Planning results for different case studies.

EMS	Trip Planning	Fuel consumption (MPG)		
		Case-1	Case-2	Case-3
Rule-based	No	97	102	102
A-ECMS	No	93	113	114
Route-based EMS	Yes	94	118	116

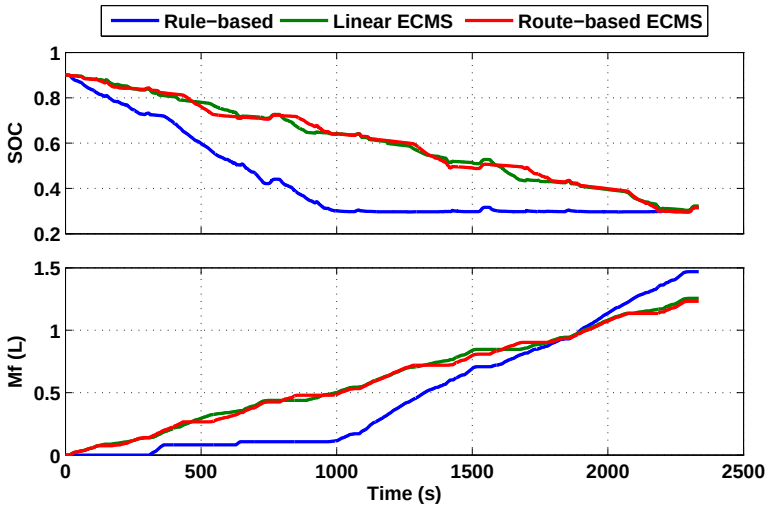

Figure 3.23: Simulation results for following 3xHWFET drive cycle without changing in the trip plan.

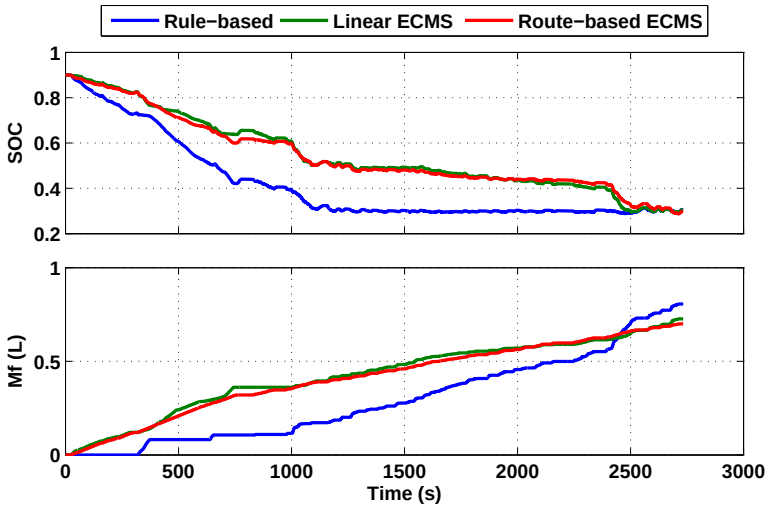

Figure 3.24: Simulation results for following EPA-HU drive cycle without changing in the trip plan.

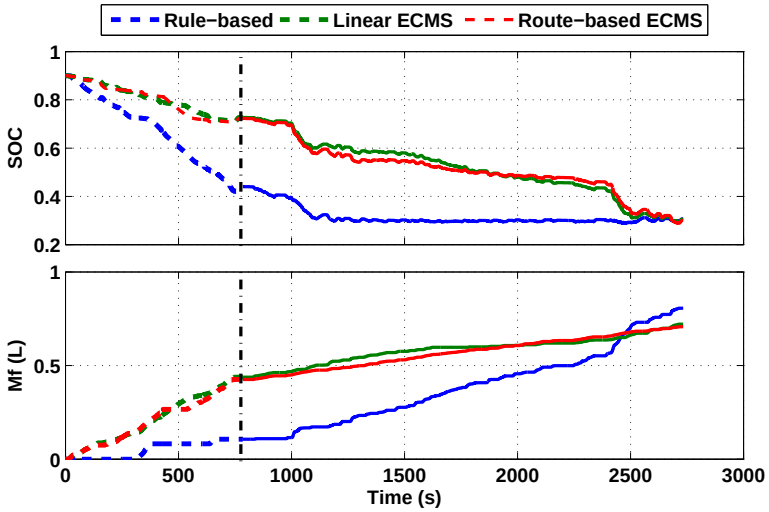

Figure 3.25: Simulation results for following EPA-HU drive cycle when trip plan is changed after passing the first HWFET cycle.

3.6 HIL testing

Electronic Control Units (ECUs) have been widely used in many automotive applications such as engine controller, transmission controller, cruise controller, driver assistance system, and entertainment systems. ECU development process has become a critical phase toward launching a new vehicle and 90% of automotive novelties are related to electronic systems, especially advanced ECUs [96]. Testing and validating ECUs have become crucial tasks in the automotive development process. The most effective way to validate an ECU is to connect it to a real plant. However, in many cases, hardware-in-the-loop (HIL) tests are more efficient. In fact, HIL testing systems provide a virtual vehicle model for ECU validation. The main advantages of validating ECU by HIL testing are as follows:

- The controller development can be done and verified prior to manufacturing of the

prototype vehicle. Therefore, HIL systems enable simultaneous development of ECU and vehicle, which can significantly reduce the vehicle development process time;

- Validation time and cost can be reduced by replacing expensive field experiments by laboratory experiments. HIL test often requires significantly less hardware than physical prototyping. This makes the procedure faster and cheaper;

- HIL testing has lower risk, especially in the extreme or hazardous ambient conditions such as typical winter test drives, cold-start tests, or validating adaptive cruise ECU in severe situation with the risk of collision;

- HIL systems can support more comprehensive tests in a shorter time. HIL testing can significantly increase repeatability and provide simulation over much broader range of operating conditions than what is feasible via purely physical prototyping;

- HIL systems also provide the initial calibration of ECUs which is a starting-point for the later development phases; and

- Damage to the vehicle can be avoided in a test scenario where failures or errors can occur. HIL simulation makes it possible to simulate destructive events without incurring a costly destruction.

This PhD research uses dSPACE systems for HIL testing. dSPACE GmbH (Digital Signal Processing And Control Engineering) is one of the top providers of instruments for developing ECUs especially for automotive applications. dSPACE systems are used at many vehicle manufacturer such as Toyota, Audi, BMW, Ford, General Motors, Honda,

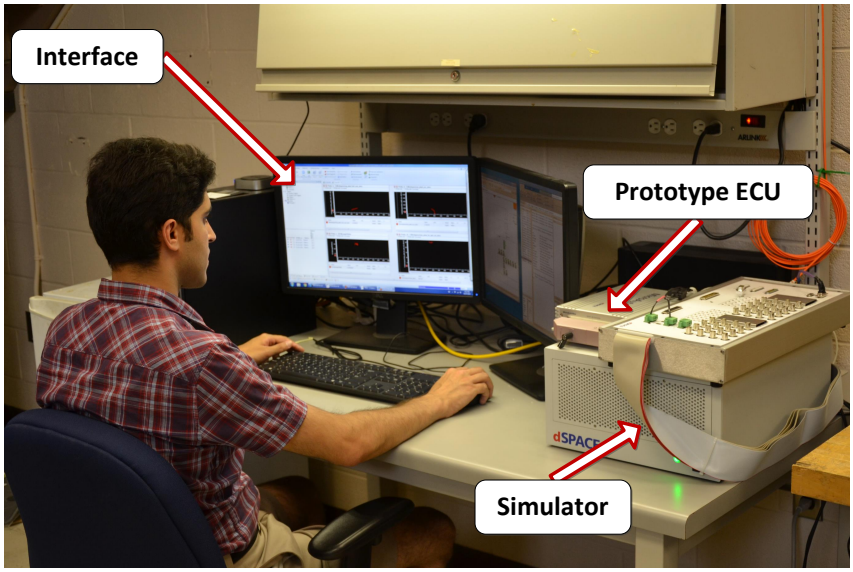

Figure 3.26: Schematic of HIL test platform.

Nissan, and some automotive suppliers [97]. dSPACE supports different phases of ECUs development process, in particular, Rapid Control Prototyping (RCP) and ECU testing and calibration.

In general, HIL testing requires a high-performance simulator with special I/O (e.g. CAN interface), real-time model, and prototype ECU. Fig 3.26 shows the architecture of the HIL test platform. It consists of three main components: a real-time simulator (DS1006 processor board), prototype ECU (MicroAutoBox II), and interface (Computer).

The real-time simulator is a very fast processor that executes the Autonomie high-fidelity model in real-time. The high-fidelity model includes the powertrain, driver, and environment models. In each time step, it sends the powertrain variables and driver commands to the ECU through a Controller Area Network (CAN). The ECU calculates the

Table 3.7: Specification of the dSPACE HIL components.

Component	Part	Specification
Real-time simulator	Processor	DS-1006 Quad-Core AMD, 2.8 GHz
	Memory	1 GB local, 4 x 128 MB global memory
	HIL I/O Board	DS-2202
ECU: MicroAutoBox II	Processor	DS-1401 PowerPC 750GL 900 MHz
	Memory	16 MB main, 16 MB nonvolatile memory
	I/O interface	DS-1511
Interface	Processor	Core i7, 3.4 GHz
	Memory	16 GB

optimal control commands and sends them back to the real-time simulator. An interface is used to set up the test, to program both the real-time simulator and ECU, and to record the desired outputs. The specifications for the HIL components are shown in Table 3.7.

3.6.1 Controller prototyping

To develop an ECU which can be implemented in the vehicle, the proper hardware should be designed for the desired application. Then, an optimized code should be generated for the target ECU platform. This process makes the ECUs development very challenging. To reduce the difficulties and enhance the process time, RCP systems have been developed, that support both hardware and code generation. This research used the dSPACE MicroAutoBox II as the prototype ECU for testing the real-time performance of the energy-optimal control strategy. The MicroAutoBox has two dedicated CAN controllers (4 CAN channels) that enable communication with the simulator over the CAN bus.

dSPACE provides some libraries in the MATLAB software to generate a C-code for different devices (MicrroAutoBox II and DS1006 processor board). These libraries handle all features of the target device (for example, reading from analog and digital inputs and communicate with other devises through CAN communication). The host service code is also uploaded to the simulator and prototype ECU for data exchange between the real-time hardware and an interface computer.

First, two separate Simulink models are generated for the PHEV high-fidelity model and the designed controller. Then, the designed control code should be prepared to be implemented in the dSPACE sytems by incorporating the dSPACE Real Time Interface (RTI) blocks. For instance, the RTI CAN Controller Setup Block is employed in both real-time model and designed controller to configure the CAN communication. The RTI CAN Receive and Sent are used for receiving and sending data.

The next step to generate a C-code for rapid control prototyping is to compile the Simulink model using the Real Time Workshop code generator. For each hardware platform, the corresponding compiler and code generator is used (for instance, rti1401.tlc and rti1006.tlc for the MicrroAutoBox (DS1041) and Simulator (DS1006), respectively). The Real Time Workshop creates the following files after code generation process: system description file (*.sdf) for uploading the executable file from interface computer using ControlDesk software, executable file (*.ppc) for the processor in the hardware platform,trace file (*.trc) for navigating through the model, and map file (*.map) for the memory address. The dSPACE ControlDesk software is an interface used to connect with RCP hardware platform, upload the executable file, manage the HIL test, and record the desired signals.

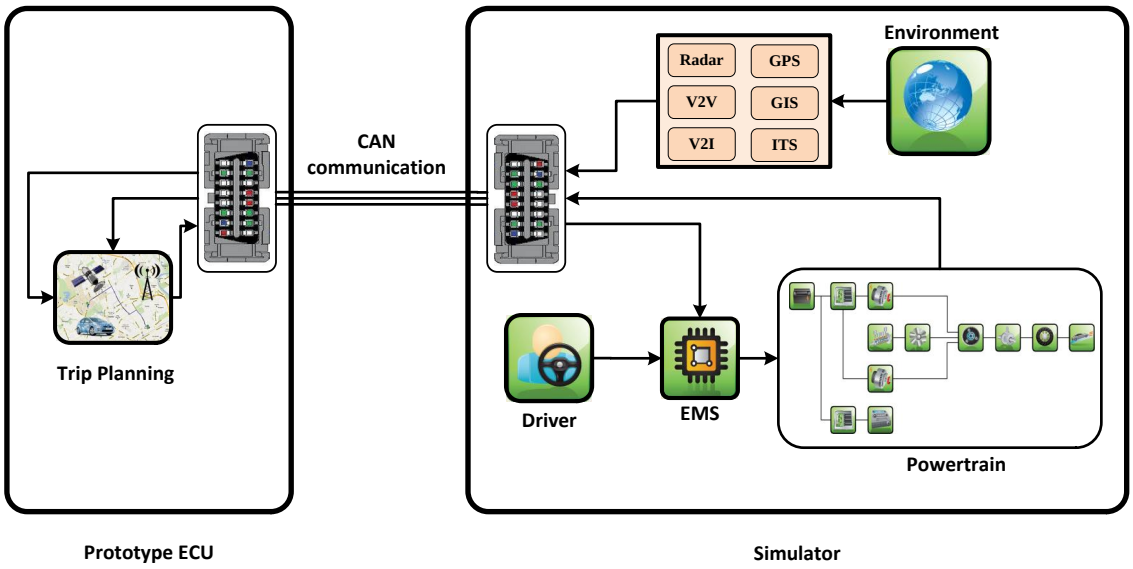

Figure 3.27: Schematic of the Simulink models for HIL testing of the Trip Planning module.

Figure 3.27 shows the software architectures for both the prototype ECU and simulator. The prototype ECU runs the Trip Planning and the simulator executes both the environment and powertrain models. These modules are communicated over the CAN bus. Table 3.8 represents the input and output signals and their characteristics in CAN communication.

3.6.2 HIL testing results

To validate the real-time capability of the ECU, the turnaround time of the controller should be less than the desired time step. Turnaround time is the amount of time taken to execute the controller code and to provide the required ECU output. To implement

Table 3.8: Specification of the input and output signals of the Trip Planning module.

CAN signal	Variable name	CAN ID	Bit length
ECU inputs	Position	100	32
	Speed	101	32
	SOC	102	16
ECU outputs	Slope of Ref. SOC	120	16
	Initial position of Ref. SOC	121	16
	Initial SOC of Ref. SOC	122	16

the HIL testing, first the time step of the system should be determined. Generally, the response time of the system or the update-rate of the impute signals are considered as a time step. One of the main input signals to the Trip Planning module is traffic data which is approximately updated in one minute. Therefore, the time step of this module is considered to be one minute.

The HIL results of the on-line Trip Planning module are shown in Fig. 3.28. The results show that the turnaround-time of Trip Planning in the MicroAutoBox hardware platform is less than 5 sec, which is significantly less than the desired time step (1 min). Therefore, the designed Trip Planning can be implemented in real-time.

3.7 Summary

This chapter has presented the Trip Planning for PHEV platforms that can optimize the total expenditure of electricity and fossil fuel. The designed algorithm utilizes look-ahead trip and driving information to predict optimum SOC profiles.

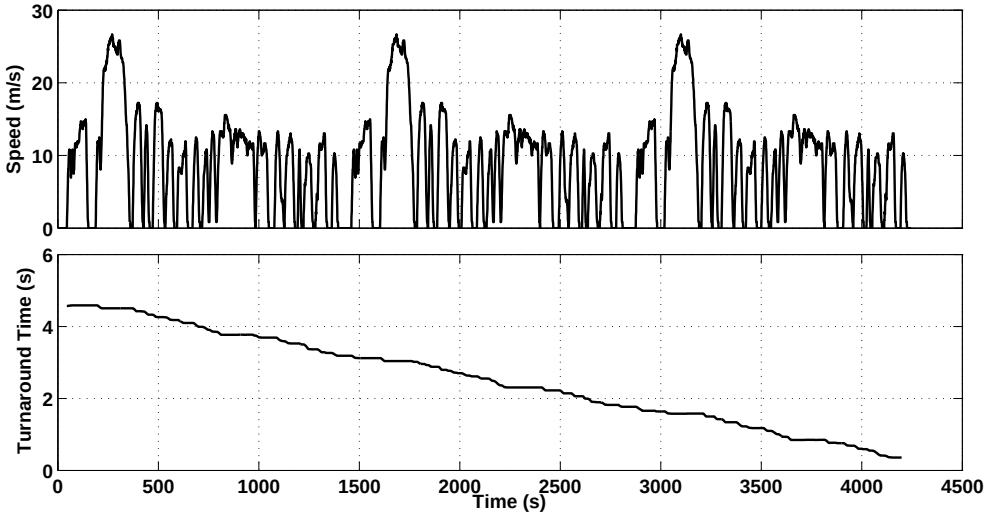

Figure 3.28: Trip Planning HIL test results under 3xUDDS drive cycle.

In the first step, PHEV online-optimization model are developed and validated against the high-fidelity PHEV model. The speed trajectory is predicted using the math-based trip model. The optimization problem is then solved in real-time using the RCO algorithm. Results show that at low speeds, the low-efficiency engine is turned off and the vehicle is operated in full electric mode. Conversely, the engine is dominant during acceleration, when power demand is high.

The RCO results are evaluated against those generated using a global optimization approach, DP. The real-time results are very promising as they show good agreement with the DP data and are achieved at much less computational expense. The results also show that online optimization can compensate changes in trip data.

The HIL results demonstrate that the computational time of the RCO algorithm is significantly less than one minute that validate the real-time Trip Planning module.

Chapter 4

Route-based energy management system development and evaluation

This chapter covers steps to design a real-time Route-based EMS for a power-split PHEV. The EMS controller adjusts power distribution between two energy sources, the engine and the battery. A schematic of the Route-based EMS is shown in Fig. 4.1. Trip Planning module employs the simple powertrain model and predicted speed trajectory to find optimum power distribution, while Route-based EMS calculates the optimum power distribution, based on actual momentary power demand. Therefore, this EMS can handle any sudden speed or propulsion power variations during a trip. Finally, the low-level controllers adjust the engine, the electric motors, and the battery operations to provide the demanded power based on the optimum power distribution.

The Route-based EMS is compared against popular EMS strategies, based on different

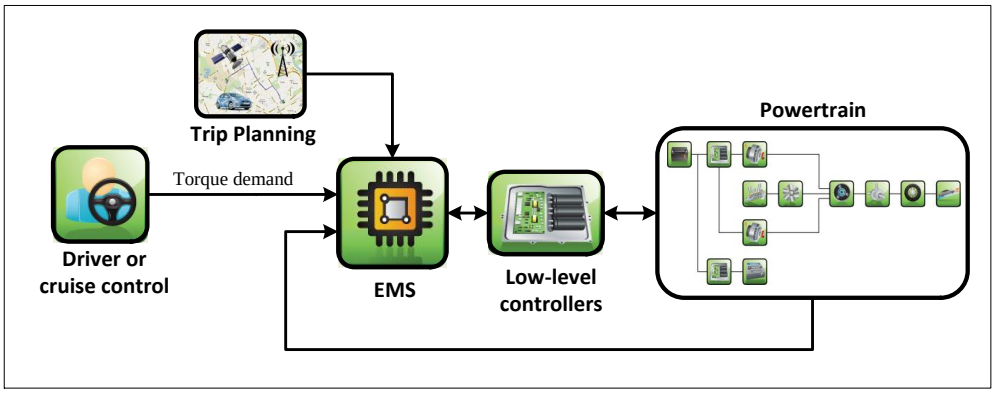

Figure 4.1: Schematic of the real-time Route-based EMS strategy.

levels of trip information. Also, the real-time implementation of the devised Route-based EMS is evaluated using HIL testing. Portions of this chapter have been published in [98–102].

4.1 Control-oriented modelling

The control-oriented model is developed to obtain the power of powertrain components based on the battery power. This model is same as the online optimization model, which is presented in Section 3.3. The only difference is that the control-oriented model calculates power demand based on the command of driver or cruise controller system, while the online optimization model predicts future speed using the math-base trip model. In the control-oriented model, the power distribution between the engine and the battery is calculated based on the Power Ratio (PR):

$$P_d = \left(m\dot{v} + \tfrac{1}{2}\rho A C_d v^2 + mgf\cos\theta + mg\sin\theta\right) v \tag{4.1}$$

$$P_e = \frac{1 - PR}{\eta_t} P_d \tag{4.2}$$

$$P_b = \eta_m^{-k} PR.P_d \tag{4.3}$$

The objective of the controller is to minimize the total energy cost of the vehicle, including the fuel and grid electrical energy, which is formulated in Eq. 4.4:

$$Cost = k_f \dot{m}_f + \ k_e \eta_{ch} Q_{max} \dot{SOC} \tag{4.4}$$

where m_f is fuel consumption, Q_{max} is the maximum battery capacity, η_{ch} is the charger efficiency, and k_f, k_e are the unit price of gas and grid electrical energy, respectively.

4.2 Optimum energy management development

To establish an optimum EMS of PHEV, the power distribution between the engine and the battery is calculated to minimize the total energy cost considering the constraints on the system. The optimal control problem can be derived by considering SOC as a state of

the system, power ratio (PR) as an input, and total energy cost as a cost function:

$$J = \int_0^{t_f} Cost\ dt = \int_0^{t_f} \left(k_f \dot{m}_f - k_e \eta_{ch} Q_{max} S\dot{O}C \right) dt \tag{4.5}$$

$$Subjected\ to: \qquad S\dot{O}C = -\frac{\eta_b}{Q_{max}} P_b$$

$$SOC(0) = SOC_0$$

$$SOC(t_f) = SOC_f$$

The constraints on the system are:

$$SOC_{min} \leq SOC \leq SOC_{max}$$

$$P_{b,min} \leq P_b \leq P_{b,max}$$

$$P_{e,min} \leq P_e \leq P_{e,max}$$

Based on the control-oriented model, the power capacity of the powertrain components can be calculated as functions of the power ratio (PR). Therefore, the constraints can be combined to reach equivalent constraints in terms of battery power and SOC:

$$SOC_{min} \leq SOC \leq SOC_{max} \tag{4.6}$$

$$PR_{min} \leq PR \leq PR_{max} \tag{4.7}$$

$$PR_{max} = \min \left(1, (1 - \eta_t \tfrac{P_{e,min}}{P_d}), (\eta_m \tfrac{P_{b,max}}{P_d}) \right) \tag{4.8}$$

$$PR_{min} = \max \left(0, (1 - \eta_t \tfrac{P_{e,max}}{P_d}), (\eta_m \tfrac{P_{b,min}}{P_d}) \right) \tag{4.9}$$

To solve this problem, we apply the PMP technique to find the global optimum solution. Then, we develop a real-time algorithm based on ECMS (Route-based EMS), that includes future driving conditions.

4.2.1 Pontryagin's minimum principle

PMP is an optimal control approach used to find the global optimal solution for control problems [103]. Assuming the objective of the optimal control problem is to minimize the cost function (J) as a function of time (t), and the state of the system is x:

$$J = \int_{t_0}^{t_f} L(x(t), t)dt \tag{4.10}$$

$$Subjected\ to:$$

$$\dot{x} = f\left(x(t), u(t), t\right) \tag{4.11}$$

with the following constraints:

$$\Psi\left(x(t), t\right) \leq 0 \tag{4.12}$$

To solve this problem, the Hamiltonian function must first be derived:

$$H = L(x(t), t) + \lambda f\left(x(t), t\right) + \nu\Psi\left(x(t), t\right) \tag{4.13}$$

$$\nu = \nu_0 \qquad if\ \psi\left(x(t), t\right) = 0$$

$$\nu = 0 \qquad if\ \psi\left(x(t), t\right) < 0$$

Then, the state and co-state equations should be solved simultaneously:

$$\dot{x} = \frac{\partial H}{\partial \lambda} = f\left(x(t), u(t), t\right) \tag{4.14}$$

$$\dot{\lambda} = -\frac{\partial H}{\partial x} \tag{4.15}$$

The optimum input, $u^{\star}$, is obtained by minimizing the Hamiltonian function:

$$u^{\star} = argmin\left\{H\left(x(t), u(t), t\right)\right\} \tag{4.16}$$

In the optimum EMS of the baseline PHEV, the cost-function is the energy cost. Therefore, according to Eq. 4.13, the Hamiltonian equation can be derived as:

$$H = Cost(P_b) + \lambda(-\frac{\eta_b}{Q_{max}}P_b) + \nu_1(soc_{min} - soc) + \nu_2(soc - soc_{max}) \tag{4.17}$$

$$\nu_1 = \nu \qquad soc_{min} = soc$$

$$\nu_1 = 0 \qquad soc_{min} < soc$$

$$\nu_2 = \nu \qquad soc = soc_{max}$$

$$\nu_2 = 0 \qquad soc < soc_{max}$$

The equations for the state and co-state that should be solved simultaneously are:

$$\begin{aligned} S\dot{O}C &= -\frac{\eta_b}{Q_{max}} P_b \\ SOC(0) &= SOC_0 \\ SOC(t_f) &= SOC_f \\ \dot{\lambda} &= -\frac{\partial H}{\partial SOC} \end{aligned} \tag{4.18}$$

Also, based on the PMP algorithm, the optimum control law will be:

$$u^\star = P_b^\star = argmin\ \{H(P_b, SOC)\} \tag{4.19}$$

This problem is a Two Point Boundary Value (TPBV) problem, in which the initial and final values of the SOC are known and the initial value of λ is unknown. The Simple Shooting Method (SSM) is a common approach to solving TPBV problems. This method converts the TPBV problem into an initial value problem, and adjusts the initial values to satisfy the end constraints. In this problem, first, an initial value for the co-state $\lambda(t_0)$ is assumed. Then, the state and co-state equations are solved simultaneously. At the terminal time (end of trip), the difference between the final SOC ($SOC(t_f)$), and its desired value (SOC_f), is used to correct the initial guessed value of $\lambda(t_0)$. This procedure is repeated until the final SOC value approaches the desired value. Since the state and co-state equations depend on power demand, upcoming driving conditions are required to solve the TPBV problem and calculate the initial λ.

Since the SSM is very sensitive to the initial guessed value of the co-state, we employ

the Modified Simple Shooting Method (MSSM), which is a more accurate method, to solve the TPBV problem. This method is similar to the SSM, but defines the passes through a trajectory in order to guide the final state to its desired value [104]. In this problem, the pass through trajectory is represented by a line between the initial and final states:

$$\Phi = SOC_0 + \frac{SOC_f}{t_f} t_k \tag{4.20}$$

In each step, the SSM is solved for the reduced trip in time interval $[0, t_k]$, with the desired final state of $SOC_f^k = \Phi(t_k)$. The solution of this step, λ_0^k, is considered as an initial guess of the next step, time interval $[0, t_{k+1}]$. This process continues until the problem is solved for the entire time interval $[0, t_f]$, [105].

Lewis [106] has proved the stability of the PMP technique. This technique solves the optimal control problem for an infinite horizon. In this problem, there are constraints on both states and input of the system. Therefore, if the power demand is feasible and can satisfy the powertrain constraint, the solution can stabilize the system.

4.2.2 Route-based EMS

The ECMS was initially developed to address the real-time EMS of HEVs. Since HEVs have only one external power source, vehicle performance can only be evaluated if the electrical energy generated by the battery is converted to an equivalent fuel consumption value. The total equivalent fuel consumption represents the consumption of both energy resources,

electrical energy and fuel, which should be minimized in the optimal EMS strategy:

$$J = \int_{t_0}^{t_f} \dot{m}_{eq}\, dt \tag{4.21}$$

$$\dot{m}_{eq} = \dot{m}_f + \boldsymbol{S}\frac{\eta_{ch}\eta_b}{H_{LHV}}P_b$$

where η_b is the battery efficiency, H_{LHV} is a low heat value of the fuel, and S is the equivalency factor.

Conversely, PHEVs have two external energy sources and can store electric energy directly from the grid. Furthermore, the electrical energy stored in the battery is not provided by the engine and is independent from the fuel. Therefore, the total energy cost during the trip is considered as a cost function of the problem.

$$J = \int_{t_0}^{t_f} \boldsymbol{F}(Pb, S)\, dt \tag{4.22}$$

$$\boldsymbol{F}(Pb, S) = k_f\dot{m}_f + \boldsymbol{S}k_e\eta_{ch}\eta_b P_b \tag{4.23}$$

In comparing the PMP and ECMS approaches, the main difference is that the PMP solves the TPBV problem to calculate $\lambda(t)$, while the ECMS assigns an equivalency factor as a design parameter.

The equivalency factor has a significant effect on the power distribution between the two energy sources. If the battery energy capacity is unlimited, the equivalency factor is equal to one, $S = 1$, and the total energy cost can be used to evaluate vehicle performance. However, there is a constraint on the battery capacity; therefore, the equivalency factor is

defined to regulate the supply and demand of electrical energy. For instance, if we assume that the electrical energy cost is less than the fuel cost, and the trip distance is more than the full electric range of the vehicle, the demand for electrical energy will be more than the battery capacity. Increasing the equivalency factor raises the cost of electrical energy, which allows us to find a more optimal point for consuming the battery electrical energy.

In general, reducing the equivalency factor decreases electrical energy cost. According to the control law, this reduction in the cost of electrical energy leads to increased battery power and decreased engine power. Therefore, more electrical energy is consumed if the equivalency factor is decreased, and vice versa: increasing the equivalency factor increases the fuel consumption.

The optimal equivalency factor depends on the driving cycle and future power demand. To overcome this problem and ensure the ECMS approach is independent of the driving cycle, an A-ECMS is employed. In this algorithm, the equivalency factor $S(t)$ is obtained based on the reference SOC. In the literature it has been shown that the linear profile of SOC with respect to driving distance is a near optimum solution for the PHEV energy management problem, and it is considered as a reference SOC in the A-ECMS method.

In the Route-based EMS, the Trip Planning scheme first uses future driving conditions to find the optimum SOC profile and then employs it as a reference SOC. A PID controller is employed to generate an equivalency factor based on the reference SOC, as shown in Fig. 4.2.

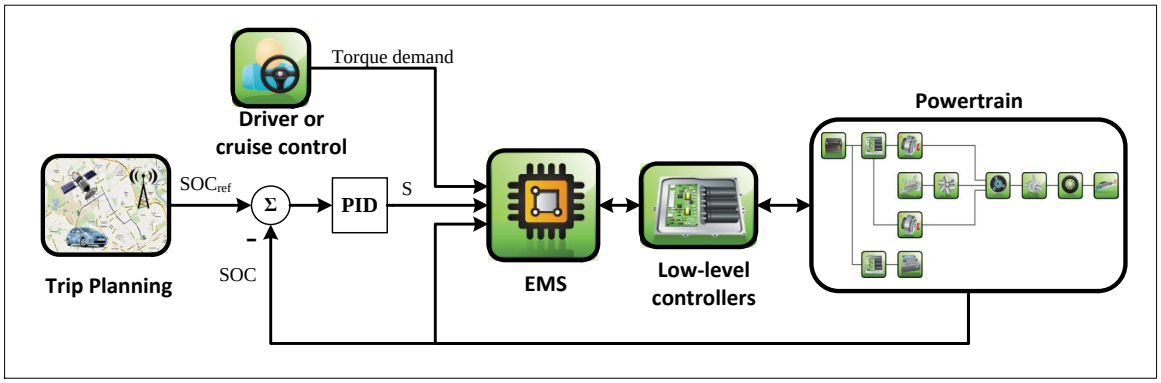

Figure 4.2: Schematic of the Route-based EMS.

4.2.3 Level of trip information

As mentioned, preview knowledge of a trip can significantly improve EMS performance. In this way, we can take advantage of advancements in vehicle intelligence and communications technologies, such as GPS, ITS, GIS, radar, and other on-board sensors to provide look-ahead trip data. These data can be utilized to predict the future driving conditions and increase the performance of EMS strategies. In terms of the level of access to the trip preview information, the EMS strategies can be categorized into three groups: I) no access, II) travelling distance, and III) speed trajectory.

Reactive EMS strategies such as rule-based, CDCS, and Manual CDCS require no preview of trip information. The Autonomie default control strategy is rule-based and similar to CDCS, except that the engine operates in CD mode when power demand is high.

In A-ECMS technique, the travelling distance is known in advance, and a linear battery depletion profile is used as a reference SOC. In the Route-based EMS, the Trip Planning

module use sensors to acquire traffic conditions and thus find an optimum reference SOC profile.

The global optimum solution is obtained by employing the PMP technique to evaluate other strategies. In this technique the exact future driving conditions and speed trajectory are known in advance (due to complete preview information).

This thesis evaluated the real-time Route-based EMS against three existing EMS strategies, taking into consideration different levels of trip information.

4.3 MIL testing

This section investigates performance of the popular EMS strategies: rule-based, CDCS, Manual CDCS, A-ECMS, and Route-based EMS, based on different levels of trip information. In particular, performance of the Route-based EMS is compared against MPC controller, which is developed by A.Taghavipour [44].

4.3.1 Following standard driving cycles

The simulation results for EMS strategies without any preview trip information according to EPA-UHU drive cycle are shown in Fig. 4.3, 4.4, and 4.5, respectively. The control system accurately follows the reference speed trajectory with a margin of error of less than 1 km/h.

The engine operates more efficiently at higher speeds than lower speeds. As a result, the better engine operation while driving on highways can improve fuel economy. While

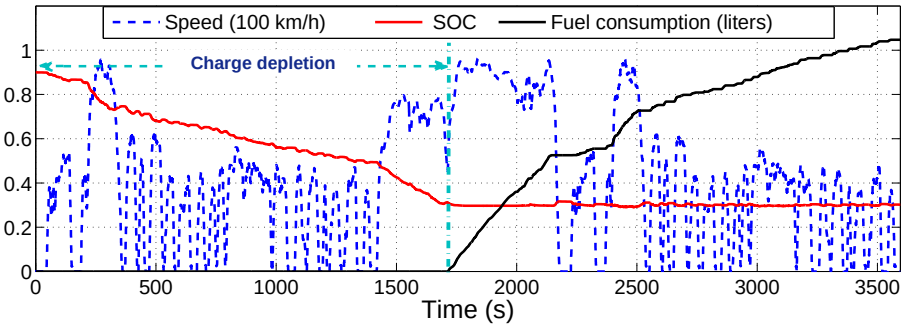

Figure 4.3: CDCS strategy performance over 3xUDDS driving schedule

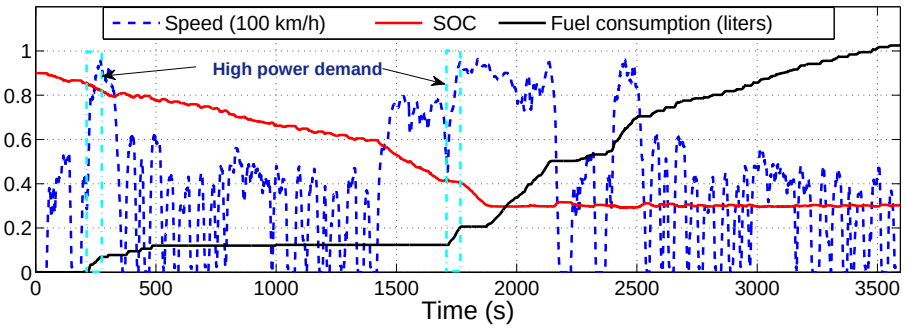

Figure 4.4: Autonomie's default rule-based strategy performance over 3xUDDS driving schedule

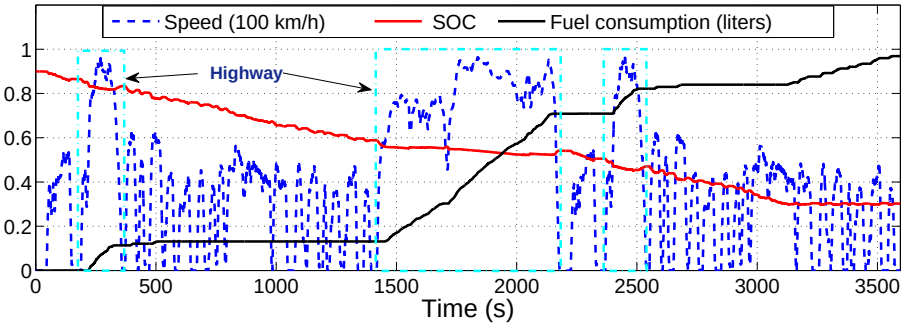

Figure 4.5: Manual CDCS strategy performance over 3xUDDS driving schedule

driving in urban areas, using electrical energy is preferable. So, in Manual CDCS, the driver can manually switch between EV mode (CD) and HEV mode (CS) depending on traffic conditions. Doing so can improve fuel economy further. The Manual CDCS strategy utilizes more engine power in the highway rather than rule-based strategy, and extends CD operating mode until $t = 3100\,s$. This strategy enhances the fuel economy by 5.6% compared to the default rule-based controller in Autonomie software.

In CDCS strategy, the battery energy propels the vehicle for approximately the first half of the trip ($t = 1715\,s$), then the operating mode switches to CS and the engine takes over (Fig. 4.3). The rule-based controller of Autonomie has a similar approach, but it starts the engine even when SOC is more than the predefined value. As shown in Fig. 4.4, for acceleration at $t = 220\,s$ and $t = 1720\,s$, the engine assists the electric drive to propel the vehicle. This leads to a longer charge depletion period and a 2.1% improvement in fuel economy (MPG) over CDCS.

The global optimum solution is obtained using the PMP technique. The resulting TPBV problem is very sensitive to initial value of λ. Figures 4.6 - 4.9 show the simulation results for different initial λ values. In low λ_0, the battery power mainly propels the vehicle until the SOC reaches the minimum value, while in high λ_0, the engine is the main power source. The modified simple shooting method is employed to solve the TPBV problem, and the optimum λ_0 satisfies the constraint $SOC(t_f) = SOC_f$.

Based on the level of trip information, A-ECMS or Route-based EMS strategies can be used to find optimal power distribution. A linear reference SOC can be developed based on trip distance or an optimum SOC profile can be generated by Trip Planning

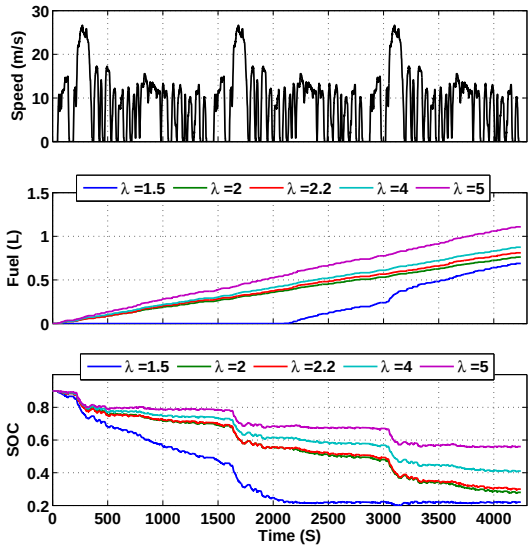

Figure 4.6: Simulation results for 3xUDDS drive cycle using different initial λ values.

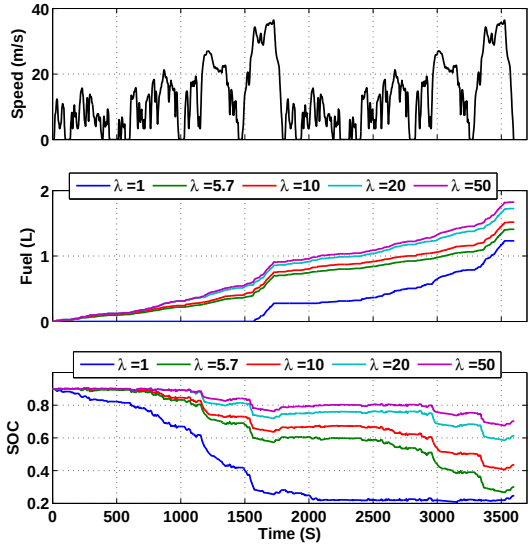

Figure 4.7: Simulation results for 2xWLTP drive cycle using different initial λ values.

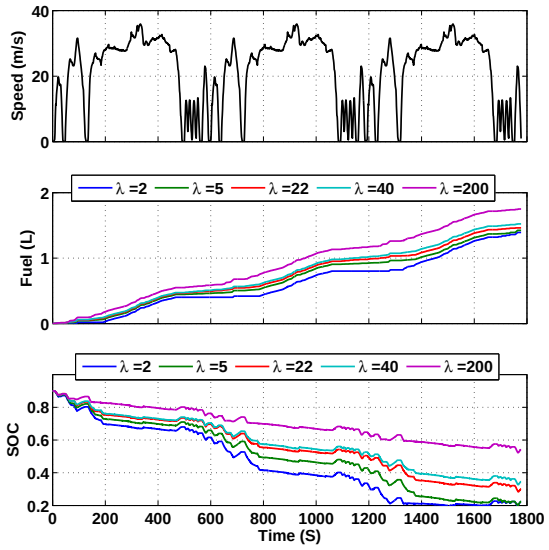

Figure 4.8: Simulation results for 3xSFTP-US06 drive cycle using different initial λ values.

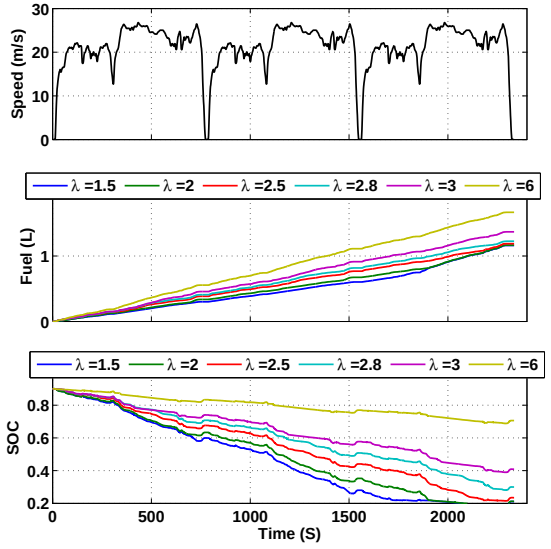

Figure 4.9: Simulation results for 3xHWFET drive cycle using different initial λ values.

Table 4.1: Fuel consumption results for each EMS strategy

Drive cycle	Fuel consumption (MPG)					
	Rule-based	CDCS	Manual	A-ECMS	Route-based EMS	PMP
3xUDDS	97.7	94.9	99.6	104.7	107.7	108.4
3xHWFET	79.3	75.8	88.0	92.8	94.6	96.9
3xSFTP	52.1	50.3	59.0	58.4	60.5	62.2
2xWLTP	72.7	69.7	80.4	78.0	80.3	82.3
EPA-UH	129.0	125.5	156.0	148.0	159.6	190.2
EPA-UHU	95.1	93.1	100.5	98.3	103.4	103.8

described in Chapter 3. The optimum fuel consumption and SOC profiles generated by the A-ECMS and Route-based EMS for various drive cycles are shown in Figures 4.10 - 4.15. The results show that both Route-based EMS and A-ECMS strategies extend the charge depleting mode until the end of trip. Therefore, both controllers can optimally use the battery and engine power for longer range compare to rule-based controller. The results also demonstrate the Route-based EMS can significantly improve the energy cost.

Table 4.1 shows the results of the EMS strategies. The best results are achieved by the real-time Route-based EMS, which closely approximated the results of the global optimum solution based on PMP technique. When no preview information is available, the Manual strategy shows the best results.

4.3.2 Comparison with MPC controller

This study also compares two optimal route-based control approaches- the MPC controller and the devised Route-based EMS- for different levels of trip information. The MPC energy

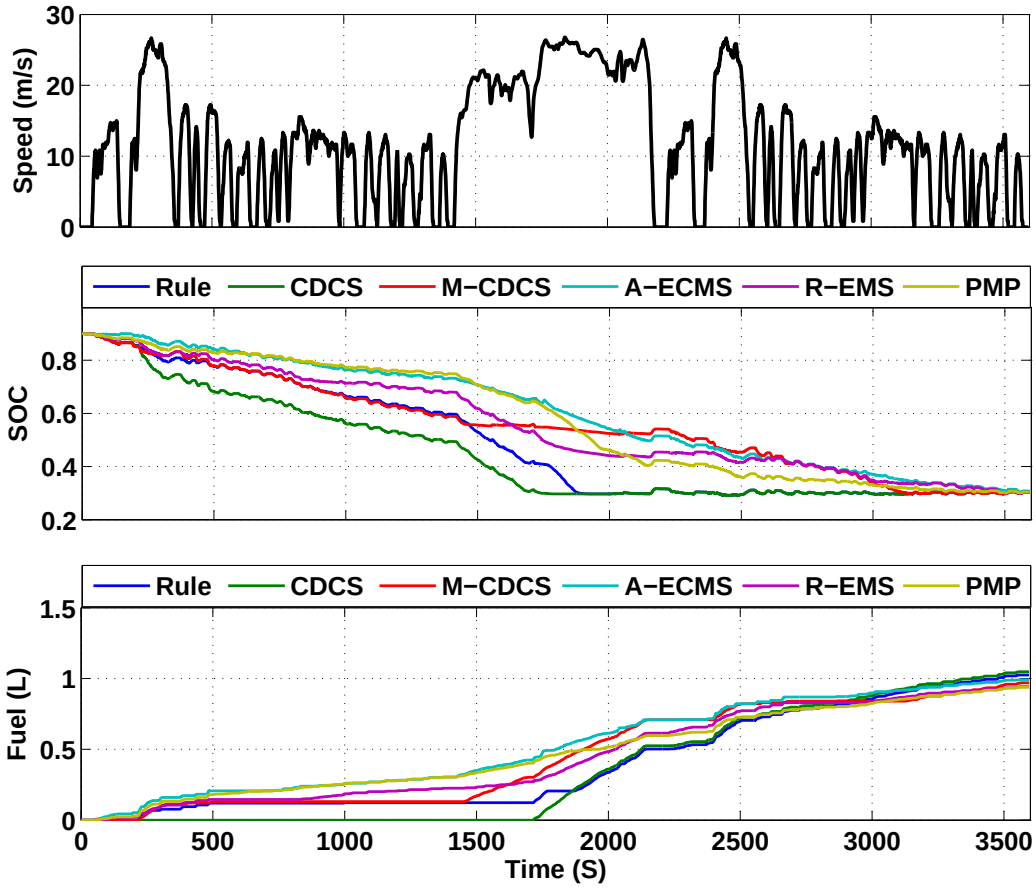

Figure 4.10: Simulation results for each EMS strategy when tracking EPA-UHU drive cycle.

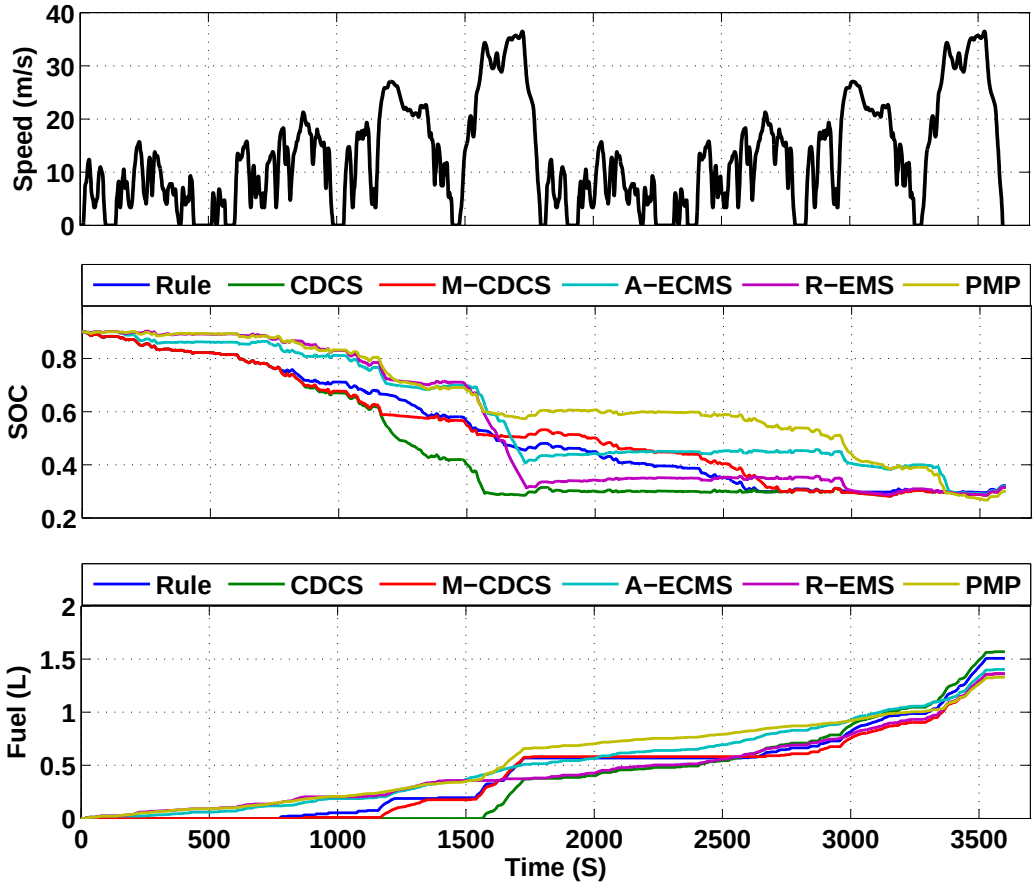

Figure 4.11: Simulation results for each EMS strategy when tracking 2xWLTP drive cycle.

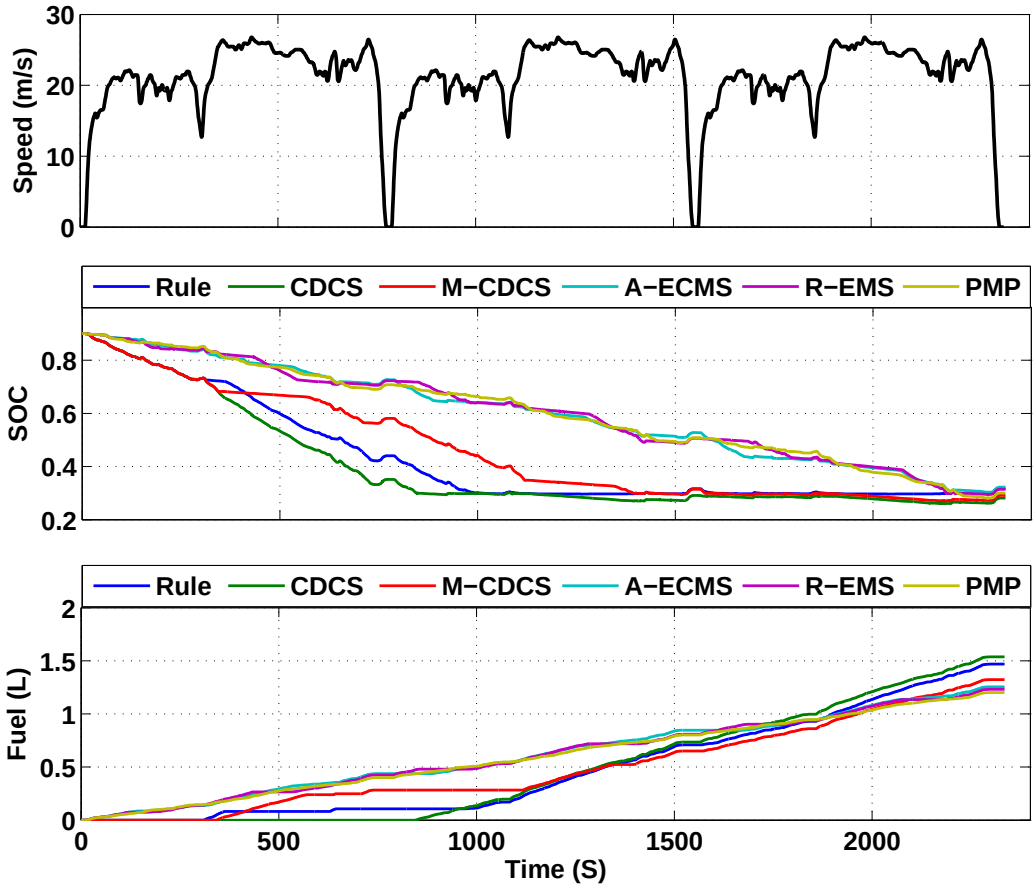

Figure 4.12: Simulation results for each EMS strategy when tracking 3xHWFET drive cycle.

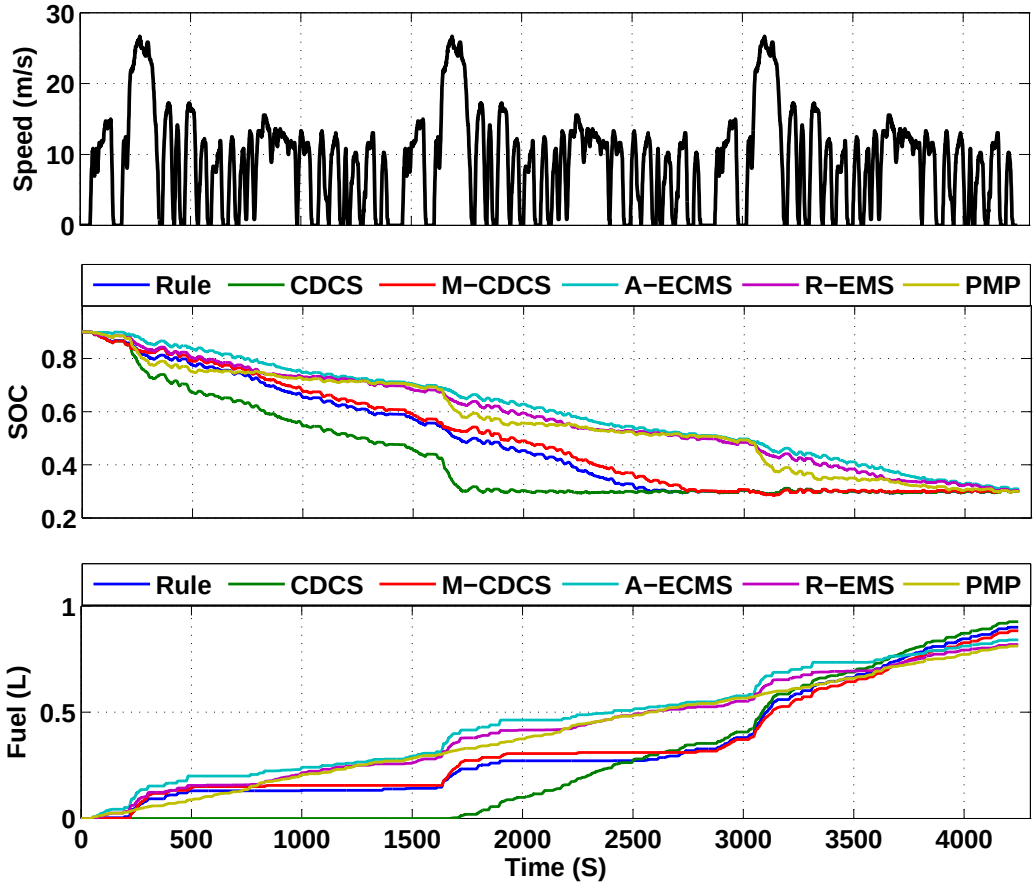

Figure 4.13: Simulation results for each EMS strategy when tracking 3xUDDS drive cycle.

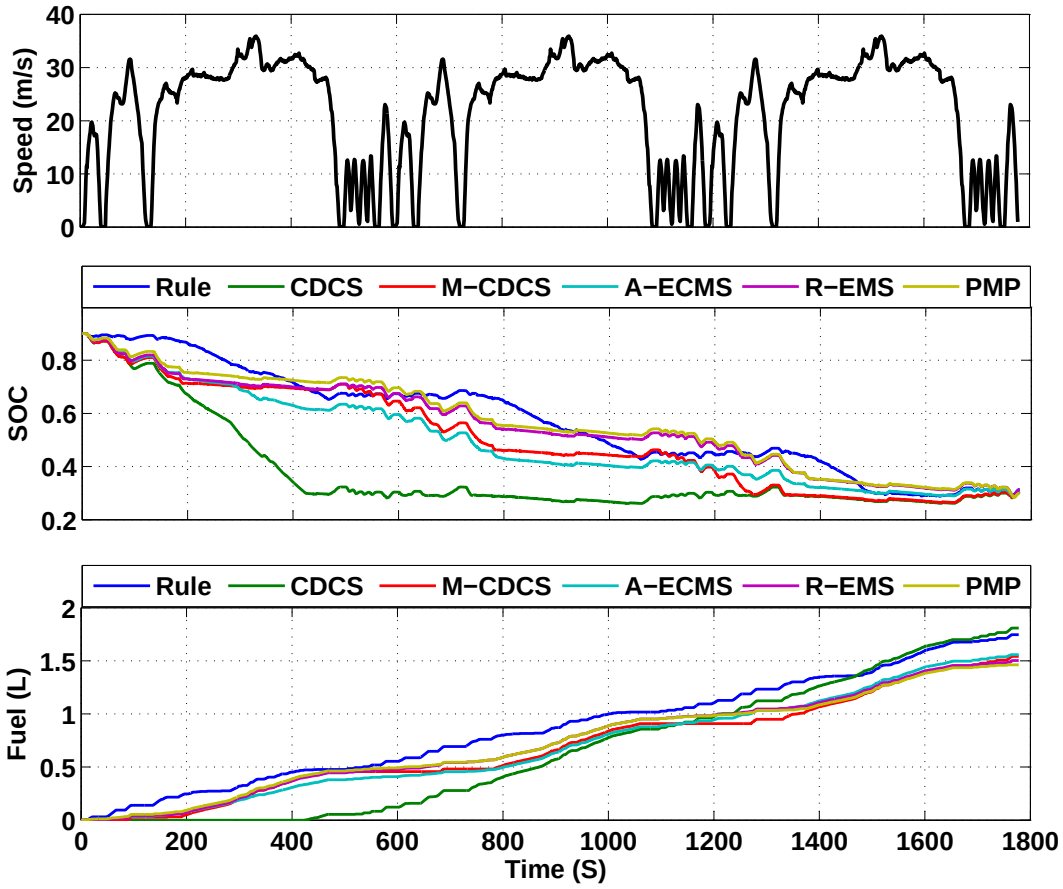

Figure 4.14: Simulation results for each EMS strategy when tracking 3xSFTP-US06 drive cycle.

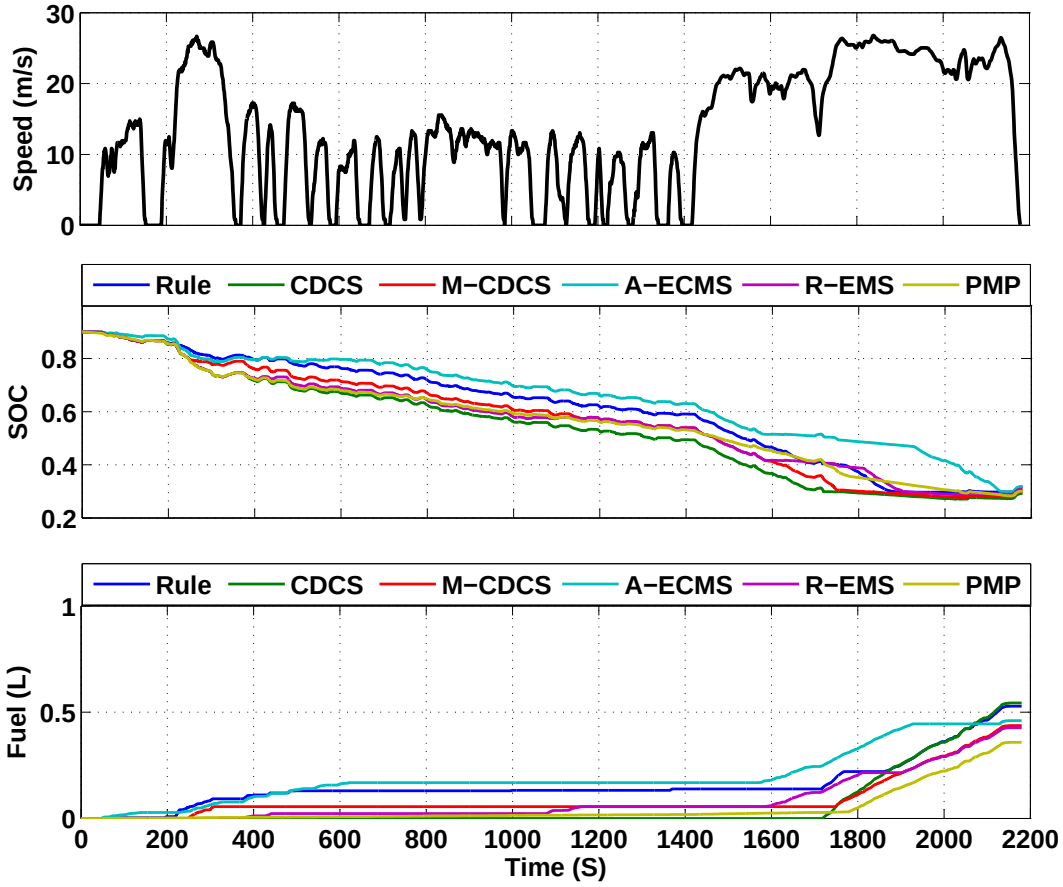

Figure 4.15: Simulation results for each EMS strategy when tracking EPA-UH drive cycle.

management strategy was developed in our research group by A. Taghavipour [3]. Both controllers are implemented in the high-fidelity model.

MPC energy management strategy

The MPC technique has been recently applied to many control applications because of its ability to handle constraints on states and inputs of the system. It solves the optimal control problem in a finite horizon time, which makes the controller capable of real-time implementation.

The MPC controller uses the control-oriented model in order to predict the future. In each prediction horizon, a cost function is minimized that results in maximum fuel economy and tracking a reference SOC trajectory while following a drive cycle. The cost function is:

$$J(k) = \sum_{i=1}^{N_p} (w_1(SOC_{ref}(k+i) - SOC(k+i))^2 + w_2(\dot{m}_f(k+i))^2). \tag{4.24}$$

In Eq. 4.24, w_1 are w_2 weighting parameters that are chosen according to the predicted maximum value of the weighted variables. The performance of the control system can deteriorate significantly when the control signals from the original design meet with the

constraints. There are some constraints on this problem that are defined as follows:

$$T_{min-i} < T_i < T_{max-i} \qquad i \in \{e, m, g\} \tag{4.25}$$
$$\omega_{min-i} < \omega_i < \omega_{max-i} \qquad i \in \{e, m, g\}$$
$$SOC_{min} < SOC < SOC_{max}$$

Stabilizing the MPC controller requires consideration of extra constraints or auxiliary objective functions, which affects the global optimality of the original problem [107–109]. It also increases the computational time and makes real-time implementation more challenging. In addition, adding constraints might make the optimal solution infeasible. Zheng et. al [110] show that closed-loop MPC controllers are asymptotically stable if the optimization problem is feasible. Therefore, MPC stability can be achieved by ensuring that the solution is always feasible and the constraints are satisfied.

Simulation results

To evaluate the designed EMS strategies performance (MPC controller and Route-based EMS), they are implemented to the high-fidelity model in Autonomie. Two different driving schedules for urban driving and combined highway and urban driving are used for the simulation. The first one is a combination of three UDDS drive cycles (3xUDDS drive cycle) and the latter is two UDDS and a HWFET drive cycles (EPA-UHU drive cycle).

The trip information helps improving the EMS strategy performance. Moreover, the battery depletion profile affects the PHEV fuel economy. If the travelling distance is

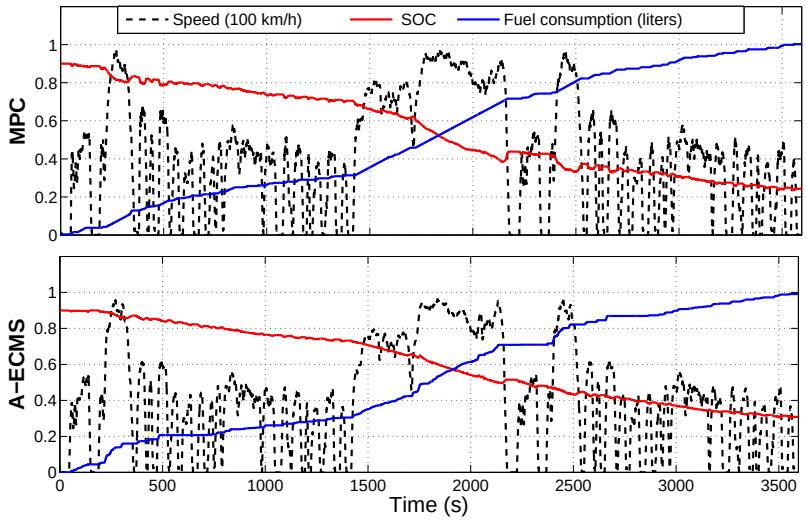

Figure 4.16: Results of EMS strategies with linear reference SOC.

available beforehand, the linear depletion profile is used as the reference SOC. In the case of modern vehicle with on-board sensors, the optimum depletion profile is generated by Trip Planning in real-time and applied to the EMS strategy. The simulation results of A-ECMS and MPC controller for linear reference SOC are shown in Fig. 4.16. It is shown that both EMS strategies satisfy the constraint on SOC at the end of the trip.

MPC uses more battery power while the vehicle is accelerating (at $t = 210\ s$ and $t = 2400\ s$). So, electrical power provides smoother engine operation, since the engine operates inefficiently in transients. On the other hand, A-ECMS uses more engine power for acceleration in order to follow the SOC reference trajectory.

The simulation results with optimized reference SOC are shown in Fig. 4.17. In highway, Route-based EMS first utilizes more engine power for acceleration part and then employs battery power to track the reference SOC. But MPC propels the vehicle by battery power in

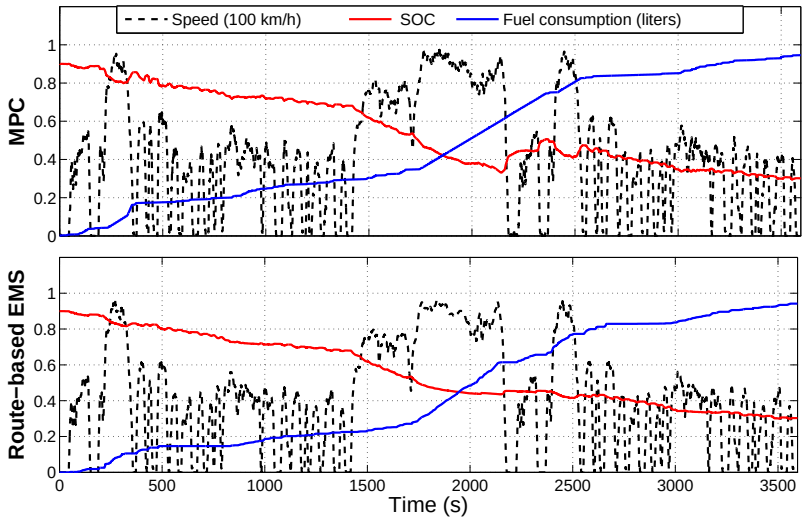

Figure 4.17: Results of EMS strategies with optimized reference SOC.

acceleration mode then uses engine power to restore battery energy and track the reference SOC. For instance, in the second segment, in the time period of 180s to 360s, the fuel consumption and ΔSOC are 0.122 L, 0.032% for MPC, and 0.087 L, 0.049% for Route-based EMS, respectively. Therefore, MPC increases SOC (decrease ΔSOC of the segment) by utilizing more engine power at the end of the segment.

To evaluate these EMS strategies in a different driving schedule, 3xUDDS drive cycle is applied to the model. Fig. 4.19 shows the simulation results. By comparing the results of Route-based EMS and MPC strategies for different driving schedules, it is found that the fuel consumption of the two EMS strategy are close to each other.

The fuel consumption for different EMS strategies with different levels of trip information in EPA-UHU and 3xUDDS drive cycles are shown in Table 4.2. When the future trip information is not available, the Manual CDCS has the best performance. If the travel-

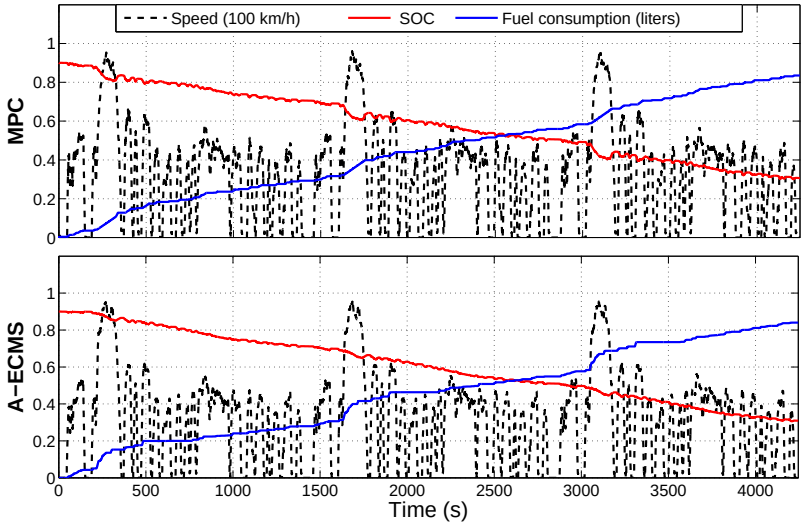

Figure 4.18: Results of EMS strategies with linear reference SOC over the 3xUDDS driving schedule.

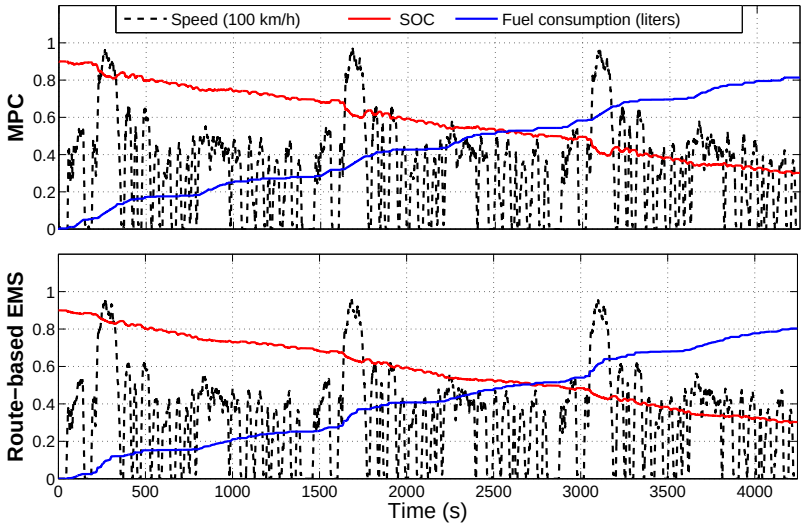

Figure 4.19: Results of EMS strategies with optimized reference SOC over the 3xUDDS driving schedule.

Table 4.2: Fuel economy for different levels of trip information

Strategy	Level of trip information	Fuel consumption (MPG)	
		EPA-UHU cycle	3xUDDS cycle
CDCS	No	93.1	94.9
Rule-based	No	95.1	97.7
Manual CDCS	No	100.5	99.6
A-ECMS	Distance	98.3	104.7
MPC	Distance	97.4	105.4
Route-based EMS	Speed	103.4	107.7
MPC	Speed	102.9	108.4
PMP	Speed	103.8	108.4

ling distance is known in advance, Manual CDCS or A-ECMS results are close. In urban drive cycle (3xUDDS), A-ECMS strategy has a better performance because the electrical energy is available until the end of the trip. In the combined urban and highway driving (EPA-UHU), Manual CDCS operates the engine more efficiently, and therefore, leads to better fuel economy.

If the predicted future speed trajectory is available, the devised Trip Planning module that generates optimum SOC profile can improve the performance of both MPC and Route-based EMS strategies. Using these control approaches, the fuel consumption is improved by 8.5% (102.9 vs. 95.1) and 10.2% (107.7 vs. 97.7) for EPA-UHU and 3xUDDS drive cycles comparing to the results of the default rule-based controller of Autonomie software.

The other criteria that should be considered in the EMS controller design is the computational effort in order to implement controls in real time. To compare the computational effort, all simulations are run on a PC with Intel Core 2 Duo CPU (E8500, 3.17GHz) and

4GB RAM. The average computation time of MPC and Route-based EMS strategies are 240, 208s for EPA-UHU drive cycle, and 290, 252 s for 3xUDDS drive cycle, respectively.

4.4 HIL testing

HIL simulation is an essential part of the ECU development process that evaluates and validates the ECU functions and communications between ECUs. The HIL simulations enable ECU testing under a variety of scenarios that may be very expensive or time consuming for vehicle drive test. In the HIL testing, ECUs are connected to a simulator instead of being connected to a real vehicle. The first step of HIL testing is prototype ECU preparation.

4.4.1 Controller prototyping

The dSPACE MicroAutoBox II hardware platform is used as the prototype ECU for testing the real-time performance of the Route-based EMS strategy. The control signals generated by the EMS strategy are sent to the high-fidelity vehicle model in the simulator over the CAN network. Figure 4.20 illustrates the schematic of software architecture for both prototype ECU (MicroAutoBox) and simulator (DS1006 processor).

Figure 4.21 shows the control architecture of Toyota Prius Plug-in Hybrid provided by Toyota Information System (TIS) [111]. By comparing the current controller of the Prius with the designed energy-optimal controller, the difference is that the latter employs Trip Planning module to provide reference SOC profiles and also incorporate Route-based EMS instead of using rule-based control strategy.

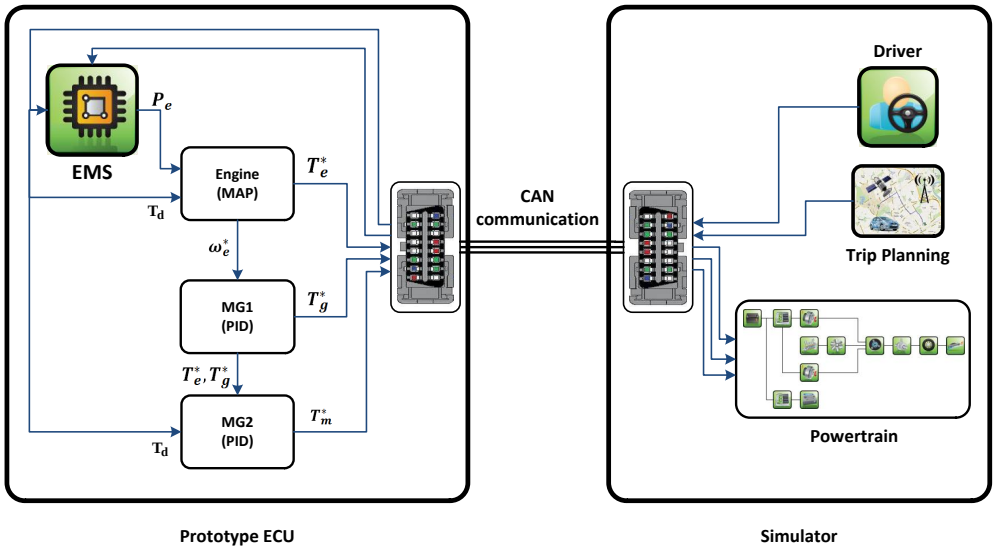

Figure 4.20: Schematic of the Simulink models for HIL testing of the Route-based EMS strategy.

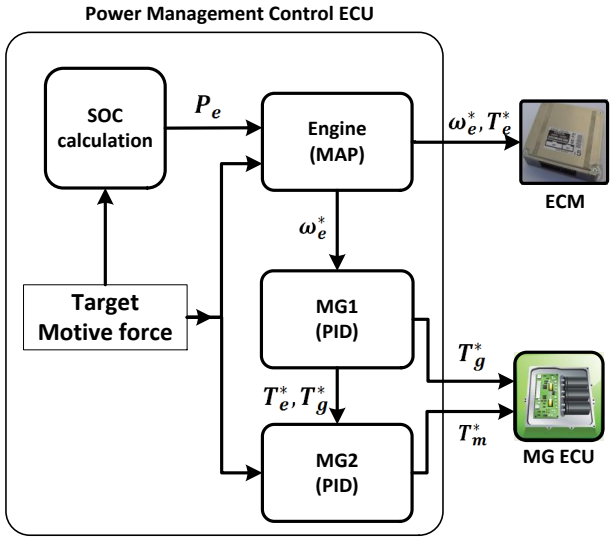

Figure 4.21: Schematic of the Prius EMS from the TIS document [111].

Table 4.3: Specification of the input and output signals of the Route-based EMS.

CAN signal	Variable name	CAN ID	bit length
ECU inputs	Position	100	32
	Speed	101	32
	SOC	102	16
	Slope of Ref. SOC	120	16
	Initial position of Ref. SOC	121	16
	Initial SOC of Ref. SOC	122	16
	Demand torque	140	32
	Engine speed	151	32
	Motor speed	152	32
	Generator speed	153	32
ECU outputs	Engine torque	141	32
	Motor torque	142	32
	Generator torque	143	32

The input signals to the prototype ECU are driver or cruise controller commands, Trip Planning signals, and feedbacks from the high-fidelity powertrain model; the output signals are the engine and motor-generators desired torques. These signals transfer to the simulator hardware through CAN bus. Table 4.3 represent the input and output signals and their characteristics in CAN bus.

4.4.2 HIL testing results

The results of the Route-based EMS system for different driving cycles are shown in Fig. 4.22 and 4.23. The HIL and MIL results are in complete agreement. The control

systems are basically the same. The only differences are in the solver program (C-code or Simulink) and the hardware (ECU or PC). The results show that the controller turnaround-time is less than 25 μs, which is less than the desired time step (1 ms). Therefore, the Route-based EMS is validated.

4.5 Summary

This chapter has presented a new real-time EMS system for PHEVs based on the ECMS approach. The designed controller takes advantage of preview trip information through optimum SOC profiles. The controller is implemented in the high-fidelity PHEV model and compared against the results of several different EMS strategies, including the CDCS, Manual CDCS, rule-based, PMP, and MPC methods. The real-time Route-based EMS system showed promising results and improved fuel consumption up to 11% compared to the rule-based controller. The HIL test results showed that the turnaround-time is less than 25 μs, and the Route-based EMS system can be implemented in real-time.

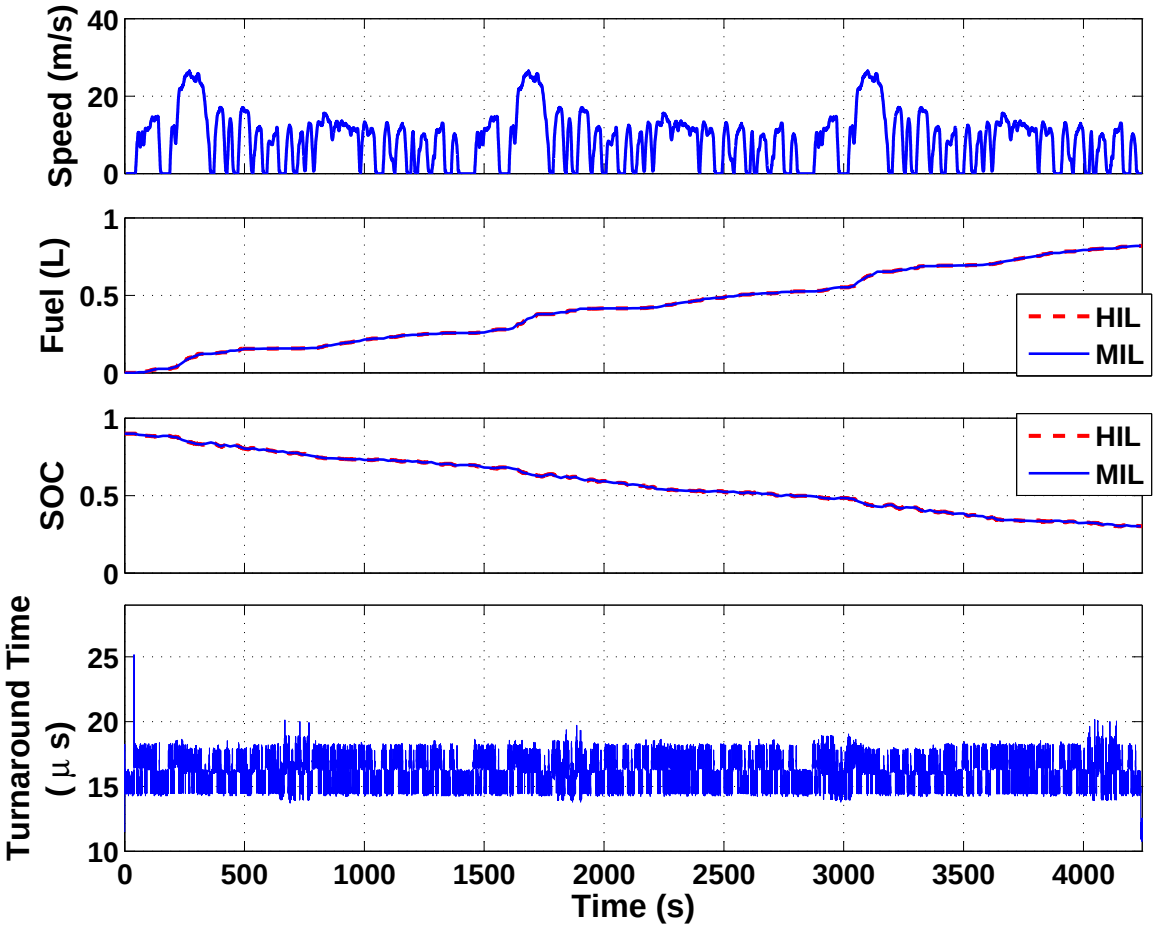

Figure 4.22: HIL test results for the Route-based EMS over the 3xUDDS driving schedule.

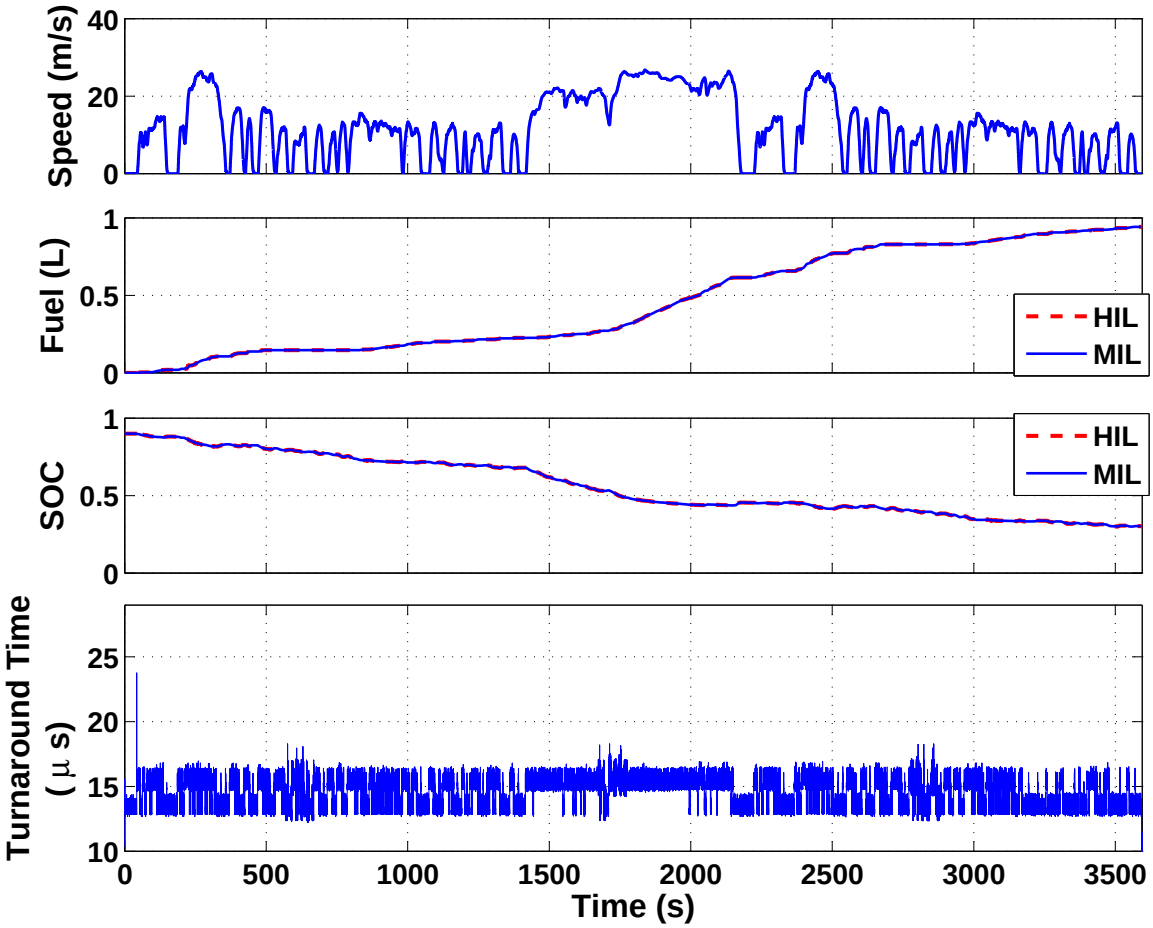

Figure 4.23: HIL test results for the Route-based EMS over the EPA-UHU driving schedule.

Chapter 5

Ecological cruise controller development and evaluation

In this chapter, an Eco-Cruise controller is developed to improve energy cost while maintaining a safe distance from the preceding vehicle. We show that the Eco-Cruise system can improve total energy costs, as well as vehicle safety, simultaneously. The developed controller is equipped with an onboard sensor to capture upcoming trip data to optimally adjust the speed of baseline PHEV. The NMPC technique is used to optimally control the vehicle's speed. To prepare the NMPC controller for real-time applications, a fast and efficient control-oriented model is developed. The NMPC controller is compared against three different controllers, i.e. PID, linear MPC, and PMP. Also, the real-time implementation of the controller is verified by HIL testing. Portions of this chapter have been published in [112–114].

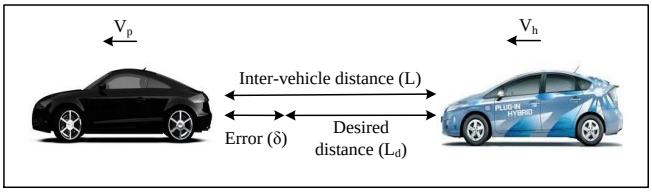

Figure 5.1: Schematic of two consecutive vehicles.

5.1 Control-oriented modeling

In this section, a control-oriented model is developed to be used at the heart of the Eco-Cruise controller. The main goal of the proposed Eco-Cruise controller is to simultaneously maintain the safe distance of the host vehicle from the preceding vehicle and minimize its total energy costs. The tasks can be fulfilled by optimally adjusting the vehicle's speed for any given driving condition. In our control-oriented model formulation, speed and distance of the host vehicle and preceding vehicle are considered as the states of the system, and the wheels' torque is considered as the input of the system. Thus, the Eco-Cruise controller should adjust the wheels'torque to comply with the required tasks.

In the rest of this section, we derive the model equations and consequently develop a proper objective function based on the input and states of the system.

5.1.1 Inter-vehicle distance modelling

Fig. 5.1 shows the schematic illustration of two consecutive vehicles in the traffic flow, in which L presents the inter-vehicle distance, L_d shows the desired inter-vehicle distance, and δ delegates the distance error.

According to the vehicle longitudinal dynamics theory, the considered system can be modeled as below:

$$\begin{pmatrix} \dot{x}_h \\ \dot{v}_h \\ \dot{x}_p \\ \dot{v}_p \end{pmatrix} = \begin{pmatrix} v_h \\ u - \frac{1}{m}F_d \\ v_p \\ a_p \end{pmatrix} \tag{5.1}$$

$$F_d = \frac{1}{2}\rho A C_d (v_h)^2 + mg\sin\theta + mgf\cos\theta$$

where v_h and x_h are the speed and position of the host vehicle, and v_p and x_p are the speed and position of the preceding vehicle, u is input, F_d is resistance force, and a_p is the acceleration of the preceding vehicle. In this equation u is equal to $u = \frac{1}{m.r}T_d$, where T_d is wheel torque, and r is wheel radius.

To develop the controller for practical application and also to make sure the controlling commands always fall within a safe range, the desired inter-vehicle distance is adaptively changed by increasing the speed, as below:

$$L_d = L_0 + hv_h \tag{5.2}$$

where L_0 is stationary distance, and h headway time. The inter-vehicle distance error is calculated using Eq. 5.3 :

$$\delta = L_d - L = (L_0 + hv_h) - (x_p - x_h) \tag{5.3}$$

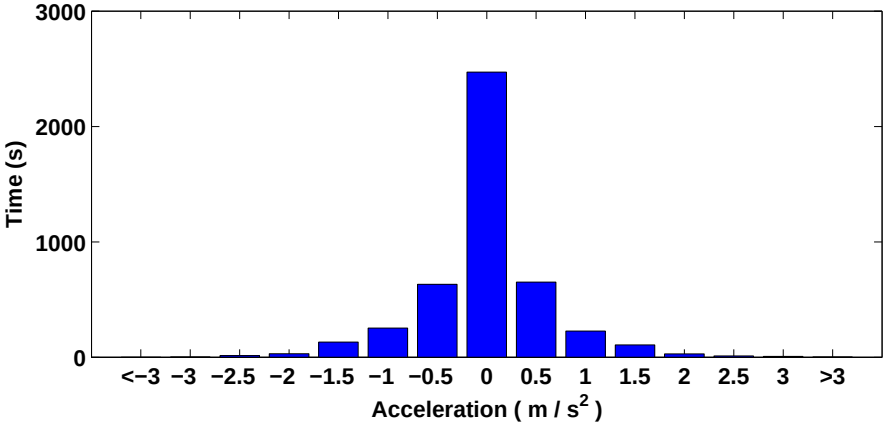

Figure 5.2: Acceleration distribution in a combined UDDS, WLTP, HWFET, and SFTP drive cycle.

It is assumed that we have access to the speed and acceleration of the preceding vehicle through measurement or through the vehicle communication system. To improve the accuracy of the prediction model and enhance the controller performance, the acceleration of the preceding vehicle is adjusted during the prediction horizon.

By investigating the acceleration distribution in several drive cycles, it is found that the vehicle mostly drives at low acceleration and a constant speed (see Fig. 5.2). Therefore, the future acceleration of the preceding vehicle decreases gradually from the measured value.

$$\hat{a}_p(\tau) = e^{-\lambda\tau} a_p(t_k) \tag{5.4}$$

where $\hat{a}_p$ is the predicted future acceleration of the preceding vehicle, $a_p(t_k)$ is the measured acceleration of the preceding vehicle, t_k is the previous time step, τ is prediction time, and λ is a constant positive parameter.

5.1.2 Powertrain modelling

This model is same as Route-based EMS control-oriented powertrain model, described in Section 4.1. The amount of supplied engine and battery power strictly depend on the EMS strategy. It is assumed that the power distribution does not vary during a time step, and that the power distribution rate is the same as previous time-step values.

$$\hat{P}_b(\tau) = \frac{P_b(t_k)}{P_d(t_k)} P_d(\tau) \tag{5.5}$$

$$\hat{P}_e(\tau) = \frac{P_e(t_k)}{P_d(t_k)} P_d(\tau) \tag{5.6}$$

where P_d is power demand, $\hat{P}_e$, $\hat{P}_b$ are predicted engine power and battery power, $P_e(t_k)$, $P_b(t_k)$ are measured engine power and battery power in the previous time step, and τ is prediction time, respectively.

5.1.3 Model evaluation

To evaluate the control-oriented model, the Autonomie high-fidelity model is used as a reference. The combination of three EPA driving cycles (UDDS, HWFET, and SFTP-US06) is applied to a high-fidelity model. The simulation data are collected in each time step. Fig. 5.3 schematically illustrates the designed Simulink model to compare the results of a high-fidelity model and a control-oriented model. The maximum error for fuel consumption, SOC, and energy cost are 2.4%, 1.6%, and 3.6%, respectively (Fig. 5.4).

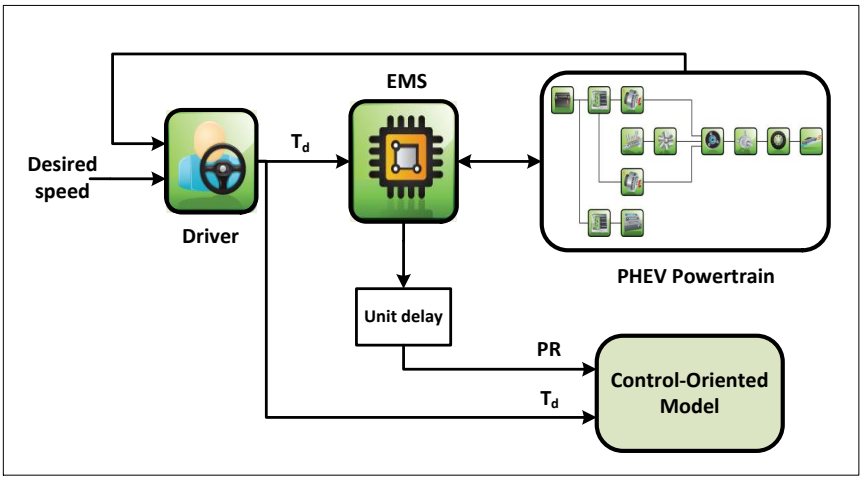

Figure 5.3: Schematic for validating the control-oriented model.

5.2 Control design

This section gives the mathematical steps required for the implementation of the controller. Fig. 5.5 clarifies the details of this controller schematically. The simulation model includes four main blocks: the environment, Eco-Cruise controller, EMS controller, and PHEV powertrain model.

Based on the vehicle's position, the inter-vehicle distance, preceding vehicle speed, and road grade are obtained and fed to the Eco-Cruise controller. The controller optimally calculates the wheel torque considering driving safety and energy cost. The EMS distributes the power demand between the two energy sources and determines the optimum torques of the engine and motor-generators. Finally, in the high-fidelity PHEV powertrain model, vehicle speed, fuel consumption, and SOC are calculated. This chapter investigates and compares four different control techniques for the Eco-Cruise controller: PMP, NMPC, LMPC, and PID.

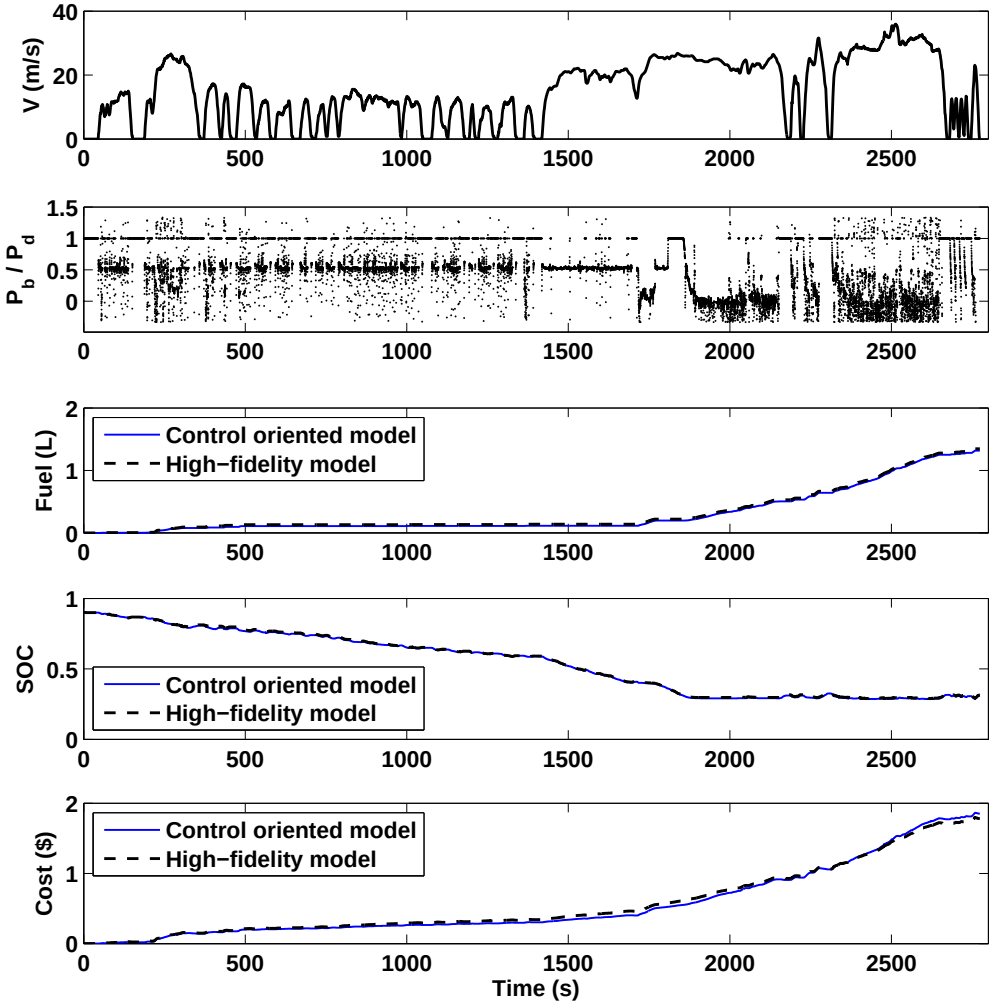

Figure 5.4: Simulation results for validating the control-oriented model.

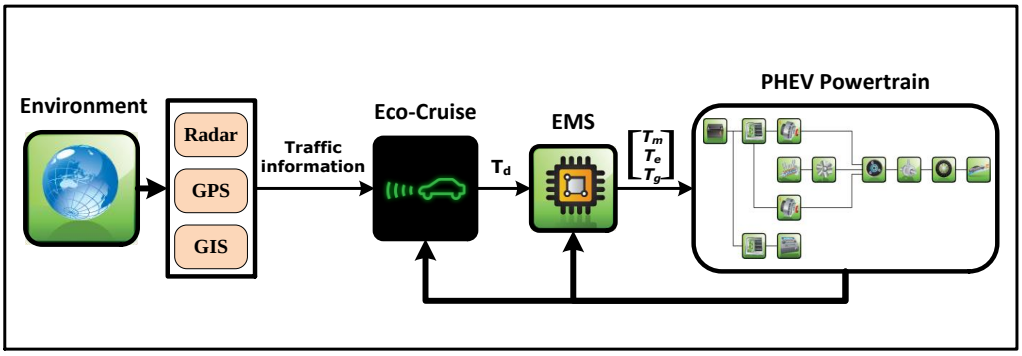

Figure 5.5: Schematic of Eco-Cruise controller for PHEVs.

5.2.1 Pontryagin's minimum principle

The PMP technique can provide a global optimum solution for an optimal control problem. The objectives of the controller are to minimize the total energy cost as well as to ensure the vehicle follows the preceding vehicle at a safe distance. The PMP technique requires future trip information to evaluate the global optimum solution. In other words, to calculate optimum speed trajectory, the position and velocity of preceding vehicle are considered to be known variables. In this case, the state variables of the system are reduced to $X = [x_h \; v_h]^T$. The optimal control problem is stated in Eq. 5.7:

$$J = \int_0^{t_f} \left(\omega_1 \, \delta^2(X) + \omega_2 \, Cost(X, u, PR)\right) dt \tag{5.7}$$
$$\dot{X} = \mathcal{F}(X, u)$$

The constraints of the system are:

$$v_{min} \leq v_h \leq v_{max}$$

$$u_{min} \leq u \leq u_{max}$$

where $PR = [\frac{P_b}{P_d}, \frac{P_e}{P_d}]$ is the power ratio between the two energy sources in previous time step, ω_1, ω_2 are respectively the weights of safety and cost in the objective function, and $\mathcal{F}$ represents the system model, which is described in the Section 5.1, (Eq. 5.1). ω_1 adaptively changes, considering the safe distance, as described in Eq. 5.8:

$$\omega_1 = \begin{cases} e^{\beta_1(\delta - 0.6\delta_{max})} & 0.6\,\delta_{max} \leq \delta \\ 1 & -0.6\,\delta_{max} < \delta < 0.6\,\delta_{max} \\ e^{\beta_2(-\delta - 0.6\delta_{max})} & \delta \leq -0.6\,\delta_{max} \end{cases} \tag{5.8}$$

The optimum input is obtained by:

$$\dot{X} = \mathcal{F}(X, u, t), \qquad X(0) = [0\ 0]^T \tag{5.9}$$

$$\dot{\lambda} = -\frac{\partial H}{\partial X}, \qquad \lambda(t_f) = [0\ 0]^T \tag{5.10}$$

$$u^\star = argmin\{H\} \tag{5.11}$$

These states and co-states equations are categorized as two-point boundary value problems, that the initial value of states and the final value of co-states are known. Here, the single shooting method is applied to solve this problem. First, the initial value of the co-states

is assumed. Next, Eq. 5.9- 5.11 are solved simultaneously. By comparing the final value of the co-states with the desired value, $\lambda(t_f) = [0\ 0]^T$, the co-states' initial values will be updated. This procedure continues until the final co-states converge to the desire value.

5.2.2 Nonlinear model predictive control

In this section, the Eco-Cruise controller is designed based on the NMPC approach to find the optimum wheel torque. In contrast to PMP formulation, the future position and speed of the preceding vehicle are unknown. Eq. 5.4 is applied to predict the acceleration of preceding vehicle. The problem formulation is given in Eq. 5.12:

$$
\begin{aligned}
J &= \int_0^{t_f} \left(\omega_1\, \delta^2(X) + \omega_2\, Cost(X, u, PR)\right)\ dt \qquad (5.12)\\
&\dot{X} = \mathcal{F}(X, u, \hat{a}_p)\\
&v_{min} \leq v_h \leq v_{max}\\
&u_{min} \leq u \leq u_{max}
\end{aligned}
$$

Using the control-oriented model, the states of the system are predicted for any given prediction horizon (τ), and consequently, the objective function is evaluated in each time step. To solve the above optimal control problem, an optimization algorithm should be taken into account. Many researches apply Particle Swarm Optimization (PSO) to solve the optimization inside MPC technique and calculate controlling commands [115–120].

PSO is a stochastic and population-based optimization search algorithm which is mainly inspired by social behavior of natural systems. Let us consider a large group of individuals

interacting within a social system, such as in flocks of birds or swarms of bees seeking a location with abundant food. In such system, each individual has two properties, a current position and a velocity. Also, each individual has knowledge of its best position so far plus the knowledge of the best-found position of the group. Now each individual can correct its properties (position and velocity) according to this information.

The PSO algorithm works based on the same principle as that of the social system described above. It simulates a simplified social system with moving particles in a multi-dimensional search space. Each particle is dynamically adjusting its own velocity and position in each step based on its history (its best position experienced so far) and those of its peers. Thus, PSO can obtain the global optimum in optimization problems as a result of a global behavior and interaction between all of the particles [121, 122].

Fig. 5.6 shows the schematic of particle position adjustment in the PSO algorithm. The velocity and position of each particle is updated in each iteration using Eq. 5.13, 5.14.

$$V_i^{t+1} = \Omega V_i^t + C_1 \Phi_1 (P_i - X_i) + C_2 \Phi_2 (P_g - X_i) \tag{5.13}$$

$$X_i^{t+1} = X_i^t + V_i^{t+1} \tag{5.14}$$

where, V, X are velocity and position of the particle, i is the index for particle number, t is the iteration number, ω is the inertia weight, Φ_1, Φ_2 are random numbers, P_i is the best position of the particle, and P_g is the best position of the swarm.

The meta-optimization is used to tune PSO algorithm. Figure 5.7 shows the schematic

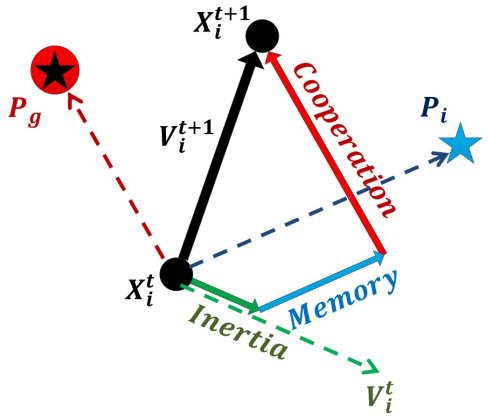

Figure 5.6: Velocity and position adjustment of a particle in the PSO algorithm.

of the meta-optimization. The optimization parameters are number of particles, maximum iteration, maximum particle velocity, and inertia weight. The objective is to minimize computation time of the PSO optimization. The DP algorithm is applied to solve the meta-optimization problem off-line and tune the PSO algorithm.

5.2.3 Linear model predictive control

To design and implement a LMPC for the Eco-cruise controller, the model is linearized and the objective function is derived in the quadratic form.

$$\mathcal{J} = \int_0^{t_f} \left(Q\left(v_h - v_{ref}\right)^2 + R\left(u - u_{ref}\right)^2 + \omega_1\, \delta^2 + \omega_2\, Cost \right)\, dt \tag{5.15}$$

$$\dot{X} = AX + Bu$$

$$v_{min} \leq v_h \leq v_{max}$$

$$u_{min} \leq u \leq u_{max}$$

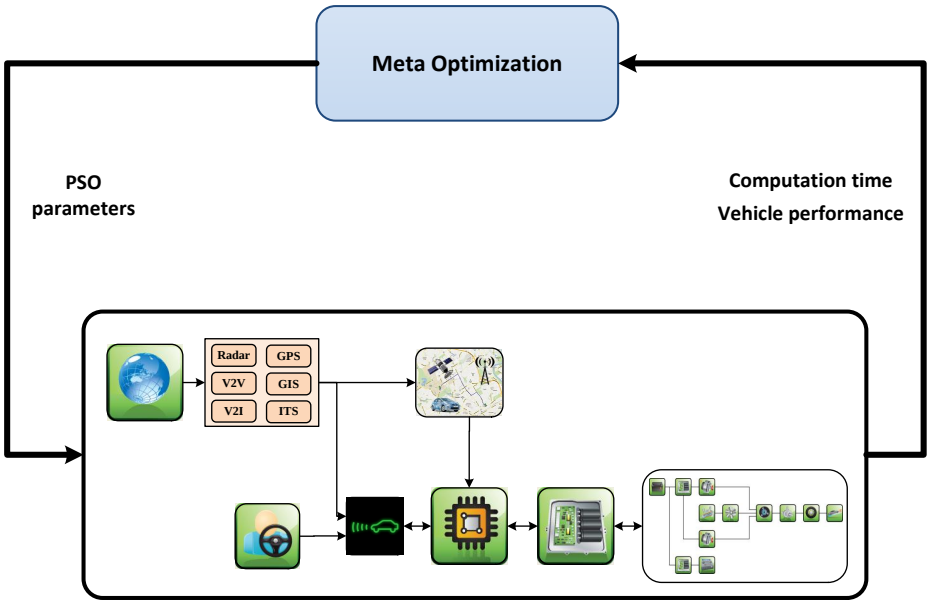

Figure 5.7: Schematic of the meta-optimization algorithm to tune PSO optimization.

where Q, R are positive definite matrices, and v_{ref}, u_{ref} are the reference values of speed and control input, respectively.

The objective is to follow the preceding vehicle, the reference speed is considered to be the speed of the preceding vehicle in previous time step. Reference control input is required input for tracking reference speed, and can be obtained from Eq. 5.1 based on $\dot{v}_h = 0$, $v_h = v_{ref}$. MATLAB toolbox is used to solve the optimal control problem.

5.3 MIL testing

To reliably check the authenticity and efficacy of the devised controller, here, the controller is evaluated for different driving scenarios, i.e. driving over a hill, and car-following.

5.3.1 Scenario-1: driving over a hill

In this scenario, it is assumed that the vehicle drives over a hill while there is no other preceding vehicle. We investigate the efficacy of the designed controller for finding the optimum speed trajectory that minimizes energy costs and neglect the inter-vehicle distance ($\omega_1 = 0$).

Since the hill length (travelling distance) is less than the All-Electric-Range (AER) of the baseline PHEV ($AER = 18km$), the propulsion of the vehicle is guaranteed by the electrical motor, and the resulting fuel consumption is zero. Thus, the entire driving range is considered as part of a longer trip (total trip distance = 40 km). The optimal power distribution is obtained by the designed A-ECMS strategy. In this strategy, two energy sources optimally propel the vehicle simultaneously and SOC is gradually decreased during the trip until it reaches the minimum value at the end of the trip ($SOC_{min} = 0.3$). In this case, the cost of both electrical and fuel consumption should be considered.

The PMP technique can find the global optimum solution of the cruise problem because it takes advantage of all trip data. The single shooting method is applied to solve the PMP problem. Fig. 5.8 shows the speed trajectory for different initial values of co-states. Based on the PMP technique, the final values of co-states should be zero at final time. The result of the single-shooting method is $\lambda(t_0) = [0.002,\ -0.2]$.

Fig. 5.9 shows the results obtained with the cruise controller. The simulation results verify that PMP leads to best energy economy. However, this technique is computationally expensive and cannot be implemented in real-time. Therefore, the optimum solution of PMP is used to evaluate the designed controllers.

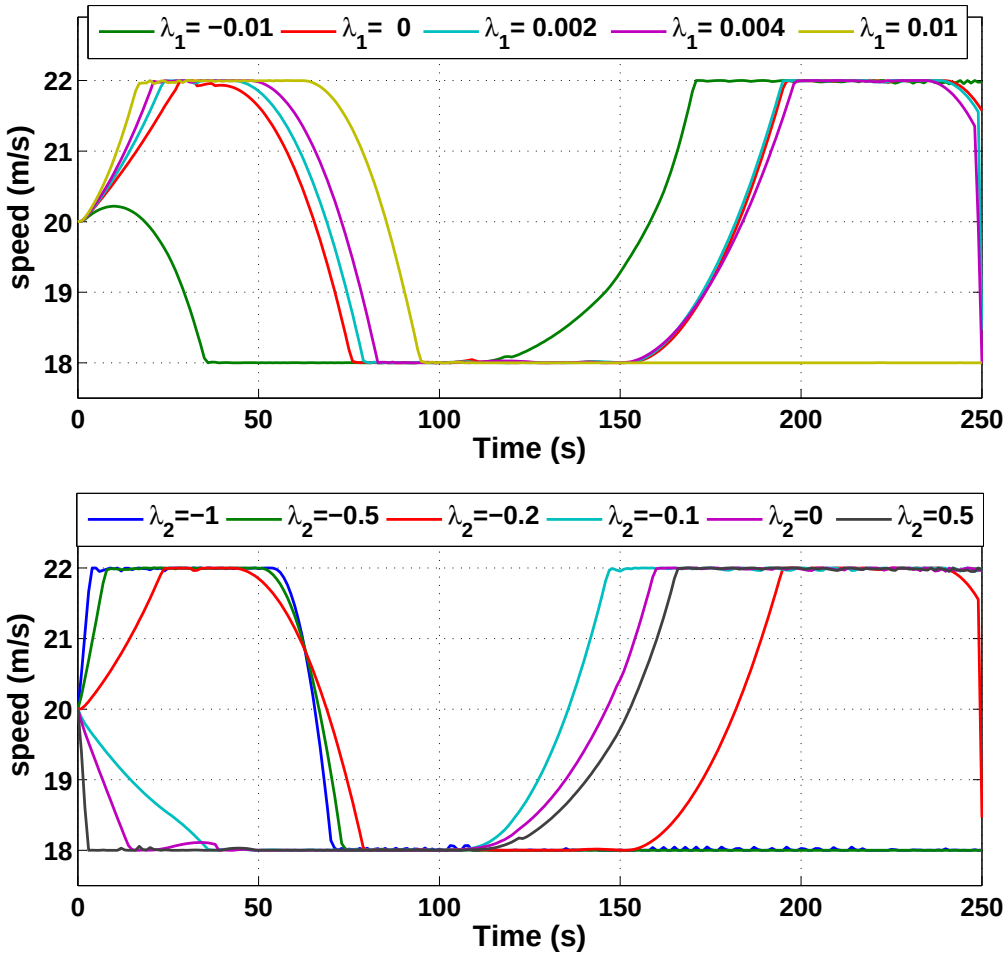

Figure 5.8: Cruise controller results for different initial co-states when driving over a hill.

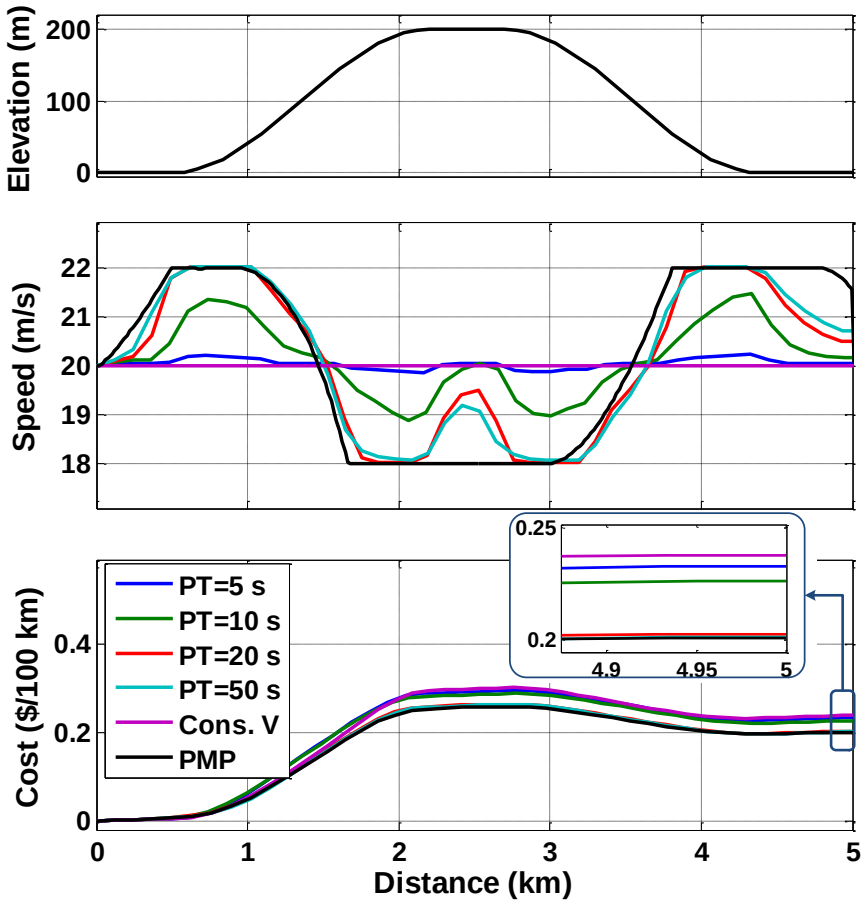

Figure 5.9: Cruise controller result when driving over a hill using A-ECMS strategy, with different prediction horizons.

It is determined that the prediction horizon is the most important controlling parameter affecting the performance of NMPC (see Table 5.1). Based on the results, it can be concluded that increasing the prediction horizon improves the performance of the NMPC. When the prediction horizon is low ($PT = 5s$ and $PT = 10s$), after ascending the uphill, the car speeds up, reaching the reference value (20 m/s) in a very short period of time. By increasing the prediction horizon ($PT = 20s$ and $PT = 50s$), the speed remains low until the vehicle descends the hill and uses gravity to increase both the acceleration and speed. These speed trajectories are closed to the optimum solution of the PMP technique.

On the other hand, increasing the prediction horizon increases the computational time, which is not appropriate for real-time implementation. Thus, the minimum acceptable prediction horizon is more desirable. In this case, the optimum prediction horizon is $PT = 20s$.

In general, the optimum prediction horizon depends on the dynamics of the system and variation rate of the inputs. In this problem, the prediction horizon should be set according to the variation rate of trip data such as road grade or traffic speed. To show the effect of trip data on prediction horizon, we repeat the simulation on a shorter hill while all other parameters remain constant. The results of the simulation are shown in Fig. 5.10.

The simulation results show that the optimum prediction horizon is reduced to $PT = 10s$. In other words, by decreasing the distance between uphill and downhill, the controller with smaller prediction horizon (10s) can still see the upcoming changes (going down-hill), and maintain the speed in a low rate to improve fuel economy. The Eco-Cruise controllers results with different prediction time are shown in Table 5.1.

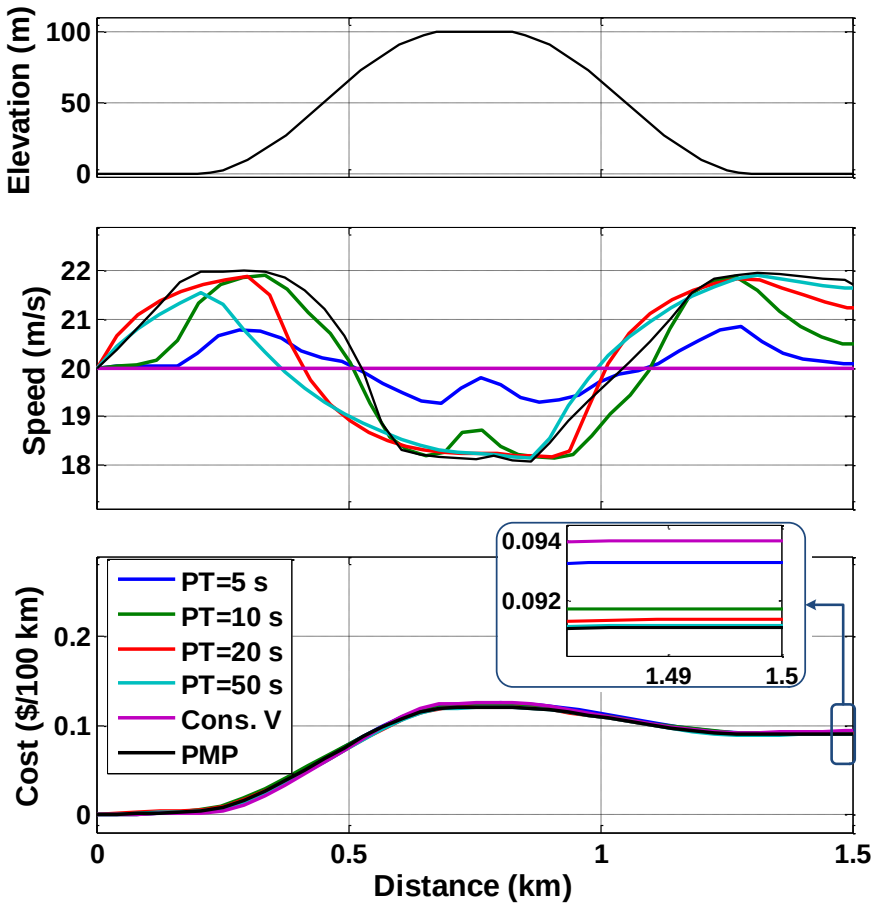

Figure 5.10: Cruise controller result when driving over a hill using A-ECMS strategy, with a distance of 1.5 km.

Table 5.1: Improvement of energy cost for different Eco-Cruise controllers compared to cruise with constant speed.

Hill number (length)	PT=5	PT=10	PT=20	PT=50	PMP
Hill-1 (5 km)	2.5 %	5.0 %	15.1 %	15.5 %	15.7 %
Hill-2 (1.5 km)	0.7 %	2.6 %	2.8 %	3.0 %	3.1 %

Table 5.2: Parameters of car-following model.

Traffic condition	L_0	h	δ_{max}
Congested low traffic flow	2	4	1
Uncongested low traffic flow	4	8	3

In the case of following a preceding vehicle, calculation of the optimum value of prediction horizon length depends on the time between acceleration, cruise and deceleration of the preceding vehicle. To predict all future events in MPC, the prediction horizon should be equal to a travelling time. Unfortunately, this makes the controller computationally expensive, and cannot be implemented in a real-time manner. Consequently, the remainder of this chapter will consider that the prediction horizon is equal to $PT = 20s$.

5.3.2 Scenario-2: car-following

This section presents the simulation results for energy-optimal controller with all three modules: Trip Planning, Route-based EMS, and Eco-Cruise controller. The objective of Eco-Cruise controller is to maintain a safe distance from the preceding vehicle while considering energy cost.

The safe distance between vehicles depends on speed and traffic conditions. The desired inter-vehicle distance is obtained based on the stationary distance and headway time in Eq. 5.2. This thesis considers two different traffic conditions, congested and uncongested low traffic flow, and obtained optimum traffic parameters from [123], as reported in Table 5.2.

The results of the NMPC controller are compared with those of two other controllers,

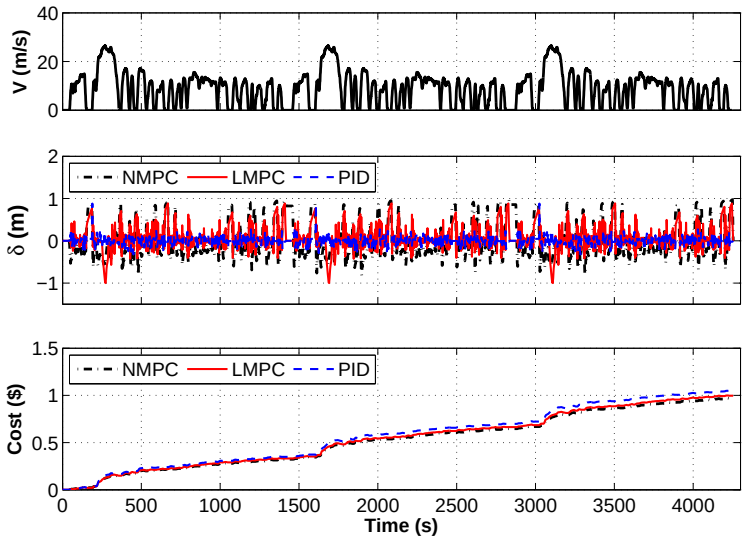

Figure 5.11: Car-following simulation results in congested traffic conditions for following 3xUDDS cycle.

the LMPC and PID controllers. For an unbiased comparison, a fine-tuning procedure is carried out on the controllers.

Fig. 5.11- 5.13 show the simulation results for following a vehicle with different speed trajectories in congested low traffic flow. All controllers follow the preceding vehicle with the acceptable distance error, $(-1 < \delta < 1)$, but the control performances are all different. The results show that the NMPC yields the lowest energy cost, compared to the other controllers.

Fig. 5.14- 5.16 show the results of Eco-Cruise controller for both congested and uncongested conditions. In the congested condition, the acceptable inter-vehicle distance error is relatively small, $\delta_{max} = 1$, and the cruise controller primarily considers safety as an objective function. In the uncongested condition, the acceptable inter-vehicle distance error

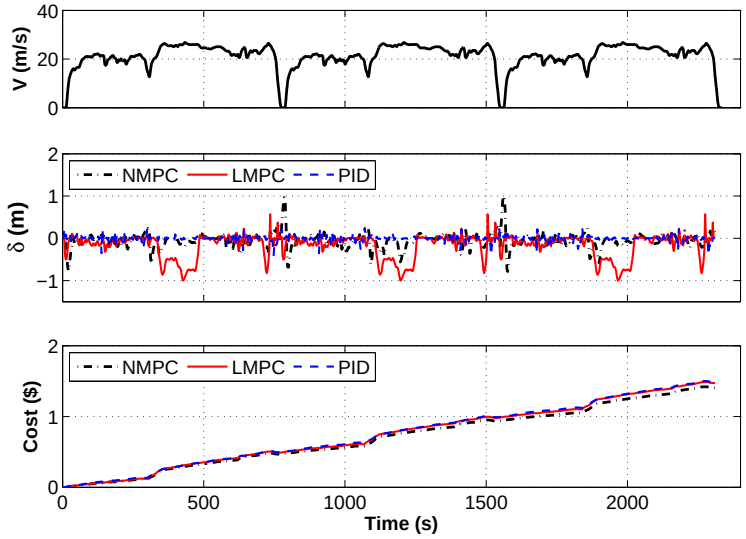

Figure 5.12: Car-following simulation results in congested traffic conditions for following 3xHWFET cycle.

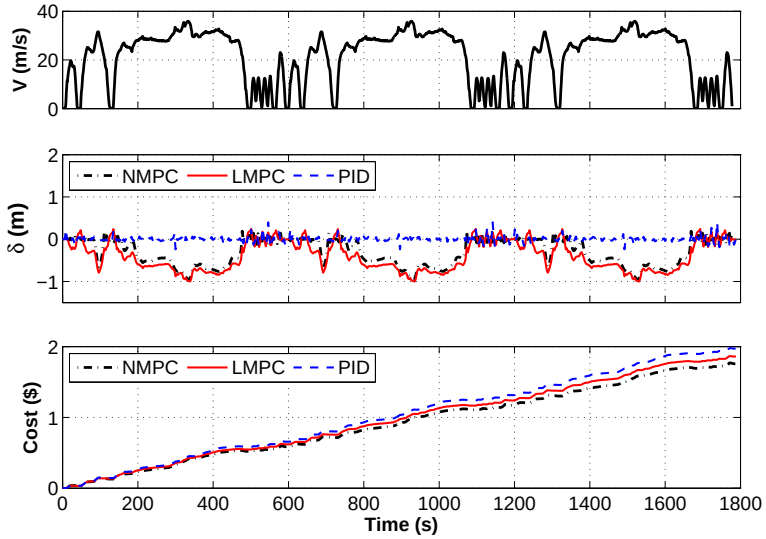

Figure 5.13: Car-following simulation results in congested traffic conditions for following 3xSFTP-US06 cycle.

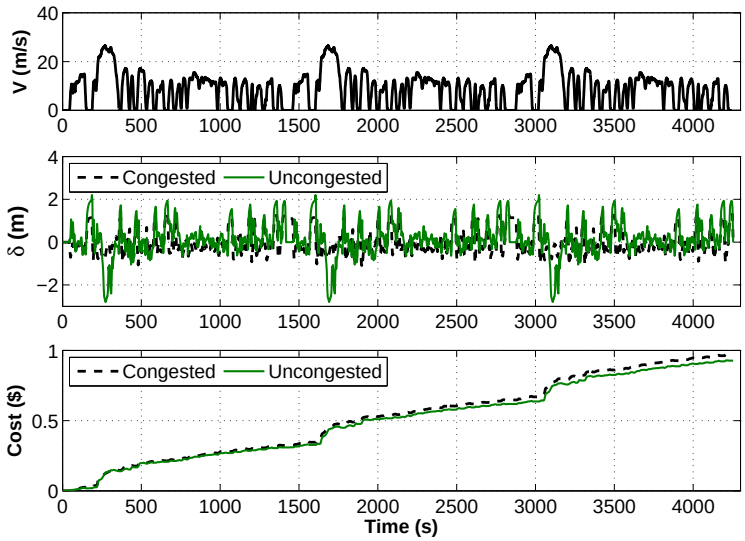

Figure 5.14: Camparison of Eco-Cruise controller results in congested and uncongested traffic conditions for following 3xUDDS cycle.

is more than the congested one ($\delta_{max} = 3$). Therefore, the cruise controller can adjust the speed cost effectively by accepting a small inter-vehicle distance error, while improving the performance of the vehicle.

Until now, the Route-based EMS is applied to calculate optimal power distribution. To find the effect of each module in energy-optimal control scheme, the cruise controllers are applied to the rule-based EMS of the Autonomie model. The simulation results for different control strategies under different conditions are shown in Table 5.3.

The results show that the NMPC controller can improve energy costs by up to 20% while maintaining driving safety. This improvement is achieved through optimizing the speed profile and reducing the acceleration of the vehicle. Fig. 5.17 illustrates the acceleration distribution of different control strategies for the combined UDDS, HWFET, and SFTP

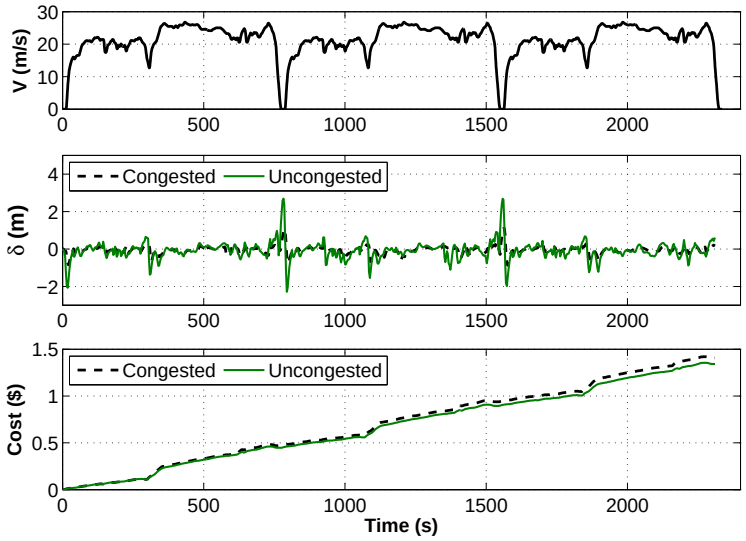

Figure 5.15: Camparison of Eco-Cruise controller results in congested and uncongested traffic conditions for following 3xHWFET cycle.

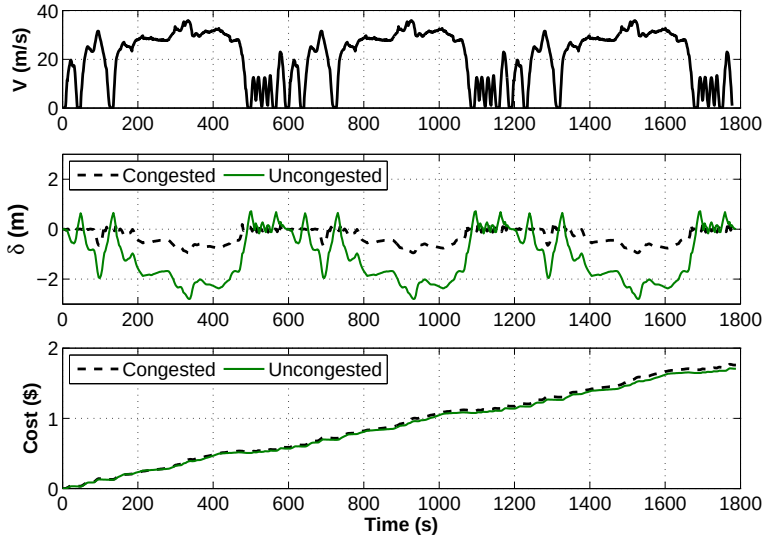

Figure 5.16: Camparison of Eco-Cruise controller results in congested and uncongested traffic conditions for following 3xSFTP-US06 cycle.

Table 5.3: Fuel economy for different cruise controllers.

Cruise controller	EMS	Traffic condition	Fuel consumption (MPG)		
			3xUDDS	3xHWFET	3xSFTP
PID	Route-based EMS	Congested	101	89	51
		Uncongested	101	89	51
	Autonomie controller	Congested	93	75	47
		Uncongested	93	75	47
LMPC	Route-based EMS	Congested	108	90	54
		Uncongested	114	95	58
	Autonomie controller	Congested	96	77	51
		Uncongested	102	81	56
NMPC	Route-based EMS	Congested	111	95	58
		Uncongested	118	100	60
	Autonomie controller	Congested	97	78	54
		Uncongested	107	85	63

drive cycles. NMPC has smaller acceleration than the PID controller. In congested traffic conditions the acceleration is increased. That observation justifies the fact that, in such a condition, the cruise controller function mainly focuses on vehicle safety and cannot widely adjust its speed.

5.4 HIL testing

Real-time HIL testing promises an effective approach for validation of vehicle control systems. There has been increasing need for real-time simulation and support for HIL in automotive applications. Section 3.6 described the HIL test platform. It consists of a real-time simulator, prototype ECU, and interface computer. These components are

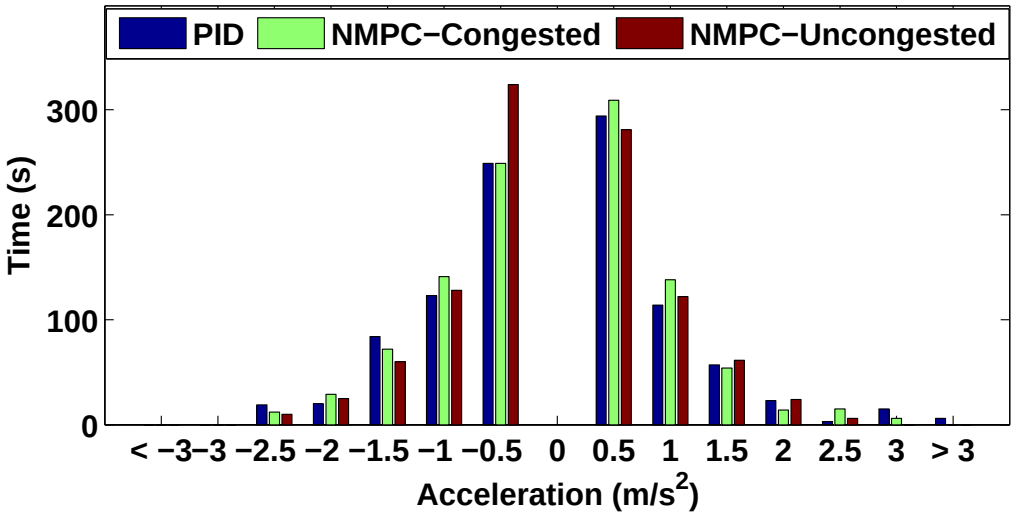

Figure 5.17: Acceleration distribution of different cruise control schemes when following combined UDDS, HWFET, and SFTP-US06 cycles.

connected through a CAN bus. The prototype ECU executes the controller and obtains optimal controller commands. The real-time simulator runs the high-fidelity model and calculates powertrain variables. These variables are fed back to the controller. An interface computer is used to set up an HIL test, program the ECU and simulator, and record the desired outputs and variables.

5.4.1 Controller prototyping

Figure 5.18, 5.19 show the cruise controller architectures of Toyota Prius (from TIS documents [124]) and the designed energy-optimal controller. Both controllers use input signals from radar and feedback signals from powertrain, and send command signals to energy management ECU. The main difference between these two controllers is the control

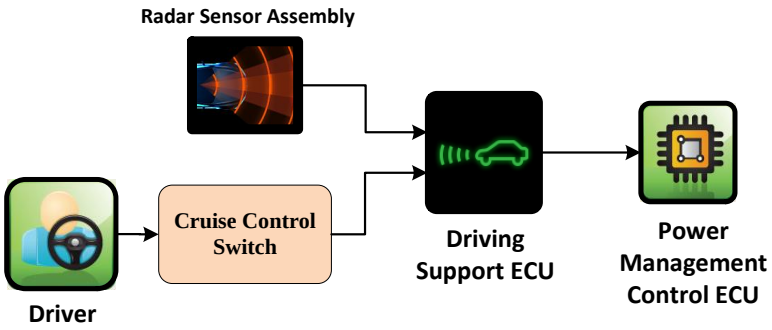

Figure 5.18: Schematic the Prius Cruise controller from TIS document [124].

Table 5.4: Specification of the input and output signals of the Eco-Cruise controller.

CAN signal	Variable name	CAN ID	bit length
ECU inputs	Speed	101	32
	Intervehicle distance	180	16
	Acceleration of the preceding vehicle	181	16
	Speed of the preceding vehicle	182	16
	Rate of SOC	160	16
	Rate of fuel	161	16
ECU outputs	Demand torque	140	32

techniques.

Tabale 5.4 characterizes the CAN communication signals between the simulator and prototype ECU. It should be noted that it is assumed that the raw radar signals are pre-processed by another algorithm. Therefore, intervehicle distance, speed, and acceleration of preceding vehicle are available for the Eco-Cruise controller.

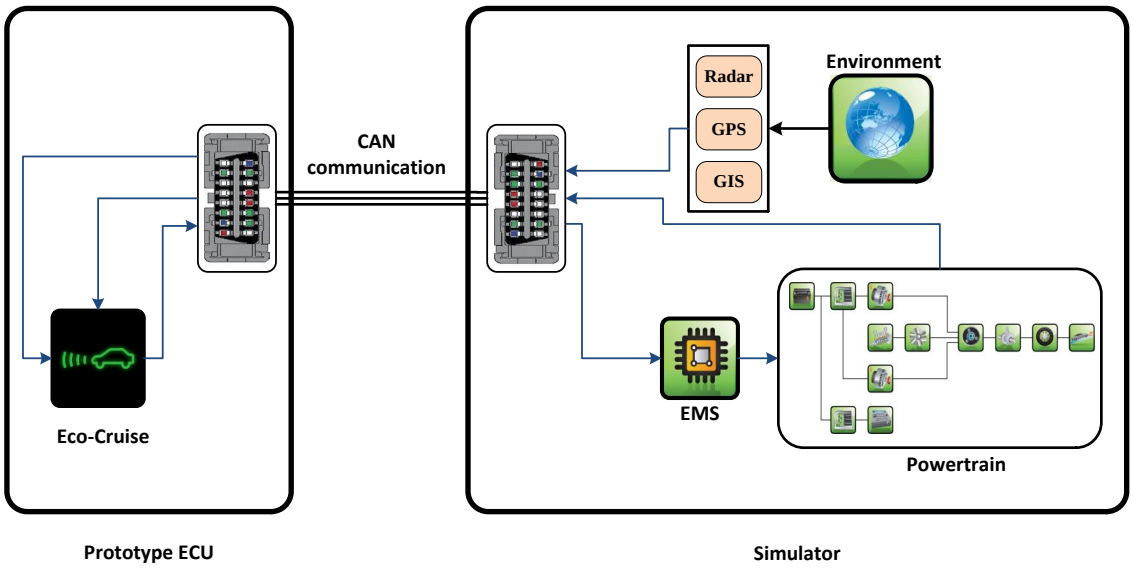

Figure 5.19: Schematic of the Simulink models for HIL testing of the Eco-Cruise controller.

5.4.2 HIL testing results

The HIL and MIL results of the NMPC controller for different driving cycles are shown in Fig. 5.20 and 5.21. The HIL and MIL results are in complete agreement. The HIL results show that the turnaround-time in the prototype ECU is less than 55 μs. The desired sample time in the Prius adaptive cruise ECU is 1 ms. The HIL tests verify that the turnaround-time is less than the desired time step. Hence, the NMPC controller can be implemented in real-time.

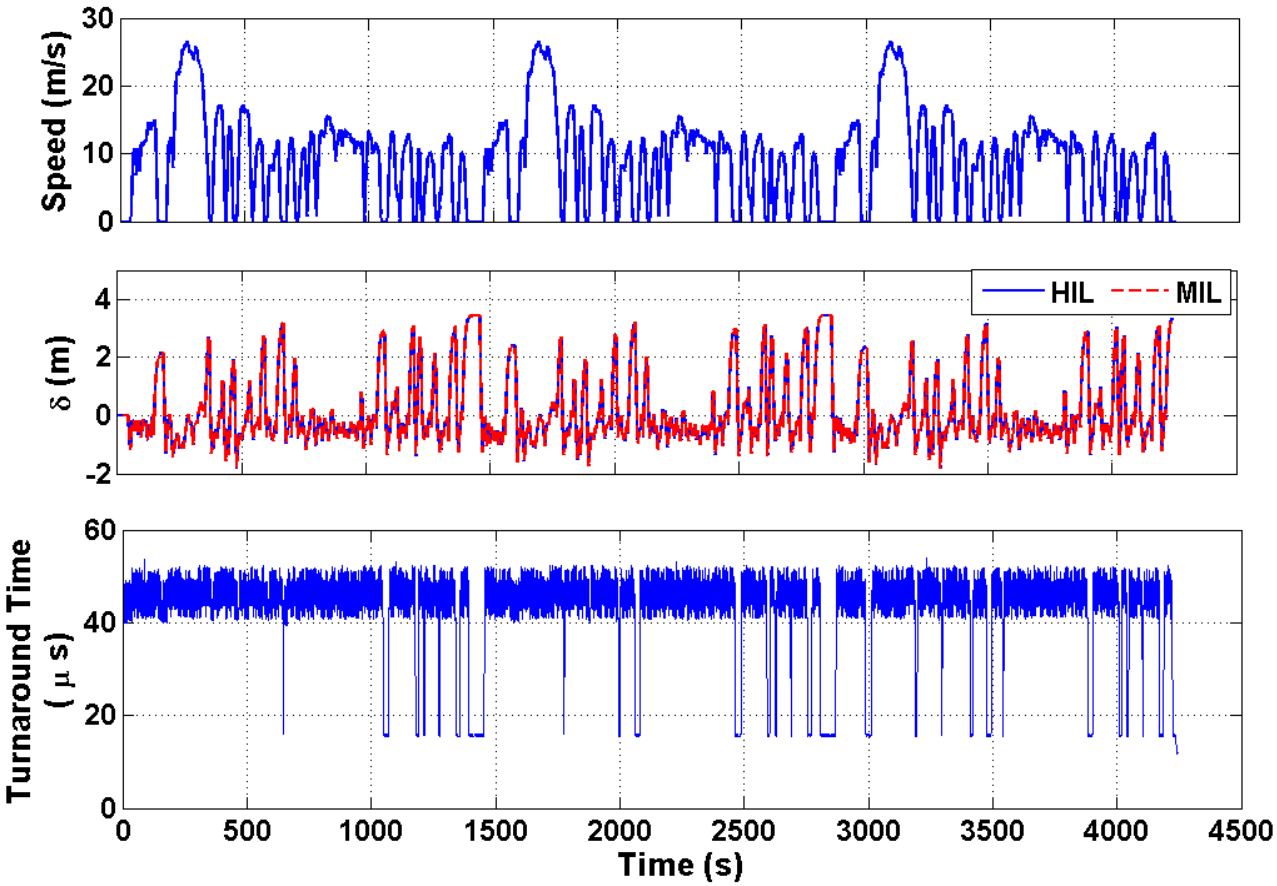

Figure 5.20: HIL test results for the NMPC Eco-Cruise controller following the 3xUDDS driving schedule.

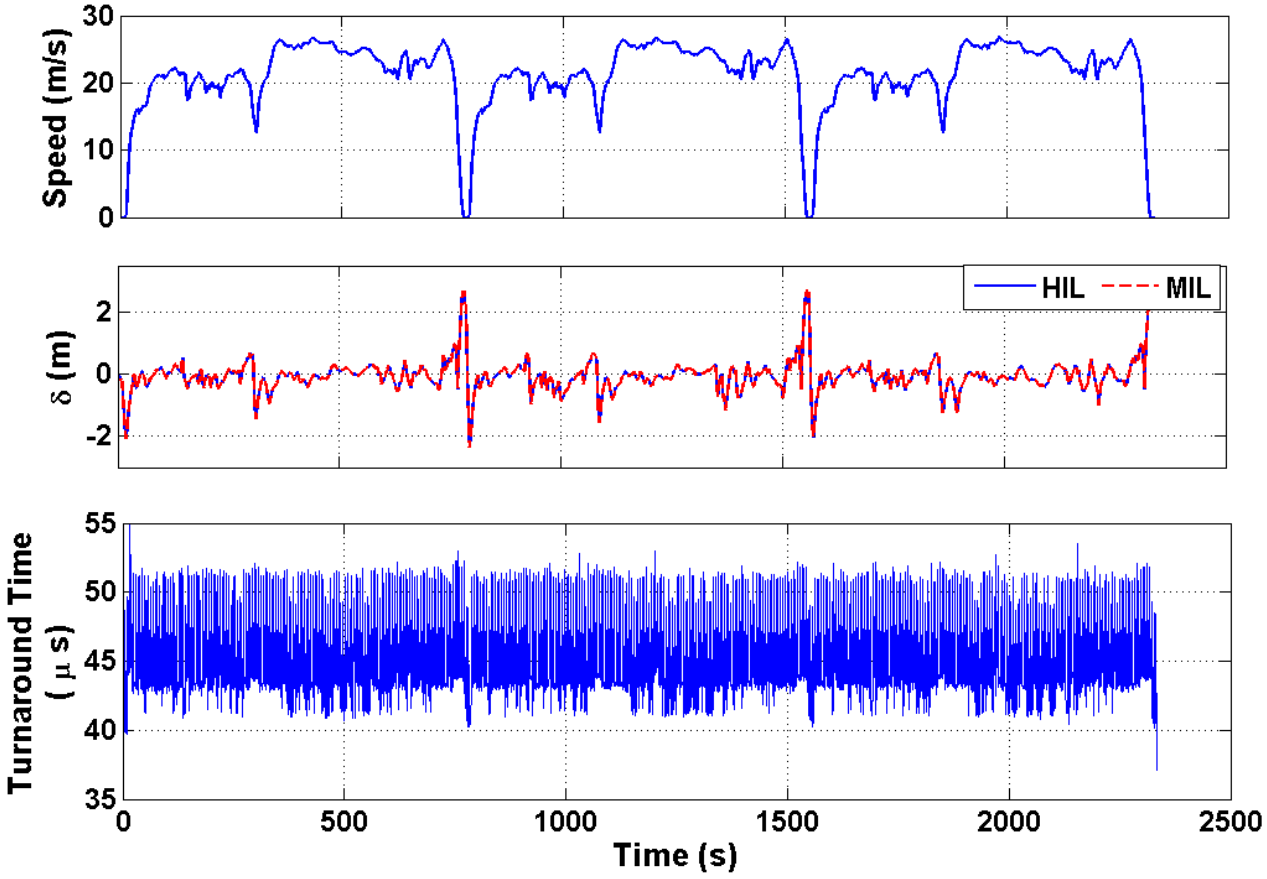

Figure 5.21: HIL test results for the NMPC Eco-Cruise controller following the 3xHWFET driving schedule.

5.5 Summary

In this chapter, an Eco-Cruise controller was designed for a PHEV based on nonlinear model predictive control. The controller optimally adjusts the vehicle speed to enhance driving safety and minimizes total energy costs.

First, the control-oriented model is developed and validated using the high-fidelity PHEV model. The simulation results show that the control-oriented model can predict vehicle performance with an error of less than 3.6%. Thereafter, the model is used at the heart of the NMPC technique to design the Eco-Cruise controller. PMP technique is applied to find the global optimum solution of the cruise control problem. To endorse the efficacy of the NMPC, its performance is evaluated against the PID, LMPC, and PMP controllers under different driving conditions.

The results indicate that for a vehicle driving over a hill, the Eco-Cruise controller takes advantage of the trip information to speed up the vehicle before the uphill, which improves the energy cost up to 15%. The results show that NMPC results are in agreement with the global optimum solution.

For the car-following scenario, the results show that the NMPC technique outperforms the PID and LMPC controllers. It is found that the performance of the Eco-Cruise controller depends on traffic conditions. In congested low traffic flow conditions, the cruise controller mainly considers the safety criteria and, as a result, the bound of allowable control command is very narrow due to small inter-vehicle distance. For uncongested low traffic flow conditions, the acceptable intervehicle distance error is relatively large, which enables the controller to improve the performance while considering the safety criterion.

The feedback of the simulation revealed that NMPC shows promising results and can improve energy costs of a vehicle by up to 20%.

HIL test results show that the turnaround-time is less than 55 μs, and the NMPC-based Eco-Cruise controller can be implemented in real-time.

Chapter 6

Conclusion

This thesis has described the development of an energy-optimal controller for a PHEV. The controller consists of three main modules: the Trip Planning, Route-based EMS, and Eco-cruise control. The Trip Planning module takes advantage of trip information to predict future speed trajectory and optimizes SOC profiles to minimize total energy cost. Route-based EMS calculates optimal power distribution between the battery and engine. The Eco-Cruise controller optimally adjusts speeds in real-time to improve diving safety and total energy cost.

The control-oriented models are developed for each module, and validated against the high-fidelity PHEV model of the Toyota Prius in Autonomie. Then, the controllers are evaluated using MIL and HIL testing.

In Trip Planning, the RCO algorithm is developed based on data clustering technique. The results are evaluated against DP results. The RCO algorithm is very promising and

can find the optimum SOC profile with less than 2.4% error with respect to the DP results.

Route-based EMS is developed based on ECMS strategy. The controller performance compared against CDCS, Manual CDCS, rule-based, PMP, and MPC techniques under various driving conditions. The Route-based EMS results are in agreement with the results from PMP and MPC techniques. They can improve fuel consumption up to 11% compared to rule-based controllers. The designed controller is evaluated using HIL testing and showed a turnaround time of less than 25 μs. Thus, the devised controller is capable of real-time implementation in the ECU hardware.

The Eco-Cruise controller is designed based on the NMPC technique. To evaluate the efficacy of the controller, its performance is compared against the PID, LMPC, and PMP controllers under variety of driving conditions. The NMPC results are in agreement with the global optimum solution of PMP controller. It is also observed that the NMPC technique can improve energy economy by up to 20% compared to the PID controllers. HIL test results show that the turnaround time of the controller is less than 55 μs, and then the real-time Eco-Cruise controller is validated.

6.1 Summary of contributions

This section summarizes the major contributions of the research.

1. Design of a new algorithm for Trip Planning, which

    - Employs future driving conditions in a real-time optimization; and

- Incorporates a novel RCO algorithm that is feasible for real-time implementation.

2. Design of a new Route-based EMS strategy for a power-split PHEV, which include
   - Development of a novel architecture that use trip data to obtain a nearly optimal solution; and
   - Implementation in real-time.
3. Development of a novel technique for an Eco-Cruise controller, which
   - Considers both fuel consumption and safety in the cruise controller;
   - Is independent from the EMS system; and
   - Implements in real-time.

6.2 Future work

This thesis demonstrates the performance of an energy-optimal controller for improving total energy cost and driving safety through MIL and HIL simulations. However, further research is needed to expand this study. This section provides some recommended future work for each control system.

1. Trip Planning module:
   - Improve the control-oriented model by considering the engine transient effect;

- Include traffic light time schedules in the traffic model; and
- Improve the robustness of the designed controller in cases of data loss and missed prediction situations.

2. Route-based EMS:

   - Improve the controller performance using short-horizon speed prediction; and
   - Improve the robustness of the control system.

3. Eco-Cruise controller:

   - Include a radar model to make the high-fidelity model more accurate;
   - Add powertrain delay into the control-oriented model; and
   - Improve the robustness of the control system against disturbances.

References

[1] N. Unger, T. Bond, J. Wang, D. Koch, S. Menon, D. Shindell, and S. Bauer, "Attribution of climate forcing to economic sectors.," in *National Academy of Sciences of the United States of America*, 2010.

[2] W. Reinhardt and A. Hadrovic, "Roadmap on ict for energy efficiency," tech. rep., 2010.

[3] A. Taghavipour, "Real-time optimal energy management system for plug-in hybrid electric vehicles," *PhD thesis, University of Waterloo*, 2014.

[4] M. Chehresaz, "Modeling and design optimization of plug-in hybrid electric vehicle powertrains," *Master's thesis, University of Waterloo*, 2013.

[5] L. Shen and M. Huang, "Assessing Dynamic Neural Networks for Travel Time Prediction," in *Applied Informatics and Communication International Conference*, pp. 469–477, 2011.

[6] B. Park, K. Malakorn, and J. Lee, "Quantifying Benefits of Cooperative Adaptive Cruise Control Toward Sustainable Transportation System," Tech. Rep. May, Center for Transportation Studies, University of Virginia, Charlottesville, VA, 2011.

[7] J. Park, Z. Chen, L. Kiliaris, M. Kuang, M. A. Masrur, A. M. Phillips, and Y. L. Murphey, "Intelligent Vehicle Power Control Based on Machine Learning of Optimal Control Parameters and Prediction of Road Type and Traffic Congestion," *IEEE Transactions on Vehicular Technology*, vol. 58, no. 9, pp. 4741–4756, 2009.

[8] T. V. Keulen, B. D. Jager, D. Foster, and M. Steinbuch, "Velocity Trajectory Optimization in Hybrid Electric Trucks," in *American Control Conference*, pp. 5074–5079, IEEE, 2010.

[9] T. V. Keulen, B. D. Jager, and M. Steinbuch, "Optimal Trajectories for Vehicles with Energy Recovery Options," in *18th IFAC World Congress Milano*, pp. 3831–3836, 2011.

[10] T. V. Keulen, G. Naus, B. D. Jager, van de Molengraft, M. Steinbuch, and E. Aneke, "Predictive Cruise Control in Hybrid Electric Vehicles," *World Electric vehicle Journal*, vol. 3, no. 1, pp. 1–11, 2009.

[11] T. V. Keulen, B. de Jager, A. F. A. Serrarens, and M. Steinbuch, "Optimal Energy Management in Hybrid Electric Trucks Using Route Information," *Oil & Gas Science and Technology*, vol. 65, pp. 103–113, Aug. 2010.

[12] Q. Gong, Y. Li, and Z.-r. Peng, "Trip-Based Optimal Power Management of Plug-in Hybrid Electric Vehicles," *IEEE Transactions on Vehicular Technology*, vol. 57, no. 6, pp. 3393–3401, 2008.

[13] Q. Gong, Y. Li, and Z.-r. Peng, "Optimal power management of plug-in HEV with intelligent transportation system," in *Advanced intelligent mechatronics, 2007 IEEE/ASME international conference on*, pp. 1–6, IEEE, 2007.

[14] Q. Gong, P. Tulpule, V. Marano, and G. Rizzoni, "The Role of ITS in PHEV Performance Improvement," in *American Control Conference*, pp. 2119–2124, IEEE, 2011.

[15] Q. Gong, Y. Li, and Z.-r. Peng, "Optimal power management of plug-in HEV with intelligent transportation system," in *Advanced intelligent mechatronics, 2007 IEEE/ASME international conference on*, pp. 1–6, IEEE, 2007.

[16] Y. Bin, Y. Li, and Q. Gong, "Multi-Information Integrated Trip Specific Optimal Power Management for Plug-In Hybrid Electric Vehicles," in *American Control Conference*, pp. 4607–4612, IEEE, 2009.

[17] G.-e. Katsargyri, I. V. Kolmanovsky, J. Michelini, M. L. Kuang, A. M. Phillips, M. Rinehart, and M. A. Dahleh, "Path dependent receding horizon control policies for Hybrid Electric Vehicles," in *American Control Conference*, pp. 4613–4617, IEEE, July 2009.

[18] G.-e. Katsargyri, *Optimally Controlling Hybrid Electric Vehicles using Path Forecasting*. Master of science, Massachusetts Institute Of Technology, 2008.

[19] A. Rousseau, S. Pagerit, and D. W. Gao, "Plug-in Hybrid Electric Vehicle Control Strategy Parameter Optimization," *Journal of Asian Electric Vehicle*, vol. 6, no. 2, pp. 1125–1133, 2008.

[20] C.-C. Lin, S. Jeon, H. Peng, J. Moo Lee, and J. Moo, "Driving Pattern Recognition for Control of Hybrid Electric Trucks," *Vehicle System Dynamics: International Journal of Vehicle Mechanics and Mobility*, vol. 42, pp. 41–58, Dec. 2004.

[21] S. Bashash, A. Arbor, and S. J. Moura, "Battery Health-conscious Plug-in Hybrid Electric Vehicle Grid Demand Prediction," in *ASME 2010 Dynamic Systems and Control Conference*, pp. 1–9, 2010.

[22] S. J. Moura, J. L. Stein, and H. K. Fathy, "Battery-Health Conscious Power Management in Plug-In Hybrid Electric Vehicles via Electrochemical Modeling and Stochastic Control," *IEEE Transactions on Control Systems Technology*, vol. 1, no. 3, pp. 1–16, 2013.

[23] S. J. Moura, H. K. Fathy, D. S. Callaway, and J. L. Stein, "A Stochastic Optimal Control Approach for Power Management in Plug-In Hybrid Electric Vehicles," *IEEE Transactions on Control Systems Technology*, vol. 19, no. 3, pp. 545–555, 2011.

[24] Y. L. Murphey, "Intelligent Vehicle Power Management : An Overview," in *Computational Intelligence in Automotive Applications SE - 10*, vol. 190, pp. 169–190, 2008.

[25] C. Manzie, H. Watson, and S. Halgamuge, "Fuel economy improvements for urban driving: Hybrid vs. intelligent vehicles," *Transportation Research Part C: Emerging Technologies*, vol. 15, pp. 1–16, Feb. 2007.

[26] T. S. Kim, C. Manzie, and R. Sharma, "Two-Stage Optimal Control of a Parallel Hybrid Vehicle with Traffic Preview," *The 18th IFAC World Congress*, no. 2, pp. 2115–2120, 2011.

[27] R. Bartholomaeus, M. Klingner, and M. Lehnert, "Prediction of power demand for hybrid vehicles operating in fixed-route service," in *Proceedings of the 17th IFAC World Congress*, pp. 5640–5645, 2008.

[28] S. Ichikawa, Y. Yokoi, S. Doki, S. Okuma, T. Naitou, T. Shiimado, and N. Miki, "Novel energy management system for hybrid electric vehicles utilizing car navigation over a commuting route," in *Intelligent Vehicles Symposium, 2004 IEEE*, pp. 161–166, IEEE, 2004.

[29] J. Gonder, T. Markel, A. Simpson, and M. Thornton, "Using GPS Travel Data to Assess the Real World Driving Energy Use of Plug-In Hybrid Electric Vehicles (PHEVs)," *Transportation Research Record*, no. 2017, pp. 26–32, 2007.

[30] J. Gonder, "Route-Based Control of Hybrid Electric Vehicles," *SAE SP*, vol. 2199, no. January, p. 21, 2008.

[31] L. Serrao, S. Onori, and G. Rizzoni, "A Comparative Analysis of Energy Management Strategies for Hybrid Electric Vehicles," *Journal of Dynamic Systems, Measurement, and Control*, vol. 133, no. 3, p. 031012, 2011.

[32] C.-c. Lin, H. Peng, J. Grizzle, J. Liu, and M. Busdiecker, "Control System Development for an Advanced-Technology Medium-Duty Hybrid Electric Truck," *SAE paper*, vol. 20, no. November 2003, 2003.

[33] C.-c. Lin, H. Peng, and J. Grizzle, "Power management strategy for a parallel hybrid electric truck," *IEEE Transactions on Control Systems Technology*, vol. 11, pp. 839–849, Nov. 2003.

[34] J. Gonder and T. Markel, "Energy Management Strategies for Plug-In Hybrid Electric Vehicles," *Energy*, vol. 1, p. 0290, 2007.

[35] M. P. O. Keefe and T. Markel, "Dynamic Programming Applied to Investigate Energy Management Strategies for a Plug-in HEV," tech. rep., National Renewable Energy Laboratory, 2006.

[36] R. S. Razavian, *Design and Hardware-in-the-Loop Testing of Optimal Controllers for Hybrid Electric Powertrains*. PhD thesis, University of Waterloo, 2012.

[37] R. S. Razavian, A. Taghavipour, N. L. Azad, and J. McPhee, "Design and evaluation of a real-time fuel-optimal control system for series hybrid electric vehicles," *International Journal of Electric and Hybrid Vehicles*, vol. 4, no. 3, pp. 260–288, 2012.

[38] S. Ebbesen, P. Elbert, and L. Guzzella, "Battery State-of-Health Perceptive Energy Management for Hybrid Electric Vehicles," *IEEE Transactions on Vehicular Technology*, vol. 61, pp. 2893–2900, Sept. 2012.

[39] L. Re, P. Ortner, and D. Alberer, "Chances and Challenges in Automotive Predictive Control," pp. 1–22, 2010.

[40] L. Wang, *Model Predictive Control System Design and Implementation Using MATLAB* . Springer, 2009.

[41] T. S. Kim, C. Manzie, and R. Sharma, "Model Predictive Control of Velocity and Torque Split in a Parallel Hybrid Vehicle," in *Systems, Man and Cybernetics, IEEE International Conference on*, no. October, pp. 2014–2019, IEEE, 2009.

[42] H. Borhan, A. Vahidi, A. M. Phillips, and I. V. Kolmanovsky, "Predictive Energy Management of a Power-Split Hybrid Electric Vehicle," in *American Control Conference*, pp. 3970–3976, IEEE, 2009.

[43] H. Borhan, A. Vahidi, A. M. Phillips, M. Kuang, I. V. Kolmanovsky, and S. D. Cairano, "MPC-Based Energy Management of a Power-Split Hybrid Electric Vehicle," *IEEE Transactions on Control Systems Technology*, vol. 20, no. 3, pp. 593–603, 2012.

[44] A. Taghavipour, N. L. Azad, and J. McPhee, "An Optimal Power Management Strategy for Power Split Plug-in Hybrid Electric Vehicles," *International Journal of Vehicle Design*, vol. 60, no. 3, pp. 286–304, 2012.

[45] A. Taghavipour, R. Masoudi, N. L. A. Azad, and J. McPhee, "High-Fidelity Modeling of a Power-Split Plug-In Hybrid Electric Powertrain for Control Performance Evaluation," in *ASME 2013 International Design Engineering Technical Conferences and Computers and Information in Engineering Conference*, pp. 1–9, 2013.

[46] J. Liu and H. Peng, "Control optimization for a power-split hybrid vehicle," in *American Control Conference*, p. 6 pp., IEEE, 2006.

[47] J. Liu and H. Peng, "Modeling and Control of a Power-Split Hybrid Vehicle," *IEEE Transactions on Control Systems Technology*, vol. 16, no. 6, pp. 1242–1251, 2008.

[48] L. Serrao and G. Rizzoni, "Optimal control of power split for a hybrid electric refuse vehicle," in *American Control Conference*, pp. 4498–4503, IEEE, June 2008.

[49] P. Pisu and G. Rizzoni, "A Comparative Study Of Supervisory Control Strategies for Hybrid Electric Vehicles," *IEEE Transactions on Control Systems Technology*, vol. 15, no. 3, pp. 506–518, 2007.

[50] G. Paganelli, T. M. Guerra, S. Delprat, J.-J. Santin, M. Delhom, and E. Combes, "Simulation and assessment of power control strategies for a parallel hybrid car," *Proceedings of the Institution of Mechanical Engineers, Part D: Journal of Automobile Engineering*, vol. 214, pp. 705–717, Jan. 2000.

[51] G. Paganelli, S. Delprat, T.-M. Guerra, J. Rimaux, and J.-J. Santin, "Equivalent Consumption Minimization Strategy For Parallel Hybrid Powertrains," in *Vehicular Technology Conference, IEEE 55th*, vol. 4, pp. 2076–2081, IEEE, 2002.

[52] V. Sezer, M. Gokasan, and S. Bogosyan, "A Novel ECMS and Combined Cost Map Approach for High-Efficiency Series Hybrid Electric Vehicles," *IEEE Transactions on Vehicular Technology*, vol. 60, no. 8, pp. 3557–3570, 2011.

[53] M. Shan, *Modeling and Control Strategy for Series Hydraulic Hybrid Vehicles*. Doctor of philosophy, The University of Toledo, 2009.

[54] C. Zhang, A. Vahidi, P. Pisu, and K. Tennant, "Role of Terrain Preview in Energy Management of Hybrid Electric Vehicles," *IEEE Transactions on Vehicular Technology*, vol. 59, pp. 1139–1147, Mar. 2010.

[55] C. Zhang and A. Vahidi, "Route Preview in Energy Management of Plug-in Hybrid Vehicles," *IEEE Transactions on Control Systems Technology*, vol. 20, pp. 546–553, Mar. 2012.

[56] P. Tulpule, V. Marano, and G. Rizzoni, "Effects of different PHEV control strategies on vehicle performance," in *American Control Conference*, pp. 3950–3955, IEEE, 2009.

[57] C. Musardo, G. Rizzoni, and B. Staccia, "A-ECMS: An Adaptive Algorithm for Hybrid Electric Vehicle Energy Management," in *European Journal of Control*, pp. 509–524, IEEE, 2005.

[58] Y. He, M. Chowdhury, P. Pisu, and Y. Ma, "An energy optimization strategy for power-split drivetrain plug-in hybrid electric vehicles," *Transportation Research Part C: Emerging Technologies*, vol. 22, pp. 29–41, June 2012.

[59] J. Wollaeger and G. Rizzoni, *ITS in Energy Management Systems of PHEV's*. Master of science, Ohio State University, 2012.

[60] S. Stockar, V. Marano, G. Rizzoni, and L. Guzzella, "Optimal Control for Plug-in Hybrid Electric Vehicle Applications," in *American Control Conference*, pp. 5024–5030, IEEE, 2010.

[61] S. Stockar, V. Marano, M. Canova, G. Rizzoni, and L. Guzzella, "Energy-Optimal Control of Plug-in Hybrid Electric Vehicles for Real-World Driving Cycles," *IEEE Transactions on Vehicular Technology*, vol. 60, pp. 2949–2962, Sept. 2011.

[62] *Global status report on road safety: time for action.* World Health Organization, 2009.

[63] T. Hummel, K. Matthias, B. Jenö, and L. Antje, "Advanced Driver Assistance Systems," tech. rep., 2011.

[64] J. Piao and M. McDonald, "Advanced Driver Assistance Systems from Autonomous to Cooperative Approach," *Transport Reviews*, vol. 28, pp. 659–684, Sept. 2008.

[65] J. Zhang and P. Ioannou, "Integrated Roadway / Adaptive Cruise Control System : Safety , Performance , Environmental and Near Term Deployment Considerations," *Research Reports, UC Berkeley*, 2004.

[66] A. Vahidi and A. Eskandarian, "Research advances in intelligent collision avoidance and adaptive cruise control," *IEEE Transactions on Intelligent Transportation Systems*, vol. 4, pp. 143–153, Sept. 2003.

[67] C. Beg, M. Vajedi, M. R. Nezhad-Ahmadi, N. L. Azad, and S. Safavi-Naeini, "A cost-effective radar system for automotive powertrain control applications," in *Intelligent Transportation Systems (ITSC), 2012 15th International IEEE Conference on*, pp. 84–89, IEEE, Sept. 2012.

[68] L. Xiao and F. Gao, "A comprehensive review of the development of adaptive cruise control systems," *Vehicle System Dynamics*, vol. 48, pp. 1167–1192, Oct. 2010.

[69] J. Bengtsson, *Adaptive Cruise Control and Driver Modeling.* No. November, Department of Automatic Control, Lund Institute of Technology, 2001.

[70] X.-y. Lu, J. K. Hedrick, and M. Drew, "ACC/CACC - Control Design, Stability and Robust Performance," in *American Control Conference*, pp. 4327–4332, IEEE, 2002.

[71] C.-y. Liang and H. Peng, "Optimal Adaptive Cruise Control with Guaranteed String Stability," *Vehicle System Dynamics*, no. December 2012, pp. 37–41, 2010.

[72] D. Corona and B. D. Schutter, "Comparison of a Linear and a Hybrid Adaptive Cruise Controller for a SMART," in *Decision and Control, 2007 46th IEEE Conference on*, no. 1, pp. 4779–4784, IEEE, 2007.

[73] A. Ferrara and C. Vecchio, "Second order sliding mode control of vehicles with distributed collision avoidance capabilities," vol. 19, pp. 471–477, June 2009.

[74] S. Moon, I. Moon, and K. Yi, "Design, tuning, and evaluation of a full-range adaptive cruise control system with collision avoidance," *Control Engineering Practice*, vol. 17, pp. 442–455, Apr. 2009.

[75] W. Huang, *Design and Evaluation of a 3D Road Geometry Based Heavy Truck Fuel Optimization System*. Doctor of philosophy, Auburn University, 2010.

[76] E. Hellstrom, M. Ivarsson, J. Aslund, and L. Nielsen, "Look-ahead control for heavy trucks to minimize trip time and fuel consumption," *Control Engineering Practice*, vol. 17, pp. 245–254, Feb. 2009.

[77] X. Zhuan and X. Xia, "Speed regulation with measured output feedback in the control of heavy haul trains," vol. 44, pp. 242–247, Jan. 2008.

[78] L.-h. Luo, H. Liu, P. Li, and H. Wang, "Model predictive control for adaptive cruise control with multi-objectives: comfort, fuel-economy, safety and car-following," *Journal of Zhejiang University SCIENCE A*, vol. 11, pp. 191–201, Feb. 2010.

[79] B. Asadi and A. Vahidi, "Predictive Cruise Control : Utilizing Upcoming Traffic Signal Information for Improving Fuel Economy and Reducing Trip Time," *IEEE Transactions on Control Systems Technology*, vol. 19, no. 3, pp. 707–714, 2011.

[80] G. Naus, J. Ploeg, M. Van de Molengraft, W. Heemels, and M. Steinbuch, "Design and implementation of parameterized adaptive cruise control: An explicit model predictive control approach," *Control Engineering Practice*, vol. 18, pp. 882–892, Aug. 2010.

[81] P. Shakouri and A. Ordys, "Nonlinear Model Predictive Control approach in design of Adaptive Cruise Control with automated switching to cruise control," *Control Engineering Practice*, vol. 26, pp. 160–177, May 2014.

[82] S. Li, K. Li, R. Rajamani, and J. Wang, "Model Predictive Multi-Objective Vehicular Adaptive Cruise Control," *IEEE Transactions on Control Systems Technology*, vol. 19, pp. 556–566, May 2011.

[83] M. a. S. Kamal, M. Mukai, J. Murata, and T. Kawabe, "Ecological Vehicle Control on Roads With Up-Down Slopes," *IEEE Transactions on Intelligent Transportation Systems*, vol. 12, pp. 783–794, Sept. 2011.

[84] M. Wang, W. Daamen, S. Hoogendoorn, and B. van Arem, "Driver assistance systems modeling by model predictive control," in *2012 15th International IEEE Conference on Intelligent Transportation Systems*, pp. 1543–1548, IEEE, Sept. 2012.

[85] N. Groot, B. D. Schutter, and H. Hellendoorn, "Integrated Model Predictive Traffic and Emission Control Using a Piecewise-Affine Approach," *IEEE Transactions on Intelligent Transportation Systems*, vol. 14, no. 2, pp. 587–598, 2013.

[86] S. Lin, B. D. Schutter, Y. Xi, and H. Hellendoorn, "Integrated Urban Traffic Control for the Reduction of Travel Delays and Emissions," *IEEE Transactions on Intelligent Transportation Systems*, vol. 14, no. 4, pp. 1609–1619, 2013.

[87] M. A. S. Kamal, J.-i. Imura, T. Hayakawa, A. Ohata, and K. Aihara, "Smart Driving of a Vehicle Using Model Predictive Control for Improving Traffic Flow," *IEEE Transactions on Intelligent Transportation Systems*, vol. 15, pp. 878–888, Apr. 2014.

[88] M. A. S. Kamal, M. Mukai, J. Murata, and T. Kawabe, "Model Predictive Control of Vehicles on Urban Roads for Improved Fuel Economy," *IEEE Transactions on Control Systems Technology*, vol. 21, pp. 831–841, May 2013.

[89] M. Vajedi, M. Chehrehsaz, and N. L. Azad, "Intelligent power management of plug-in hybrid electric vehicles , part I : real-time optimum SOC trajectory builder," *International Journal of Electric and Hybrid Vehicles*, vol. 6, no. 1, pp. 46–67, 2014.

[90] M. Vajedi, A. Taghavipour, N. L. Azad, and N. L. Azad, "Traction-Motor Power Ratio and Speed Trajectory Optimization for Power Split PHEVs Using Route Information," in *ASME 2012 International Mechanical Engineering Congress & Exposition*, (Houston, Texas, USA.), ASME, Nov. 2012.

[91] A. Mozaffari, M. Vajedi, and N. L. Azad, ""Real-time immune-inspired optimum state-of-charge trajectory estimation using upcoming route information preview and neural network for plug-in hybrid electric vehicles fuel economy," *Frontiers of Mechanical Engineering*, vol. 10, no. 2, pp. 154–167, 2015.

[92] L. Slezak, "Autonomie training part 1 Overview," tech. rep.

[93] J. Liu, H. Peng, and Z. Filipi, "Modeling and Analysis of the Toyota Hybrid System," in *Proceedings of the 2005 IEEE/ASME International Conference on Advanced Intelligent Mechatronics*, pp. 24–28, IEEE, 2005.

[94] D. S. Naidu, *Optimal control systems*. CRC press, 2002.

[95] L. Rokach and O. Maimon, "Clustering methods," in *Data mining and knowledge discovery handbook*, pp. 321–352, Springer, 2005.

[96] C. Hammerschmidt, "Innovation in the car: 90% comes from electronics and software." EETimes Europe Automotive, April 29, 2014, April 29, 2014.

[97] dSPACE GmbH, *dSPACE catalog 2004: Solutions for Control*, 2004.

[98] M. Vajedi, M. Chehrehsaz, and N. L. Azad, "Intelligent power management of plug-in hybrid electric vehicles , part II : real-time route based power management," *International Journal of Electric and Hybrid Vehicles*, vol. 6, no. 1, pp. 68–86, 2014.

[99] A. Mozaffari, M. Vajedi, and N. L. Azad, "Multi-objective component sizing of a power-split plug-in hybrid electric vehicle powertrain combined with optimal power management," *Engineering and Optimization*, 2015.

[100] A. Taghavipour, M. Vajedi, N. L. Azad, and J. McPhee, "Predictive Power Management Strategy for a PHEV Based on Different Levels of Trip Information," in *Engine and Powertrain Control, Simulation and Modeling*, vol. 3, pp. 326–333, 2012.

[101] M. Vajedi, A. Taghavipour, N. L. Azad, and J. McPhee, "A comparative analysis of route-based power management strategies for real-time application in plug-in hybrid electric vehicles," in *American Control Conference (ACC)*, pp. 2612–2617, IEEE, 2014.

[102] A. Taghavipour, M. Vajedi, N. L. Azad, and J. McPhee, "A comparative analysis of route-based energy management systems for PHEVs," *Asian Journal of Control*, 2015.

[103] D. E. Kirk, *Optimal control theory: an introduction*. Courier Corporation, 2012.

[104] H. B. Keller, *Numerical solution of two point boundary value problems*, vol. 24. SIaM, 1976.

[105] R. W. Holsapple, R. Venkataraman, and D. Doman, "New, Fast Numerical Method for Solving Two-Point Boundary-Value Problems," *Journal of Guidance, Control, and Dynamics*, vol. 27, pp. 301–304, Mar. 2004.

[106] A. D. Lewis, *The Maximum Principle of Pontryagin in control and in optimal control*. 2006.

[107] H. Michalska and D. Q. Mayne, "Robust receding horizon control of constrained nonlinear systems," *Automatic Control, IEEE Transactions on*, vol. 38, no. 11, pp. 1623–1633, 1993.

[108] T. Parisini and R. Zoppoli, "A receding-horizon regulator for nonlinear systems and a neural approximation," *Automatica*, vol. 31, no. 10, pp. 1443–1451, 1995.

[109] P. O. Scokaert, D. Q. Mayne, and J. B. Rawlings, "Suboptimal model predictive control (feasibility implies stability)," *Automatic Control, IEEE Transactions on*, vol. 44, no. 3, pp. 648–654, 1999.

[110] A. Zheng and M. Morari, "Stability of model predictive control with mixed constraints," *Automatic Control, IEEE Transactions on*, vol. 40, no. 10, pp. 1818–1823, 1995.

[111] Toyota Information System, *Hybrid / battery control: hybrid control system: details 2015 My Prius PHV,Doc ID: RM000004273OOMX*, 2015.

[112] M. Vajedi and N. L. Azad, "Ecological Adaptive Cruise Controller for Hybrid Electric Vehicles Using Nonlinear Model Predictive Control," *IEEE Transactions on Intelligent Transportation Systems*, 2015.

[113] A. Mozaffari, M. Vajedi, and N. L. Azad, "A robust safety-oriented autonomous cruise control scheme for electric vehicles based on model predictive control and online sequential extreme learning machine with a hyper-level fault tolerance-based supervisor," *Neurocomputing*, pp. 1–12, Oct. 2014.

[114] B. Sakhdari, M. Vajedi, and N. L. Azad, "Ecological Adaptive Cruise Control of Connected Plug-in Hybrid Electric Vehicles for Urban Driving," in *American Control Conference (ACC)*, IEEE, 2015.

[115] M. Han, J. Fan, and J. Wang, "A dynamic feedforward neural network based on gaussian particle swarm optimization and its application for predictive control," *Neural Networks, IEEE Transactions on*, vol. 22, no. 9, pp. 1457–1468, 2011.

[116] E. Pourjafari and H. Mojallali, "Predictive control for voltage collapse avoidance using a modified discrete multi-valued pso algorithm," *ISA transactions*, vol. 50, no. 2, pp. 195–200, 2011.

[117] G. Sandou and S. Olaru, "Particle swarm optimization based nmpc: An application to district heating networks," in *Nonlinear Model Predictive Control*, pp. 551–559, Springer, 2009.

[118] Y. Song, Z. Chen, and Z. Yuan, "New chaotic pso-based neural network predictive control for nonlinear process," *Neural Networks, IEEE Transactions on*, vol. 18, no. 2, pp. 595–601, 2007.

[119] X. Wang and J. Xiao, "Pso-based model predictive control for nonlinear processes," in *Advances in Natural Computation*, pp. 196–203, Springer, 2005.

[120] M. Yousuf, H. Al-Duwaish, and Z. Al-Hamouz, "Pso based nonlinear predictive control of single area load frequency control," in *IFAC Workshop on Control Applications of Optimization*, 2009.

[121] M. Clerc, *Particle swarm optimization*, vol. 93. John Wiley & Sons, 2010.

[122] I. C. Trelea, "The particle swarm optimization algorithm: convergence analysis and parameter selection," *Information processing letters*, vol. 85, no. 6, pp. 317–325, 2003.

[123] F. Ye and Y. Zhang, "Vehicle Type-Specific Headway Analysis Using Freeway Traffic Data," *Transportation Research Record: Journal of the Transportation Research Board*, vol. 2124, pp. 222–230, Dec. 2009.

[124] Toyota Information System, *Cruise control: dynamic radar cruise control system: system diagram 2015 MY Prius PHV, Doc ID: RM00000427F01BX*, 2015.